Linda Matos Câmara

Licenciatura em Ciências da Engenharia Biomédica

Paper-based enzyme free platform for detecting falsified antibiotics using gold nanoparticles

Dissertação para obtenção do Grau de Mestre em
Engenharia Biomédica

Orientadora: Doutora Elvira Maria Correia Fortunato, Professora Catedrática da FCT-UNL

Júri:

Presidente: Doutor Jorge Alexandre de Carvalho Silva, Professor Auxiliar da FCT-UNL

Vogais: Doutora Elvira Maria Correia Fortunato, Professora Catedrática da FCT-UNL

Doutor José Ricardo Ramos Franco Tavares, Professor auxiliar com Agregação da FCT-UNL

FACULDADE DE CIÊNCIAS E TECNOLOGIA
UNIVERSIDADE NOVA DE LISBOA

September, 2019

Paper-based enzyme free platform for detecting falsified antibiotics using gold nanoparticles

Dedicado aos meus pais e à minha irmã.

Acknowledgements

É com enorme prazer e alegria que escrevo estas palavras de agradecimento a todas as pessoas que fizeram parte desta etapa muito importante da minha vida. O sucesso não se alcança sozinho e sem estas pessoas, o culminar destes cinco anos de estudo não teria sido possível. Este sucesso não é só meu, mas sim nosso.

Esta dissertação de mestrado foi realizada no Centro de Investigação de Materiais (CENIMAT|i3N) da Faculdade de Ciências e Tecnologia da Universidade Nova de Lisboa. Quero desde já, agradecer a todas pessoas que trabalham nesta instituição de excelência, por me terem proporcionado excelentes momentos e uma boa integração.

Quero agradecer à minha orientadora, Professora Elvira Fortunato, por me ter proporcionado esta oportunidade de realizar a dissertação neste estabelecimento, pela orientação ao longo desses meses, pela ajuda e pelo incentivo.

Quero agradecer à Carolina e ao Tomás, por terem sido incansáveis comigo durante todo este projeto. Mostraram sempre disponibilidade para me acompanhar, tirar dúvidas e ajudar a ultrapassar todos os contratempos. Vocês foram essenciais para a realização desta dissertação e estou-vos eternamente grata.

Um obrigado especial ao meu namorado, aos meus pais e à minha irmã, por me terem apoiado todos os dias, por terem acreditado nas minhas capacidades e por me terem motivado a continuar. Estiveram sempre lá para mim e fizeram com que não me faltasse nada. Foram sem dúvida, das pessoas mais importantes ao longo deste processo. Quero também agradecer a todos os meus amigos, que me proporcionaram momentos de festa, alegria e descontração. Após estes cinco anos de curso, levo comigo grandes amizades e boas memórias.

Abstract

The emergence of counterfeit and substandard medicines is a worldwide problem that has been growing over the years. The use of these medicines puts people's health at risk, which can even result in death. It is estimated that 5% of the antibiotics on the market are counterfeit and that most of these are β-lactams. Despite being a worldwide problem, its incidence is higher in less developed countries due to limited access to quality medical products at an affordable price and the lack of sophisticated means for their detection. Most of the techniques used to validate the purity of an antibiotic require specialized technicians, adequate infrastructures and expensive equipment, which makes it impossible to use in resource-poor countries.

The main goal of this dissertation is to develop an inexpensive and user-friendly device, able to detect counterfeit β-lactam antibiotics. This detection is based on checking for the presence of the active pharmaceutical ingredient (API) in the antibiotic and verifying if it is within the correct dosage. The device consists of a paper-based platform, obtained by Lab-on-Paper technology, with an enzyme-free detection, based on the use of gold nanoparticles. In the presence of the API, the $HAuCl_4$ is reduced and gold nanoparticles (GNPs) are formed, allowing a colorimetric detection. This reaction was tested with solutions of different volumes and concentrations of antibiotic and calibration curves were obtained, from digital analysis, to obtain the dosage of that antibiotic. Solutions of common drug replacements were used to verify if there is formation of GNPs without the API.

Keywords: counterfeit β-lactam antibiotics, enzyme-free platform, gold nanoparticles, paper-based sensor

Resumo

O aparecimento de medicamentos falsificados e de baixa qualidade é um problema mundial que tem vindo a intensificar-se ao longo dos anos. O uso destes medicamentos coloca a saúde das pessoas em risco, podendo resultar em morte. É estimado que 5% dos antibióticos no mercado são falsificados e que a maioria desses antibióticos são β-lactâmicos. Apesar de ser um problema mundial, a sua incidência é maior em países em desenvolvimento devido ao acesso limitado a produtos médicos de qualidade a preço acessível e à falta de meios sofisticados para a sua deteção. A maioria das técnicas utilizadas para validar a pureza de um antibiótico, requerem técnicos especializados, infraestruturas adequadas e equipamentos caros, o que impossibilita o seu uso em países com poucos recursos.

O objetivo desta dissertação é desenvolver um dispositivo barato e de fácil utilização para a deteção de antibióticos β-lactâmicos falsificados. Essa deteção é baseada na confirmação da presença do princípio farmacêutico ativo (API) no antibiótico e na identificação da sua dose. O sensor em papel é obtido através da tecnologia Lab-on-Paper e utiliza nanopartículas de ouro (GNPs) com meio de deteção. Na presença do API o $HAuCl_4$ é reduzido e são formadas GNPs, permitindo uma deteção colorimétrica e não enzimática. Esta reação foi testada com diferentes volumes e concentrações de antibiótico e foram obtidas curvas de calibração, a partir da análise digital, para obter a dose desse antibiótico. Foram utilizadas soluções de substitutos de medicamentos para verificar se há formação de GNPs na ausência do API.

Palavras-chave: antibióticos β-lactâmicos falsificados, sensor não enzimático, nanopartículas de ouro, sensor em papel

Contents

List of Figures

List of Tables

Abbreviations

6-APA	6-aminopenicillanic Acid
7-ACA	7-aminocephalosporanic Acid
API	Active Pharmaceutical Ingredient
CENIMAT	Centro de Investigação de Materiais
Cr.I.	Crystalline Index
DLS	Dynamic Light Scattering
DSC	Differential Scanning Calorimetry
EDS	Energy Dispersive Spectroscopy
FTIR	Fourier Transform Infrared Spectroscopy
GNPs	Gold Nanoparticles
GPHF	Global Pharma Health Fund
HPLC	High-Performance Liquid Chromatography
LOD	Limit of Detection
MS	Mass Spectrometry
PDMS	Polidimetilsiloxano
Penicillin G	Benzylpenicillin
Penicillin V	Phenoxymethylpenicillin

POC	Point-of-Care
SEM	Scanning Electron Microscopy
SPR	Surface Plasmon Resonance
TEM	Transmission Electron Microscopy
TLC	Thin layer chromatography
XRD	X-Ray Diffraction

1

Introduction and Objectives

According to the World Health Organization (WHO), counterfeit/falsified and substandard medical products have been increasing over the years. These products are considered medical products with a fraudulent presentation of identity, composition and origin or medical products that do not meet quality standards, respectively. Substandard medical products may be poorly manufactured, poorly packed or poorly transported. Falsified medical products may contain the correct Active Pharmaceutical Ingredient (API) in different concentrations than expected, not contain the correct API or contain the wrong compounds [1]. An API is a substance used in the manufacture of a medical product, which exerts a pharmacological, immunological or metabolic action to restore and correct physiological functions or establish a medical diagnosis. Any other substance in a medical product is referred to as an excipient [2].

The use of counterfeit and substandard medical products puts people's health in danger and leads to failures in the treatment of illness, which may even result in death. These failures result in a loss of confidence in the drugs and the health system and contribute to the expansion of drug resistance. Antibiotics and other antimicrobials are manufactured in such a way as to contain doses capable of destroying the pathogens present in the body. If they contain only a fraction of the correct dose or are poorly manufactured, only a few of these pathogens will be destroyed. Survivors are the pathogens that acquire mutations that allow them to survive low doses of medication. This could lead to the development of drug resistant infections which, due to the evolution of the means of transport, could easily be transmitted to other countries [1].

Between 2013 and 2017, 1500 counterfeit and substandard medical products were reported in various regions of the world (**Figure 1.1**) [1]. It is estimated that 5% of the antibiotics

present on the world market are counterfeit and that within these, beta-lactam (β-lactam) antibiotics are the most common [3]. Studies have shown that the most counterfeit β-lactam antibiotics of the penicillin and cephalosporin classes are amoxicillin, ampicillins and ceftazidime [4]. Although this problem is worldwide, its incidence is higher in countries where:

- Access to affordable and safe quality medical products is limited;
- There are gaps in governance, poor ethical practices in health care and corruption in the private and public sectors;
- Equipment and technical capacity to ensure good manufacturing practices, quality control, storage and distribution are limited [1].

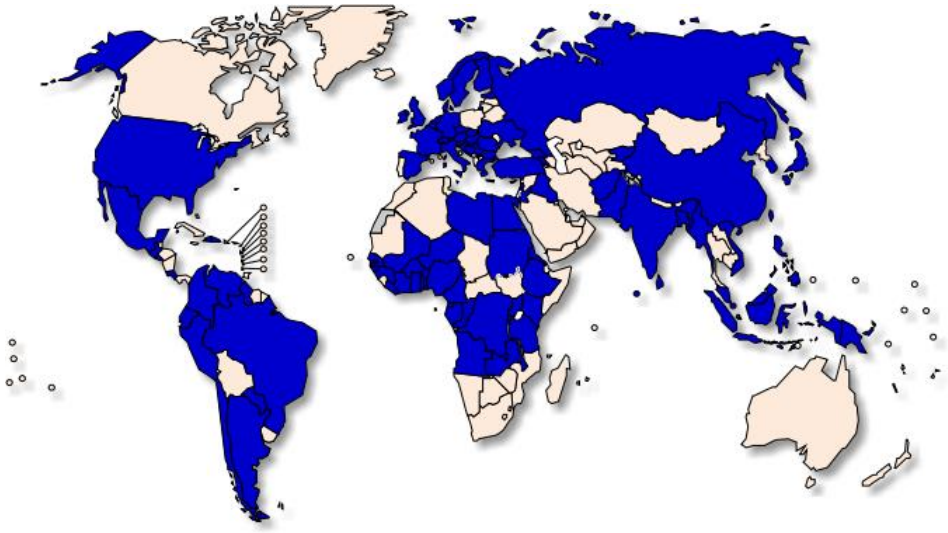

Figure 1.1 Detection of counterfeit and substandard products worldwide
The countries in which counterfeit and substandard medical products have been discovered and reported to WHO between 2013 and 2017 are represented in blue. Adapted from [1]

The standard procedure for determining the purity of a drug is based on mass spectrometry and high-performance liquid chromatography (HPLC). This requires specialized technicians, adequate infrastructures and expensive equipment, which makes it difficult to carry out these procedures in less developed countries [3]. Consequently, in conditions of few resources the assessment of the purity of the medicines is hampered. The means available for this purpose are less precise and have the disadvantage of requiring chemicals, standard samples, trained people to perform them, a high initial investment or a limited lifetime.

The purpose of this thesis is to develop an inexpensive and user-friendly device, able to distinguish legitimate from counterfeit antibiotics. As most of the worldwide counterfeit antibiotics are β-lactams, antibiotics from this group will be used, namely penicillins and cephalosporins. This device shall consist of a non-enzymatic, microfluidic paper device with a colorimetric

detection obtained through metal nanoparticles. The use of paper as diagnostic support makes the sensor inexpensive, equipment free and easy to use. The evaluation of the colour can be done using a smartphone which removes the need for specialized technicians. Another advantage of this device is the absence of enzymes, which increases the shelf life of the sensor and its resistance to transport and storage conditions. The main goals of this project are:

i. Synthesis of gold nanoparticles (GNPs) in solution by reduction of $HAuCl_4$ by the antibiotics' amine group;
ii. Application of the previous synthesis on paper substrate and establishment of protocols for each antibiotic;
iii. Testing the previous protocols with common drug replacements;
iv. Proof of concept development of a non-enzymatic paper-based device to distinguish legitimate from counterfeit antibiotics.

2

Concepts

In this chapter, the theoretical foundations necessary for a better understanding of this thesis are presented. Within the theory associated with this project, it is important to understand the function of paper-based microfluidics and colorimetric detection using gold nanoparticles. In addition, it is essential to understand the concept of sensor and antibiotic.

2.1 Antibiotics

Antibiotics are substances of biological or synthetic origin, capable of killing or inhibiting the growth of bacteria [5]. Most antibiotics result from the purification and chemical modification of colonies of microorganisms, which qualifies them as semi-synthetic antibiotics [6]. Antibiotics can be classified according to their *in vitro* behaviour, their molecular structure or according to their mode of action. According to classification based on *in vitro* behaviour, antibiotics may be designated as bactericidal or bacteriostatic. Bactericides kill bacteria while bacteriostats inhibit their growth. Classification according to molecular structure considers the molecular geometry and electronic structure of the antibiotic. The mode of action includes inhibition of cell wall synthesis, alteration of cell membrane structure or function, inhibition of nucleic acid function and structure, inhibition of protein synthesis at ribosomes, and blocking of metabolism [5].

2.2 Penicillins

The first antibiotic discovered was the penicillin, in 1928, by Alexander Fleming [5]. This antibiotic is derived from the fungus *Penicillium chrysogenum* and is part of the β-lactam antibiotic group. Its chemical structure has a β-lactam ring, a thiazolidine ring and a side chain (**Figure**

2.1). The β-lactam ring and the thiazolidine ring form the nucleus of the penicillins, called 6-aminopenicillanic acid (6-APA). The stability of the antibiotic and its activity against different bacteria is determined according to the variable side chain group (R). Altering this group allows different types of penicillin to be obtained (**Figure 2.2**) [7].

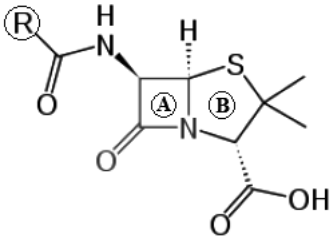

Figure 2.1 General structure of penicillins
R: side chain variable group; A: β-lactam ring; B: thiazolidine ring. Adapted from [5]

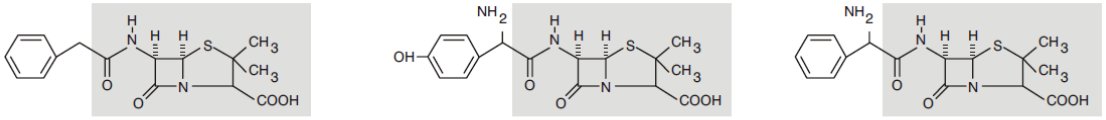

Figure 2.2 Benzylpenicillin, amoxicillin and ampicillin structure
The alteration of the side chain variable group allows obtaining different types of penicillin [8].

Penicillins act as bactericidal agents, because inhibits the bacterial cell wall synthesis and has been used to treat bacterial infections, such as ear infections, bladder infections, gonorrhoea, *Escherichia coli* or *Salmonella* infections, upper respiratory tract infections, pneumonia, skin and soft tissue infections, septicaemia, meningitis, endocarditis and gastrointestinal tract infections [7]. These antibiotics can be divided into natural penicillins and semi-synthetic penicillins. Natural penicillins result from fermentation processes of the fungus *Penicillium* and are part of this group benzylpenicillin (penicillin G) and phenoxymethylpenicillin (penicillin V). These penicillins present some drawbacks, such as their narrow spectrum of activity and their susceptibility to inactivation by β-lactamases and penicillinase. β-lactamase are enzymes produced by bacteria which break down the β-lactam ring. Penicillin-specific β-lactamases are called penicillinase.

Semi-synthetic penicillins have been developed to overcome the disadvantages of natural penicillins and result from the chemical addition of side chains to the 6-APA produced by the fungus. 6-APA is obtained by disrupting the synthesis of the penicillin molecule to obtain only the common nucleus, or by removing the side chains. The semi-synthetic penicillins are divided into penicillinase-resistant penicillins, extended spectrum penicillins and β-lactamase inhibiting penicillins. The penicillinase-resistant penicillins are not activated by the penicillinase enzyme and examples of these penicillins are methicillin, oxacillin, cloxacillin, dicloxacillin and nafcillin.

The extended spectrum penicillins have the widest antibacterial spectrum and are subdivided into aminopenicillins (amoxicillin and ampicillin), carboxypenicillins (carbenicillin and ticarcillin) and ureidopenicillins (mezlocillin and azlocillin). β-lactamase inhibiting penicillins result from the combination of penicillins with β-lactamase inhibitors and are used in treatments for infections caused by β-lactamase producing bacteria. Amoxicillin-clavulanate and ticarcillin-clavulanate are examples of penicillins of this group [7], [9].

2.3 Cephalosporins

Cephalosporins are the most used β-lactam antibiotics and have a similar structure and mode of action to penicillins (**Figure 2.3**). Its chemical structure consists of a β-lactam ring, a dihydrothiazine ring and a side chain (**Figure 2.4**). The β-lactam ring and the dihydrothiazine ring form the nucleus of cephalosporins, called 7-aminocephalosporanic acid (7-ACA). The alteration of the variable groups allows to obtain different types of cephalosporins (**Figure 2.5**) [5], [10].

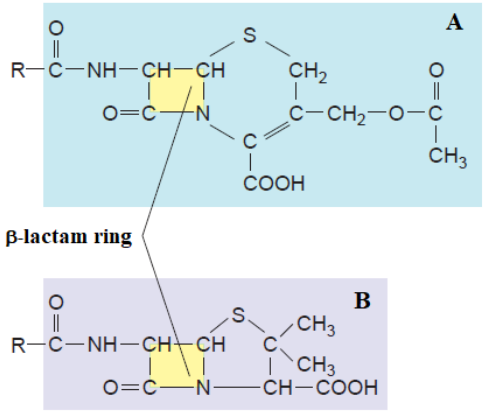

Figure 2.3 Cephalosporin and penicillin nuclear structures
A: Cephalosporin; B: Penicillin. Adapted from [11]

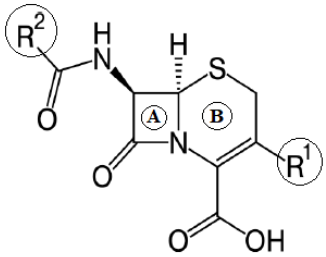

Figure 2.4 General structure of cephalosporins
R: side chain variable groups 1 and 2; A: β-lactam ring; B: dihydrothiazine ring. Adapted from [5]

The first cephalosporin antibiotic was isolated in 1945 from the fungus *Cephalosporium acremonium*. These antibiotics also act as bactericidal agents, disrupting the synthesis of the bacterial cell wall and turning the bacteria susceptible to the environment [12]. Cephalosporins are used to treat skin or soft tissue infections, urinary tract infections, ear infections, pneumonia, gonorrhoea, bronchitis, bone and joint infections [13]. These antibiotics are subdivided into five generations according to their target organism [5]. First-generation cephalosporins have a relatively restricted action spectrum, specifically against gram-positive bacteria, while the successive generations are increasingly more effective against gram-negative bacteria and have a more extended spectrum [5]. Cefaclor and cefuroxime are examples of cephalosporins of second generation and ceftazidime is an example of a cephalosporin of third generation.

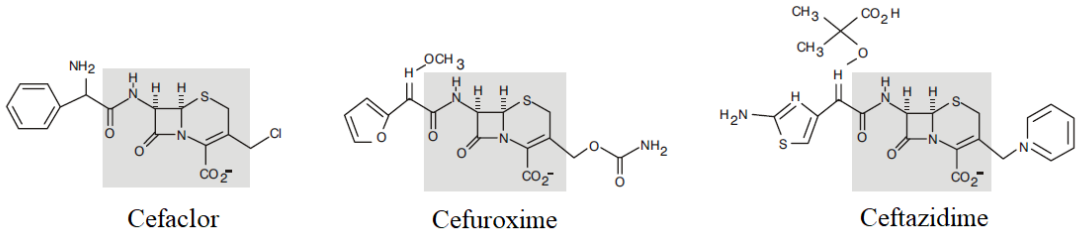

Figure 2.5 Cefaclor, cefuroxime and ceftazidime structure
The alteration of the variable groups allows to obtain different types of cephalosporins [8]

In this thesis, β-lactam antibiotics from the two different groups previously mentioned were used: amoxicillin and ampicillin from the penicillin group and ceftazidime from the cephalosporin group.

2.4 Sensors

A sensor is an element of a measuring system that is directly affected by a phenomenon, body, or substance carrying a quantity to be measured. The presence of the phenomenon, body, or substance can be indicated by a detector when a threshold value of an associated quantity is exceeded [14]. A sensor can be characterized by the following parameters:

- **Sensitivity**: quotient of the change in an indication of a measuring system and the corresponding change in a value of a quantity being measured;
- **Selectivity**: property of a measuring system, used with a specified measurement procedure, whereby it provides measured quantity values for one or more measurands such that the values of each measurand are independent of other measurands or other quantities in the phenomenon, body, or substance being investigated;

- **Dynamic range**: interval between the minimum and maximum concentration of a quantity being measured in which the sensor is sensitive;
- **Linear range**: values between which the output signal is directly proportional to the input signal;
- **Limit of detection (LOD)**: minimum value discriminated by the sensor;
- **Stability**: property of a measuring instrument, whereby its metrological properties remain constant in time;
- **Response time**: duration between the instant when an input quantity value of a measuring instrument or measuring system is subjected to an abrupt change between two specified constant quantity values and the instant when a corresponding indication settles within specified limits around its final steady value;
- **Recovery time**: amount of time until the sensor can take a new measurement;
- **Accuracy**: closeness of agreement between a measured quantity value and a true quantity value of a measurand;
- **Calibration curve**: expression of the relation between indication and corresponding measured quantity value [14], [15].

The sensors can be classified according to their measurand. In this case, we speak of sensors for temperature, pressure, flow, level, humidity, pH, chemical composition, position, velocity, acceleration, and so forth [16], [17].

2.5 Paper

Paper was discovered in China, by the imperial court official Ts'ai Lun, back in A.D. 105. He joined mulberry and other fibres with fishnets, old rags and hemp waste to produce the first sheet of paper. After the paper technology spread to the middle east, it suffered an improvement by the Arabs, in which it was enhanced with linen, flax and other vegetable fibres. After the printing invention, the demanding for paper increased and nowadays paper is used in numerous areas, such as agriculture, building, business, cars, communications, domestic products, education, electrical, entertainment, filtration, impregnated papers, industry, medical and finances [18], [19].

Paper is mostly constituted by cellulose, which is one of the most abundant biopolymers on earth and has various benefits such as low cost, availability, renewability, light weight, nanoscale dimension and unique morphology [20]. This polymer can have different origins, such as wood pulp, bacteria, cotton or other plant fibres and is composed by aldehyde sugars [21]. Each

cellulose chain is asymmetric, with a chemically reducing end and a nonreducing end that contains a pendant hydroxyl group. These chains come together, by van der Waals forces, intra-molecular and inter-molecular hydrogen bonds, to form cellulose fibres. This hydrogen-bonding and the molecular orientation can vary widely, originating different cellulose polymorphs. The cellulose chemical structure is present in **Figure 2.6**.

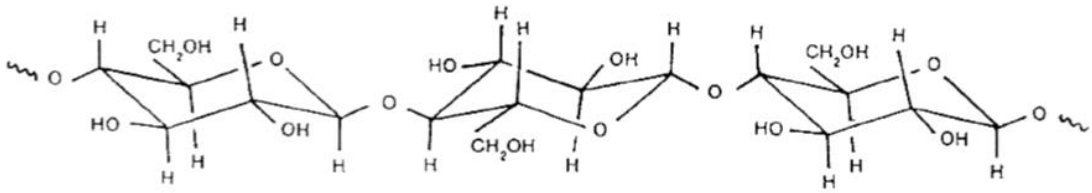

Figure 2.6 Cellulose chemical structure
[22]

A parameter termed the crystalline index (Cr.I.) has been used to describe the relative amount of crystalline material in cellulose [23]. This parameter can be calculated by the empirical method proposed by Segal [24]:

$$\boldsymbol{Cr.I.}(\%) = \frac{\boldsymbol{I_{200} - I_{am}}}{\boldsymbol{I_{200}}} \times \mathbf{100} \qquad \textbf{(2.1)}$$

where I_{200} is the maximum intensity of the (200) lattice diffraction and I_{am} is the intensity diffraction at 18º 2Θ degrees. Native cellulose or cellulose I is the most crystalline type and presents two forms I_α and I_β. In both structures, the hydrogen-bonding patterns differ, resulting in different crystalline structures. The first has a triclinic unit cell, while the second has a monoclinic unit cell. The ratio in native cellulose depends on their source: cellulose from bacteria and algae have mainly I_α, while higher plants present both I_α and I_β [20], [21].

The use of paper as diagnostic support in sensors contains several benefits, such as the price, the high surface to volume ratio, the large supply with different formats and properties, the compatibility with various chemicals, the disposability, the easy use and the presence of a white background, which allows a colorimetric detection [25]. The colorimetric detection in paper devices involves the movement of the analyte to the test zone, through capillary force, where it interacts with specific reagents. This produces a colour that can be analysed at naked eye or through additional equipment. This colorimetric detection can be performed using metal nanoparticles [26].

2.6 Microfluidics

Microfluidics involve the use of devices on a microscale that allow accurate manipulation of small volumes of fluids. This presents advantages such as reduced use of reagents and products, speed, reduced size, precise temperature control, low energy consumption, low risk of contamination and low-cost mass production. Microfluidic devices are well suited for medical diagnostic tests performed outside the laboratory and with the patients, namely Point-of-Care (POC) tests [27]. According to WHO the POC devices must be affordable, sensitive, specific, user-friendly, rapid and robust, equipment-free and deliverable to those in need [25], [28].

The manufacture of microfluidic devices consists in the production of channels on the surface of a solid substrate, in the formation of small holes to allow the entrance of the fluids, and in the encapsulation of the device. One of the methods most used for its manufacture is the soft lithography [29], which consists of the engraving of patterns in a soft polymer such as polydimethylsiloxane (PDMS) [30].

Microfluidics on paper was introduced by the *Whitesides* group of Harvard University in 2007. It was presented as an inexpensive device with the possibility of being considered a POC equipment. This Lab-on-Paper technology consists in the creation of microchannels on hydrophilic paper limited by hydrophobic polymers, wax or photoresist (light-sensitive material). The technology for standardizing paper that allows a better production-cost ratio is wax printing. In this technique, the paper is patterned with solid hydrophobic wax and then heated to melt and diffuse through the pores of the paper. This allows the creation of hydrophobic barriers that delimit the hydrophilic channels, the reaction zones and the fluid reservoirs [25].

2.7 Gold Nanoparticles

Nanoparticles are defined as particles ranging from 1 nm to 100 nm. These particles have very particular chemical and physical characteristics, namely chemical surface, size, shape-dependent electronics and optical properties [31]. Due to these characteristics, the nanoparticles can be used as biological and chemical sensors for detection of analytes [32].

Some of the nanoparticles with the most applications in the biomedical area are the gold nanoparticles (GNPs). These nanoparticles when present in solution, have a reddish colour with a maximum absorption peak at 562 nm [32], [33]. The position of the absorption peak depends on the shape and state of aggregation of the particle. The broadness of the peak provides infor-

mation on particle size distribution and state of aggregation. Its intensity of absorption is proportional to the number of nanoparticles produced [33], [34]. When aggregated, GNPs show changes in colour and maximum absorption peak position [32].

The colour change of GNPs is related to surface plasmon resonance (SPR) of nanoparticles (**Figure 2.6**) [35]. This phenomenon consists of the collective oscillation of free electrons in resonance with the incident electromagnetic radiation [36]. As the wave front of the radiation passes, the electron density in the particle is polarized to one surface and oscillates in resonance with the radiation's frequency, causing a standing oscillation [37]. The frequency of this phenomenon depends on the size and shape of the nanoparticle, the dielectric properties of the medium and the coupling interactions between nanoparticles [35]. As the shape or size of the nanoparticle changes, the surface geometry also changes, causing a shift in the electric field density on the surface and consequently, a change in the oscillation frequency [37]. For small spherical monodisperse GNPs, the SPR phenomenon causes an absorption of light in the blue-green region of the spectrum, dispersing red light. For increased size particles the wavelength of SPR shifts to higher values, absorbing red light and dispersing blue/purple light. As the particle size continues to increase, the SPR wavelengths shifts to the infrared region and the GNPs acquire a translucent colour [38]. When spherical GNPs aggregate, they increase the total particle size, leading to a colour change in the solution from red to blue. Due to the colour change of the GNPs, these can be used for colorimetric detection in sensors. In addition to this feature, GNPs are inexpensive, easy to prepare and allow quick and effective detection [32].

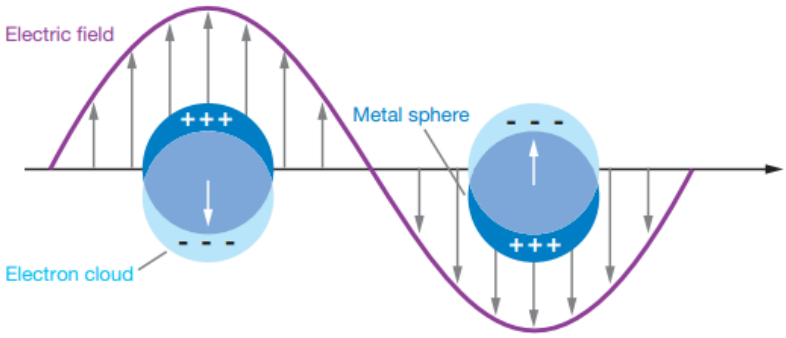

Figure 2.7 Localized surface plasmon resonance
Light interacts with particles much smaller than the incident wavelength, which leads to a plasmon that oscillates locally around the nanoparticle with a frequency known as localized surface plasmon resonance. [39]

3

State of the Art

The purpose of this chapter is to introduce the different methods for detection of falsified antibiotics in more and less developed countries. Examples of microfluidic paper-based analytical devices are presented to contextualize this theme with methods already developed to evaluate the purity of β-lactam antibiotics.

3.1 Methods for detection of falsified antibiotics

A variety of technologies have been used to detect falsified and substandard antibiotics. Qualitative tests demonstrate the presence or absence of the API while quantitative tests ensure that the API is present in the correct dosage. The range of technologies include colorimetry, chromatography, spectroscopy, X-ray diffraction and spectrometry [4], [40], [41]. The gold standard procedure to detect counterfeit antibiotics is via High-performance liquid chromatography (HPLC) and Mass Spectrometry (MS).

Chromatography allows the separation of different ingredients in a mixture by their interaction with a solid stationary phase, fixed in a column or support. Each compound of the mixture interacts with the stationary phase through a mobile phase and acquires different speeds depending on its affinity. As many compounds are colourless in the UV/Visible range, specific detectors based on refraction index changes, fluorescence or absorbance at various wavelengths, are used to reveal them. In HPLC the sample is dissolved in a solvent and pumped at high pressure through a column with silica particles [42]. This technique allows the separation, identification and precise quantification of the API in non-volatile samples, through ultraviolet-visible light

absorbance detectors and mass spectrometers. Gas chromatography is used to detect volatile components, residual solvents and undeclared ingredients. This technique is similar to HPLC except for the mobile phase, that is in a gaseous state [43], [44]. These procedures are sophisticated and efficient however they require expensive laboratory instruments.

MS allows the identification of the compounds present in an antibiotic based on their charge and mass. Different compounds exposed to an external electric field acquire different velocities or require different electric fields to be moved, which allows their identification. The results are compared with results obtained by standard samples under the same conditions [42]. It is a specific and precise technique that does not require a sample preparation yet, it is expensive and requires specialized people for the procedure [4].

X-ray diffraction can be used to analyse the physical and chemical characteristics and the structural orientation of the API and the excipients of an antibiotic. The X-rays focus on the sample and specific diffraction patterns are formed, which reflect the characteristic physical and chemical properties of each component. The specific pattern of a drug is a superposition of all the diffraction patterns from its crystalline components. Any change in the drug can be identified after comparison with the genuine drug. This technique has the disadvantage of requiring a skilled person, having to be performed in a laboratory, and being less sensitive and reliable than HPLC and MS [45], [46].

Microbiological assays can determine the bioactivity and potency of an antibiotic. These assays are performed on bacterial cultures and involve the evaluation of the biological response of bacteria to the antibiotic. They have the disadvantage of also having to be carried out in a laboratory, being longstanding and susceptible to errors, due to various factors such as incubation temperature, sample preparation and agar layer thickness [47].

As the presented techniques require expensive equipment, specialized technicians or suitable infrastructures, it is difficult to use them in less developed countries. Consequently, drug efficacy and purity are determined by visual inspection, dissolution and disintegration assays, Thin-layer Chromatography (TLC), *GPHF-Minilab*, portable spectroscopy devices and colorimetric techniques [4], [40], [41]. These techniques have the disadvantage of being less sensitive and less specific than the techniques used in developed countries. Although visual inspection of packaging and label quality is inexpensive and basic, without chemical analysis it is not possible to guarantee the purity of the drug, since most of the suppliers of these falsified products invest in the improvement of the packaging [1].

Disintegration and dissolution assays consist of placing the tablet in water at a specific temperature. The first one verifies if the antibiotic disintegrates within the prescribed time and

the second one allows to evaluate the percentage of drug released in the medium and consequently, evaluate the effectiveness of the drug. In the dissolution assay the drug is dissolved with the aid of a device which promotes constant agitation of the medium. The presence of incorrect excipients, poor manufacturing quality and poor storage conditions can lead to poor dissolution. Although the dissolution assay requires more training and more sophisticated equipment than the disintegration assay, both can identify a falsified drug even with the correct dosage of API [43].

In TLC, a small drop of sample is placed on a chromatographic plate which is then inserted into a solvent. The solvent moves through the plate by capillary forces and the different components of the sample acquire different rates of mobility, which allows their separation. The position of each component can be calculated by the ratio between the distances travelled by the component and the solvent [44]. Although it is a quick and inexpensive method, it has the disadvantage of requiring flammable or toxic reagents and trained people to perform the procedure.

The *GPHF-Minilab* is a quality control kit for medicines and is made up of laboratory equipment and chemical products that allow to carry out about a thousand tests. The quality check of the medicines by this kit involve physical inspection of the medicine and its packaging, a disintegration test and TLC tests [48]. It is a simple, reliable and inexpensive method but requires reagents, solvents, standard samples and trained people to perform it.

Spectroscopy involves the interaction between chemical compounds and electromagnetic radiation. When the sample is irradiated with a specific wavelength, the components of that sample absorb the energy and vibrate along its chemical bonds. The collection of these vibrations allows the chemical structure of the antibiotic and its constituents to be obtained. By comparing the specimens obtained with known specimen, it is possible to identify whether the antibiotic is falsified or not. In developed countries, various spectroscopy techniques have been shown to be efficient methods for the qualitative and/or quantitative analysis of antibiotic's API and excipients. Portable Raman and infrared spectrometers allow the chemical information of and antibiotic to be obtained without having to take the sample to the laboratory, which is useful for less developed countries. However, these portable devices have a high initial investment, require a preloading of a spectrum library and the presence of fluorescent material in the antibiotic may interfere with the results [42], [43].

Colorimetric techniques use the colour developed, due to the presence of reagents, to evaluate the presence or absence of specific components in the sample. The intensity of this colour allows qualitative information of these components to be obtained through specific devices or naked eye. These types of techniques can be performed by non-specialist and allow a rapid and

highly specific detection. Over the years, these tests have been improved and are now incorporated into microfluidic paper devices, making them inexpensive, equipment free and easy to use [3], [4], [42], [49].

3.2 Paper-based devices for detection of falsified β-lactam antibiotics

In 2013, Weaver et al. [49] developed a paper analytical device for detecting the purity of β-lactam antibiotics and anti-tuberculosis drugs. This device detects the APIs, such as ampicillin, amoxicillin, rifampicin, isoniazid, ethambutol and pyrazinamide, screens for substitute pharmaceuticals, such as acetaminophen and chloroquine, and can detect binders and fillers like chalk, talc and starch. It consists of twelve hydrophilic channels separated by hydrophobic barriers standardized with wax. Each channel contains different deposited reagents that allow the identification of the different components present in the drug. Of the twelve channels, five are to test the presence of functional groups expected to appear in the targeted antibiotics, six are to test the presence of excipients and substitute materials, and the other channel is to indicate when the device can be withdrawn from the water. The drug is spread over a line about 1-1.5 cm below the top of the channels, depositing at least 0.5000 mg of the solid in each channel. Once the sample is applied, the device is set in water and held upright for about four minutes. The water rises through the channels by capillary forces and different chemical reactions occur. These reactions cause the device to form a coloured bar code (**Figure 3.1**), which is then compared with standard samples. For optimal colour development, the device should dry flat for five minutes [49].

Some of the colorimetric indicators used in this device are copper (II), ninhydrin, iron (III) chloride, tosic acid, sodium nitrate, nitroaniline, sodium hydroxide, tri-iodide ion, nickel (II) and nioxime. Copper (II) acquires a dark forest green coloration in the presence of β-lactam antibiotics. Ninhydrin is used to discriminate between ampicillin and amoxicillin. It acquires an orange coloration in the presence of ampicillin and a forest green coloration in the presence of amoxicillin. The purpose of iron (III) chloride is to indicate the presence of adulterants such as baking soda, chalk or calcite. The channel to evaluate the presence of the phenol functional group, found in amoxicillin and ampicillin, and the presence of acetaminophen, contains four reagents: tosic acid, sodium nitrate, nitroanline and then sodium hydroxide. As the water moves up, the reagents successively mix and form an unstable acid, which gains a strong orange colour in the presence of amoxicillin, ampicillin or acetaminophen. The channel with tri-iodide Ion is used to detect starches and the channel with nickel (II) and nioxime serves as a timer. An intense pink spot is formed when the nioxime reaches the nickel (II), which indicates to the user that the device should be removed from the water[49].

The device was tested with multiple samples containing pure API, combinations of API and pure excipients. To simulate falsified drugs, the device was tested with samples of ampicillin with 50% of powder talc and samples with substitute API, such as acetaminophen. This pharmaceutical screening test does not require a lab and allows a qualitative analysis of the presence of API, common drug substitutes and unapproved excipients. A batch of sixty paper analytical devices can be made start to finish in under two hours and the cost per device is about $0.45 [49]. It has the disadvantage of not allowing a quantitative analysis.

Figure 3.1 Paper analytical device for detecting the purity of amoxicillin and ampicillin
Each channel contains different deposited reagents that allow the identification of the different components present in the drug. Of the twelve channels, five are to test the presence of functional groups expected to appear in the targeted antibiotics, six are to test the presence of excipients and substitute materials, and the other channel is to indicate when the device can be withdrawn from the water [49].

In 2018, Boehle et al. [3] developed another paper-based assay for detecting falsified β-lactam antibiotics. This device is based on an enzyme competition that uses nitrocefin, a chromogenic substrate, to compete with β-lactam antibiotics in a reaction with β-lactamase. Nitrocefin is hydrolysed in the presence of β-lactamase, which leads to a change of colour from yellow to red and allows a colorimetric detection. This device contains a section for antibiotic purity detection and another section for pH detection, both standardized with wax (**Figure 3.2**). β-lactamase is deposited in the antibiotic purity analysis detection zone and nitrocefin is placed along the channel. By dissolving the antibiotic in water and adding it to the device, the solution moves by capillary forces to the detection zone, which allows its passage through the dried nitrocefin. If the APIs are present in the solution they will compete, in a concentration dependent manner, for the β-lactamase active site with the dilute nitrocefin. In the case of a legitimate antibiotic, the API is at higher concentration than nitrocefin, so the detection zone remains yellow. In the case of a counterfeit antibiotic, there is a higher concentration of nitrocefin to react with β-lactamase and the detection zone turns red. The channel for pH detection is subdivided into three channels with

different pH indicators, namely bromophenol blue, phenol red and phenolphthalein. Bromophenol blue is used to indicate acidic pH values, phenol red indicates values between pH 6 and pH 8 and phenolphthalein indicates alkaline pH values. The pH indication zone can alert the user when the assay is at an acidic or alkaline pH [3].

The device was printed on Whatman chromatography paper using a *ColorQube 8870* wax printer and then placed on a hot plate and covered with a metal plate at 165 ºC, for 90 s, to allow the wax to melt through the paper pores. The sample was then added to the sample inlet and the device was left to react for 15 min before scanning and image analysis. To test common drug replacements, 50 mg mL^{-1} solutions were made of each falsified replacement (chalk, gelatine, sodium bicarbonate, acetylsalicylic acid, sucrose, D-(+)-lactose and calcium carbonate) and dissolved in water. Because the enzymatic reaction between nitrocefin and β-lactamase is pH dependent, the device only works optimally between pH 6.5 and pH 8 and does not work at acidic pHs, which can be a disadvantage [3]. The fact that this device uses β-lactamase for its functioning, does not allow a quantitative analysis of β-lactamase inhibiting penicillins, because the presence of these inhibitors can affect the assay. Other disadvantages are the storage and the enzymatic activity of the device. To store nitrocefin for more than one week, the device must be stored in a refrigerator, which might not be possible in some areas. Also, β-lactamase loses its enzymatic activity over time, affecting the life shelf of the device.

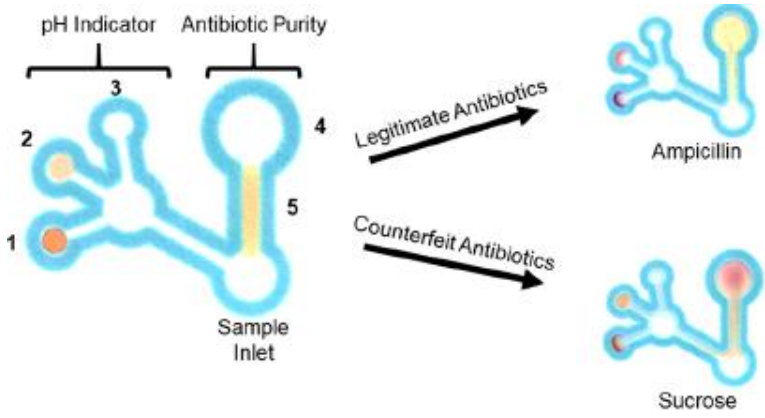

Figure 3.2 Operation of the paper device developed by Boehle et al.
The pH indicator section contains 0.45 µL of bromophenol blue (1), 0.30005 µL of phenol red (2) and 0.40 µL of phenolphthalein (3). The antibiotic purity detection section contains 2.5 µL of β-lactamase (4) and 2 µL of nitrocefin (5). 35 µL of sample is added to the sample inlet and allowed to saturate and react with the device. The fluid wicks down the channel, rehydrating and transporting the stored nitrocefin to the detection zone to react with β-lactamase. If the sample contains API, it should be present at a higher concentration relative to nitrocefin, therefore β-lactamase will react with the antibiotic and the device will stay yellow. If the sample is falsified and does not contain API, nitrocefin will be the dominant substrate, resulting in a distinct colour change from yellow to red [3].

The device designed in this thesis has several advantages over the previous devices. It allows a quantitative analysis, it can be used by β-lactamase inhibiting penicillins and it is non-enzymatic which improves the life shelf of the sensor and its resistance to storage and transport conditions.

4

Materials and Methods

In this chapter, the methods and experimental procedures used in this thesis for the sensing of falsified antibiotics in solution and paper substrate are described. These procedures are based on the one-step reduction of the gold salt by antibiotics, which synthesize stable antibiotic conjugated GNPs. The synthesis of these GNPs in solution and on paper substrate are presented, as well as the validation tests of the sensor with common materials found in falsified antibiotics and the characterization of two different types of paper, to help choose the best substrate for the device. In addition, the fabrication of the final device and its cost are also presented.

4.1 Materials

Gold (III) chloride trihydrate ($HAuCl_4 \cdot 3H_2O$), ceftazidime hydrate ($C_{22}H_{22}N_6O_7S_2 \cdot xH_2O$), ampicillin trihydrate ($C_{16}H_{19}N_3O_4S \cdot 3H_2O$), amoxicillin trihydrate ($C_{16}H_{19}N_3O_5S \cdot 3H_2O$), Sodium Bicarbonate ($NaHCO_3$), D-(-)-fructose ($C_6H_{12}O_6$) and D-(+)-galactose ($C_6H_{12}O_6$) were purchased from *Sigma-Aldrich*. Gelatine was purchased from *Merck* and calcium carbonate, precipitated, extra pure ($CaCO_3$) was purchased from *Scharlau*. All chemicals were used without further purification. Migraspirina (acetylsalicylic acid ($C_9H_8O_4$), 500 mg) was manufactured by *Bayer*, lot #BT10JT1, expiration date 11/2021.

4.2 Synthesis of GNPs in solution

The experimental procedure for the synthesis of colloidal GNP solutions was based on the study conducted by M. Demurtas and C. C. Perry, that consists on the synthesis of stable antibiotic conjugated GNPs by a one-step reaction using amoxicillin. The amoxicillin reduces the

gold salt to form nanoparticles and at the same time coats them to afford the functionalised nanomaterial [33]. In this thesis, 1447 µL of distilled water, 15 µL of $HAuCl_4 \cdot 3H_2O$ (0.010 M) and 38 µL of amoxicillin trihydrate at different concentrations were added to a 1.5 mL Eppendorf tube in this order. The Eppendorf tubes with different concentrations of antibiotic (1.0000 mM, 0.5000 mM, 0.3000 mM, 0.2500 mM, 0.1300 mM, 0.1000 mM, 0.06500 mM, 0.0325 mM and 0.0100 mM) were placed open in a 70º C water bath for 15 minutes. The same procedure was performed for ceftazidime hydrate and ampicillin trihydrate. The duration of this procedure in water bath was based on another dissertation developed in CENIMAT|i3N [50].

To verify if this reaction occurs without the heat source, the same procedure was done with the Eppendorf tubes left at room temperature for 24 hours, for the three antibiotics. The duration of this procedure was based on the study conducted by A. Rai, A. Prabhune, and C. C. Perry, that consists on the reduction of gold ions using cefaclor at 20 ºC, during 24 hours [51].

4.3 Synthesis of GNPs on paper substrate

Office paper was used as substrate to produce paper microplates with 384 wells (3.38 cm diameter) for the synthesis of GNPs. These microplates, represented in **Figure 4.1**, were produced using the Lab-on-Paper technology developed by CENIMAT|i3N [50]. As mentioned in chapter 2, Lab-on-Paper technology consists in the formation of hydrophilic microchannels delimited by hydrophobic barriers. The microplates were designed on *Adobe Ilustrator software* and printed on A5 office paper using the *Xerox ColorQube 8570* printer (**Figure 4.2 - A**). In this printer, the solid cartridge wax is melted before being ejected and thereafter solidifies on the paper surface, instantly. This technology reduces the waste of material, since these wax cartridges can be reused to form new cartridges. After wax paper is standardized, it is placed on a *SCHOTT ROBAX* heating plate (**Figure 4.2 - B**) at 120º C, during 2 minutes, to allow the vertical diffusion of the wax through the pores of the paper [25].

The procedure for the synthesis of GNPs on paper substrate consists on the deposition of $HAuCl_4 \cdot 3H_2O$ followed by the deposition of antibiotic solutions in each well, without letting the $HAuCl_4 \cdot 3H_2O$ dry. After this, the paper can dry at room temperature. The optimum volumes of $HAuCl_4 \cdot 3H_2O$ and antibiotic to use are 4 µL and 9 µL, respectively. The optimum $HAuCl_4 \cdot 3H_2O$ concentration to use is 0.010 M for amoxicillin trihydrate and ampicillin trihydrate, and 0.006 M for ceftazidime hydrate.

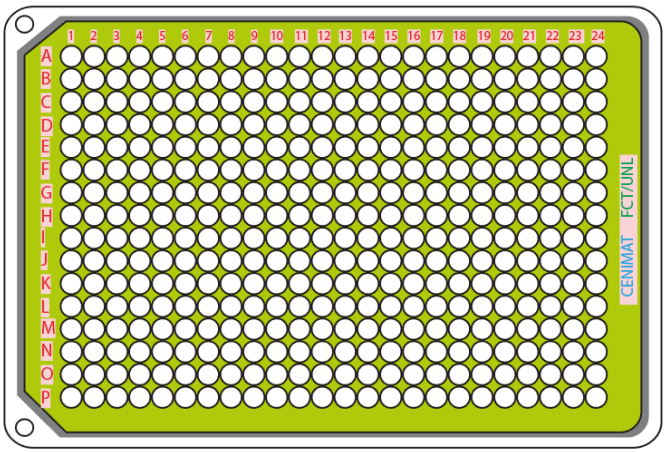

Figure 4.1 384-microplate design

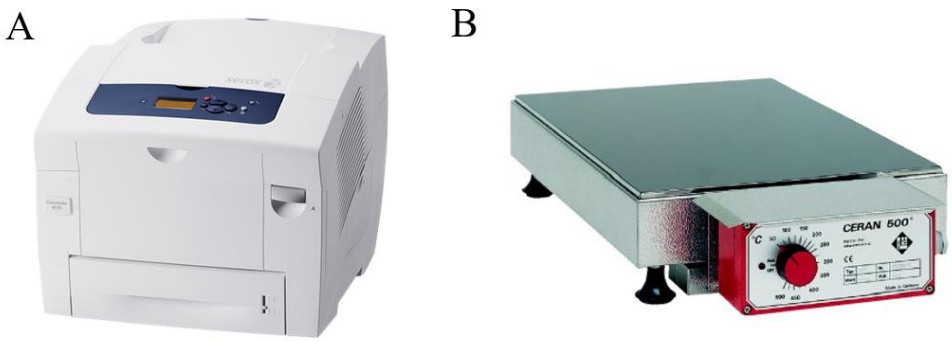

Figure 4.2 Devices used on the production of the paper microplates
A: *Xerox ColorQube 8570* printer used to print the paper microplates; B: *SCHOTT ROBAX* heating plate used to diffuse the wax through the pores of the paper. Adapted from [52], [53].

4.4 Testing common drug replacements

Selected falsified ingredients (gelatine, sodium bicarbonate, acetylsalicylic acid, calcium carbonate [3], D-(-)-fructose and D-(+)-galactose) were used in the previous procedures instead of the antibiotics, to see if there was still formation of GNPs. Each ingredient was dissolved in distilled water to obtain solutions with the concentrations of the antibiotics previously used.

To obtain the acetylsalicylic acid solution, a tablet of *Migrosapirina* was grinded with the help of a mortar and pestle and it was considered that each tablet contained 500 mg of acetyl-salicylic acid. As the molecular mass of the gelatine is unknown, the molar concentrations were obtained by approximation to the ceftazidime molar concentrations. The molar concentrations of ceftazidime previously used were converted to mass concentrations and served as guides for the preparation of the gelatine solutions. In other words, the mass concentrations used for gelatine were the same as the obtained mass concentrations of ceftazidime. These values and methods of

calculation are demonstrated in **Annex A**. As calcium carbonate has a solubility in water of 14 mg/L at 25º C, the solutions were only prepared with concentrations between 0.1300 mM and 0.0100 mM. To dissolve the gelatine, it was necessary to heat the solution up to 60º C and for this compound, only concentrations between 0.0325 mM and 1.0000 mM were used.

4.5 Characterization Methods

The purpose of this phase is to evaluate the size, shape and concentration of the GNPs produced in the previous phases and observe the differences between the Whatman No.1 chromatography paper and the office paper, in order to decide the best paper substrate for the final device. To characterize the GNPs synthesized in solution, UV-Vis spectrophotometry was used and to evaluate the GNPs synthesized on paper substrate, *ImageJ* software and Scanning Electron Microscopy (SEM) were used. To characterize the two types of paper, various characterization techniques were used, such as SEM, Fourier Transform Infrared Spectroscopy (FTIR), X-Ray Diffraction (XRD), Thermogravimetry (TG) and Differential Scanning Calorimetry (DSC).

4.5.1 UV-Vis spectrophotometry

UV-Vis spectrophotometry is based on the absorption of light by a sample. The sample is illuminated with electromagnetic rays of various wavelengths, in the visible and ultraviolet range of the spectrum, and the recording of the absorption spectra is achieved by a spectrophotometer. This equipment measures the intensity of the light that passes through the sample solution and compares it to the intensity of the initial light. This light is partially absorbed by the sample molecules in the solution. The quantity of light and its wavelength absorbed by the sample provides information that can be used to identify or quantify each substance. UV-Vis spectra allow the identification of the components present in the sample solution, by the position and profile of the absorption peaks [54]. In this thesis, this technique was used to confirm the existence of GNPs in the solutions, characterize the optical properties of the GNPs, and analyse possible changes in size and concentration resulting from the reactions. A *TECAN SPARK 10M* spectrophotometer was used to measure the absorbance of the solutions in each well of the microplate. The absorbance of a material (A) s given by:

$$A = \log T = \log \frac{I}{I_0} \qquad \textbf{(4.1)}$$

Where T is the transmittance of that material, I is the radiant flux transmitted and I_0 is the radiant flux received by that material. A microplate well with only water was use as reference and is represented in **Figure 4.3**.

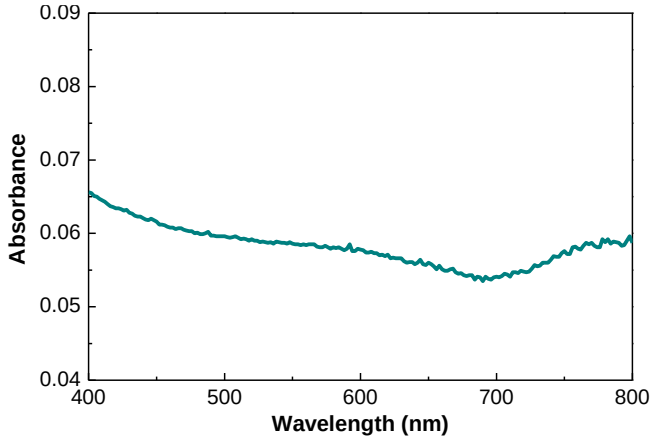

Figure 4.3 UV-Vis spectrophotometry analysis of a microplate well with only water

4.5.2 *ImageJ* software

ImageJ software is an image processing program that can display, edit, analyse, process, save and print images. It can also calculate areas and pixel values, measure distances and angles, create density histograms and perform geometric transformations [55]. This software was used in this thesis to extract the RGB (Red - Green - Blue) channel intensities of each paper microplate well, in order to calculate the ratio between Red and Green channels. This ratio was used to plot a calibration curve that relates the Red/Green Ratio of the well with each antibiotic concentration and allows the antibiotic API dose calculation. Each paper microplate was first scanned by a *Canon MG5250* scanner, in TIF format and with a 600 dots per inch resolution, in order to standardize the colour representation and the number of pixels for each paper microplate well.

4.5.3 Scanning Electron Microscopy

SEM is a technique that allows large magnifications to be made on sample surfaces, in order to obtain the morphology, microstructure and topography of its surface. The sample surface is bombarded with an electron beam and radiation is emitted, allowing for high resolution images, a digital display of absorbed electrons, an elemental chemical analysis and a chemical distribution mapping. Image formation is dependent on the acquisition of signals produced from the electron beam and specimen interactions, such as elastic and inelastic interactions. The elastic interactions are characterized by an insignificant energy loss during the collision and by a wide-angle directional change of the scattered electron. In the inelastic interactions the electron beam transfers substantial energy to the atom, which leads to the excitation of the specimen electrons and the generation of secondary electrons. These secondary electrons can be used for topographic contrast for visualization of surface texture and roughness. The topographical image depends on the number of secondary electrons that reach the detector. The electrons that don't reach the detector will

generate shadows or a darker contrast than the regions that have an unobstructed electron path. The SEM present in CENIMAT|i3N is a *Zeiss AURIGA CrossBeam FIB-SEM* and has a magnification of 5x to 3000 000x and a resolution of 3.5 nm [56]–[58]. This technique was used in this thesis to characterize the morphology of the two different types of paper. The images were taken in secondary electron mode, with an electron high tension of 5 kV, an aperture size of 30 µm and a 6.2 mm distance between the sample and the SEM column.

4.5.4 Fourier Transform Infrared Spectroscopy

FTIR is a technique used to identify the functional groups in the materials, by using a beam of infrared radiations. The infrared radiation is bombarded on the sample, which absorbs the light and creates various vibration modes. There are two modes of vibrations, namely stretching and bending vibrations. Stretching vibrations lead to an increase or decrease of the length of the bond, while bending vibrations cause a change in the bond angles and in the relative position of the atoms. Each infrared radiation frequency is absorbed by a bond in the molecule, due to the natural vibrational frequency of each bond, allowing the identification of the different functional groups present in the sample. The resultant spectrum is plotted in absorbance or % transmittance versus wavenumber (cm^{-1}) in the infrared region [59]. In this thesis, this technique was applied in the characterization of the two types of paper used for the synthesis of the GNPs. To do so, a *Nicolet 6700* from *Thermo Electron Corporation* was used, with *Attenuated Total Reflectance* configuration and the spectra were obtained in the spectral region of 525 to 4500 cm^{-1}.

4.5.5 X-Ray Diffraction

XRD is a non-destructive technique that allows the analysis of crystalline materials by providing information on structures, phases, preferred crystal orientations and structural parameters, such as average grain size, crystallinity, strain and crystal defects [60]. It is based on constructive interference of monochromatic X-rays and a crystalline sample and consequently, a diffracted ray that is detected, processed and counted. When the total incident X-ray pattern on the sample satisfies Bragg's law, constructive interference occurs and a peak in intensity appears. Conversion of the diffraction peaks to d-spacings allows identification of the compound, by comparison with standard reference patterns [60]. For this project, a *X'Pert PRO MPD system* from *PANalytcal* was used to structurally characterize the different types of paper and the diffractograms were obtained for angles between 10º and 90º (2Θ), with a scan step size of 0.03º, in continuous mode and operating at 45 kV with 40 mA.

4.5.6 Thermogravimetry and Differential Scanning Calorimetry

DSC determines the temperature and heat flow associated with material transitions as a function of time and temperature. During a change in temperature, DSC measures a heat quantity, radiated or absorbed excessively by the sample, calculated by the difference between the sample and material temperatures [61]. TG is a technique in which the mass of a substance is monitored as function of temperature or time, as the sample is subjected to a controlled temperature and atmosphere [62]. This technique provides information about physical and chemical phenomena and is used to detect evaporation, decomposition, oxidation and other effects of temperature alteration that cause mass changes. These techniques were used in this thesis to observe the resistance of the different type of papers to heat, since the procedure of synthesis of GNPs on paper substrate uses a heating plate. The CENIMAT|i3N has a *TGA-DSC STA 449 F3 Jupiter* that can operate in a temperature range between room temperature and 1550 ºC and has a thermobalance that can measure samples up to 35g [63].

4.6 Fabrication of the final device

This phase consists of the production of an easy-to-use and intuitive paper-based platform for detecting counterfeit antibiotics. This device was developed by using the Lab-on-Paper technology previously mentioned. The sensor was designed on *Adobe Ilustrator software* and is represented in **Figure 4.3**, along with all its components. The front of the design includes the identification of the sensor, the test result and the date of realization, and the test zones. The production of the sensor includes the wax printing and heating of the front, to allow the wax diffusion, followed by the wax printing of the back to encapsulate the device and prevent reagent loss between their deposition and drying. **Figure 4.4** presents the sensor after wax diffusion. Along with this device, $HAuCl_4 \cdot 3H_2O$ (0.010 M) and $HAuCl_4 \cdot 3H_2O$ (0.006 M) will be provided for the test.

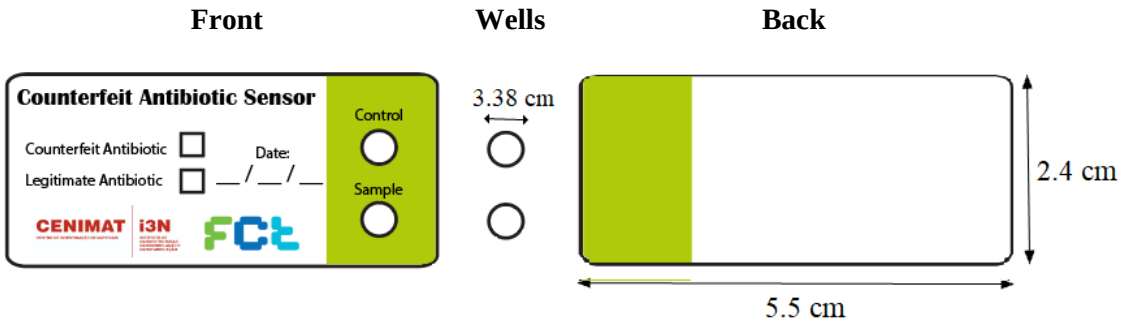

Figure 4.4 Prototype of the final paper-based sensor

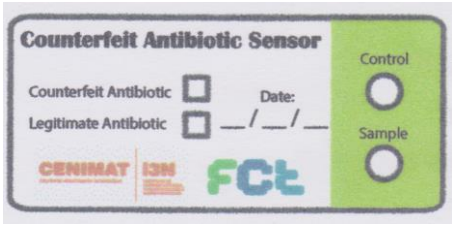

Figure 4.5 Final paper-based sensor after wax diffusion

5

Results and Discussion

In this chapter, the results of the methods and experimental procedures used for the sensing of falsified antibiotics, described in the previous chapter, are presented. These results include the study of optical properties of GNPs in colloidal solutions, the calibration curve for the final paper-based sensor and the validation tests, where common materials found in counterfeit antibiotics are tested on the paper substrate. The results obtained by the characterization of the two different types of paper to help choose the best substrate are also presented.

5.1 Synthesis of GNPs in solution

For the synthesis of GNPs by the one-step reduction of a gold salt by antibiotics, various concentrations of antibiotic between 1.0000 mM and 0.0100 mM were tested, which correspond to diluted solutions of common amoxicillin dosages, such as 125 mg/5 mL, 250 mg/5 mL and 500 mg/5 mL [64]. This process is based on the reduction of $HAuCl_4$ by the antibiotics and is presented in **Figure 5.1**. The electrons are transferred from the amine group to the metal ion Au^{3+}, resulting in the formation of Au^0, which undergoes nucleation and growth to form GNPs. This reaction can occur in acidic or neutral solutions. “Amines are used extensively as reductants and subsequent capping agents in the synthesis of metal nanoparticles, especially gold, due to its affinity to nitrogen” [61]. Antibiotics with amine groups act as stabilizing and capping agents, preventing aggregation [33], [51], [65], [66].

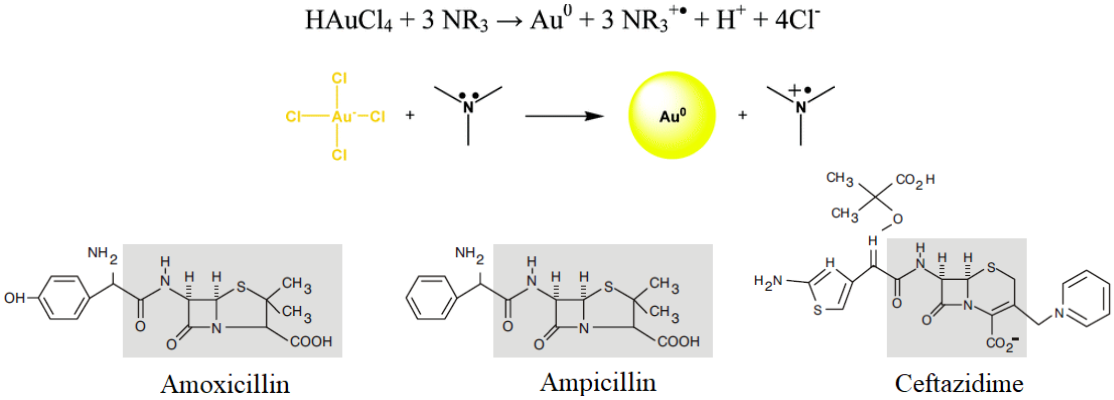

Figure 5.1 Reaction between $HAuCl_4$ and the amine group present in the antibiotics and amoxicillin, ampicillin and ceftazidime structure

The electrons are transferred from the amine group (present in the amoxicillin, ampicillin and ceftazidime structure) to the metal ion Au^{3+}, resulting in the formation of Au^0, which undergoes nucleation and growth to form GNPs [65].

The resulting GNPs in solution (**Figure 5.2**), present a decrease of colour intensity with the decrease of antibiotic concentration. It is also verified that for lower concentrations of antibiotic the colour is almost imperceptible, indicating the non-formation of GNPs. To determine the relation between the amount of antibiotic and the optical properties of the synthesized GNPs, a UV-vis spectrophotometry analysis was performed with three repetitions for each condition.

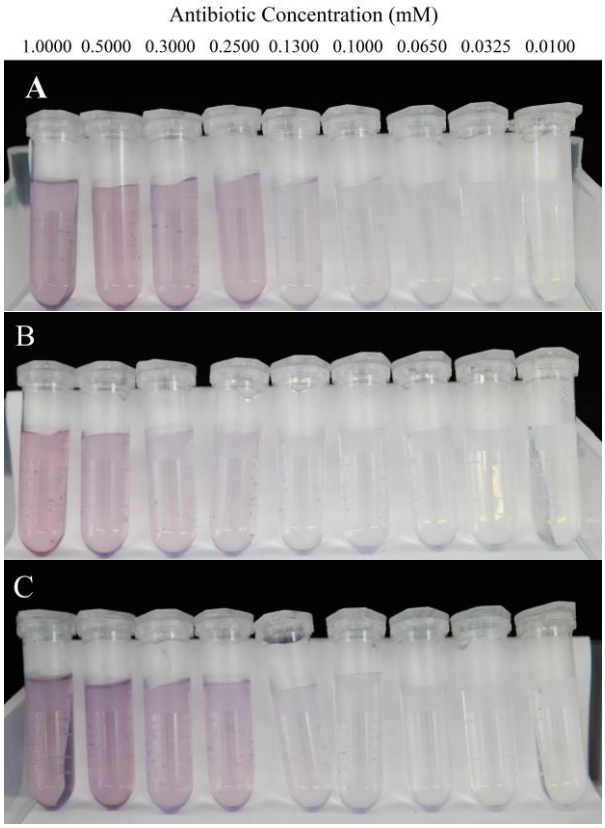

Figure 5.2 Colloidal GNPs solution obtained by gold salt reduction with antibiotics

A: Amoxicillin; B: Ampicillin; C: Ceftazidime.

Figures 5.3 - A, 5.4 - A and **5.5 -A** represent the UV-Vis spectrophotometry analysis of the colloidal GNP solutions made at 70º C, upon addition of ampicillin, amoxicillin and ceftazidime, respectively. **Figures 5.3 - B, 5.4 - B** and **5.5 - B** represent the calibration curves obtained by plotting the maximum absorbance with the corresponding antibiotic concentrations, using the mean and standard deviation values. The absorbance value used for the calibration curve plotting was the one corresponding to the approximated SPR peak position wavelength, which varied slightly for each antibiotic.

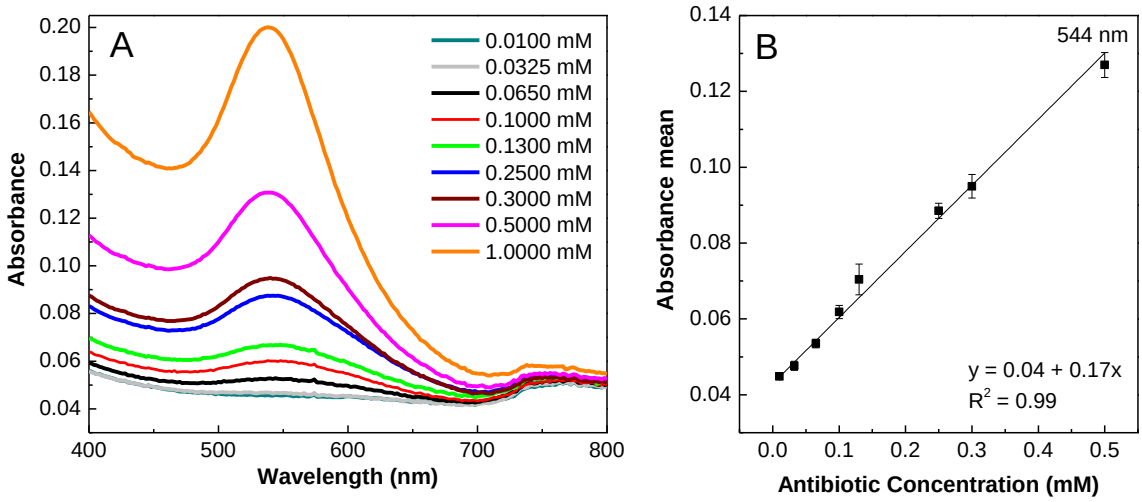

Figure 5.3 UV-Vis spectrophotometry analysis of colloidal GNP solutions upon addition of ampicillin

A: Absorbance spectrum obtained upon addition of different concentrations of ampicillin; B: Corresponding calibration curve of absorbance at 544 nm versus antibiotic concentration (n=3).

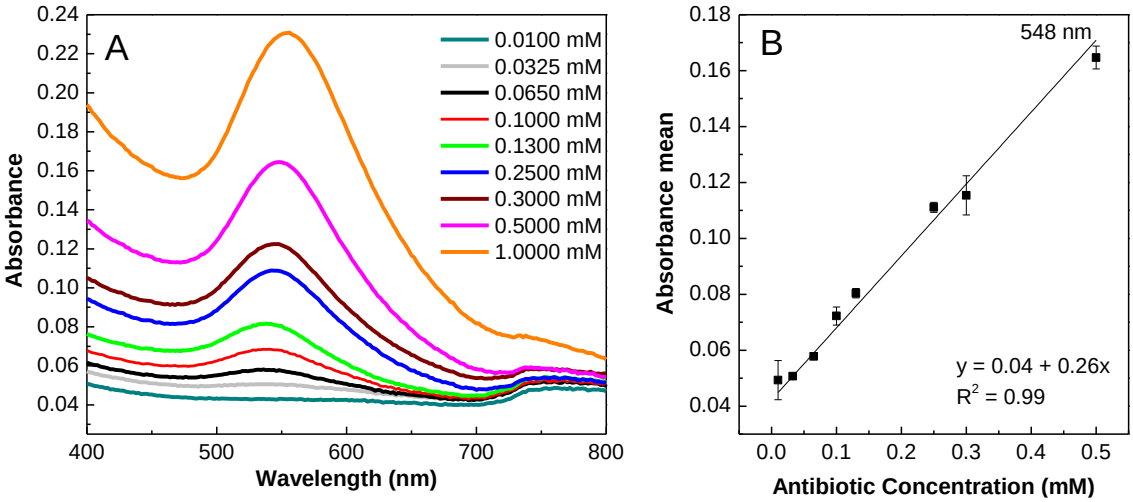

Figure 5.4 UV-Vis spectrophotometry analysis of colloidal GNP solutions upon addition of amoxicillin

A: Absorbance spectrum obtained upon addition of different concentrations of amoxicillin; B: Calibration curve of absorbance at 548 nm versus antibiotic concentration (n=3).

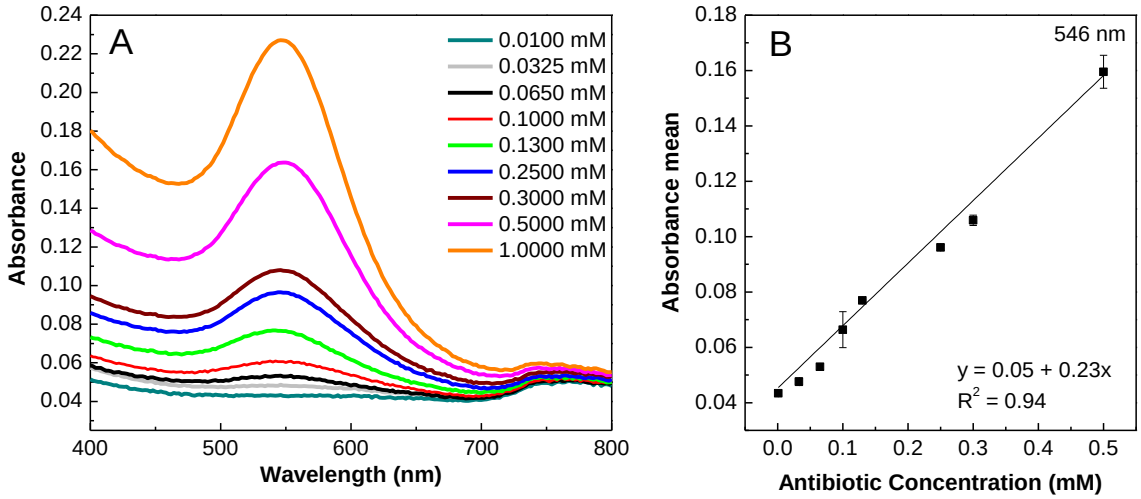

Figure 5.5 UV-Vis spectrophotometry analysis of colloidal GNP solutions upon addition of ceftazidime

A: Absorbance spectrum obtained upon addition of different concentrations of ceftazidime; B: Calibration curve of absorbance at 546 nm versus antibiotic concentration (n=3).

Analysis of **Figures 5.3 - A, 5.4 - A** and **5.5 -A** show an increase in the absorbance value with the increase of antibiotic concentration used to synthesize the GNPs. In addition, it is possible to see that the lowest concentrations (0.0100 mM and 0.0325 mM) do not form GNPs. GNPs are characterized by an absorption peak in the visible region of the electromagnetic spectrum [33], so it can be concluded that the method used for synthesis of GNPs in solution is able to produce GNPs from 0.0650 mM. This establishes a LOD of 0.0650 mM of antibiotic concentration for synthesis of GNPs in solution, indicating that the antibiotic solution to test must have a concentration above this value. Since the common dosages of amoxicillin are 125 mg/5 mL, 250 mg/5 mL and 500 mg/5 mL, which correspond to approximately 0.046 M, 0.091 M and 0.183 M, respectively, the dilution of the antibiotic must be performed to have a concentration between 0.0650 mM and 1.0000 mM.

The SPR peak position provides information about the particle shape, the broadness of the peak indicates the particle size distribution and the state of aggregation and the absorption value is proportional to the amount of GNPs produced [33]. The absorbance peak varies from approximately 0.05 to 0.20 for ampicillin, 0.06 to 0.23 for amoxicillin and 0.05 to 0.23 for ceftazidime. These variations in absorbance and the number of GNPs produced are related to the antibiotic concentration. Ampicillin presents a lower absorbance value for the highest concentration than amoxicillin and ceftazidime, indicating that ampicillin produces less GNPs than the other antibiotics, in these conditions. It can also be observed, for the three samples, that for lower concentrations of antibiotic, the SPR peak absorptions are broader than for higher concentrations.

This indicates that higher concentrations of antibiotic form GNPs with narrower size distribution and aggregation.

Calibration curves from **Figures 5.3 - B, 5.4 - B** and **5.5 -B**, which establish a relationship between the SPR peak and the antibiotic concentration, show that the absorbance value of the SPR peaks is directly proportional to the concentration of antibiotic up to 0.5000 mM. This confirms the increase of absorbance value with the increase of antibiotic concentration and indicates that the assay maintains the same sensitivity until the antibiotic concentration reaches 0.5000 mM.

Before applying this synthesis on paper substrate, the same procedure was done with the Eppendorf tubes left at room temperature for 24 hours, to see if this reaction occurs without the heat source. **Figures 5.6**, **5.7** and **5.8** represent the UV-Vis spectrophotometry analysis of the colloidal GNP solutions left at room temperature, upon addition of ampicillin, amoxicillin and ceftazidime, respectively.

Figures 5.6 - A, **5.7 - A** and **5.8 – A, C** show that the GNP synthesis occurs at room temperature in the same range of antibiotic concentrations as when synthesized at 70 ºC, that is from 0.0650 mM. The lowest concentrations (0.0100 mM and 0.0325 mM) do not form GNPs for these antibiotics, as in the previous cases. This maintains the LOD of 0.0650 mM of antibiotic concentration, for the synthesis of GNPs in solution at 70º C and at room temperature and confirms the concentration range in which the concentration of the antibiotic to test must be a part of. It can also be observed, for the three antibiotics, that for lower concentrations of antibiotic, the SPR peak absorptions are broader than for higher concentrations. This indicates that higher concentrations of antibiotic form GNPs with narrower size distribution and aggregation and was also seen in the samples left at 70º C.

In addition, it is verified that the absorbance value is higher for the cases of GNP synthesis left at room temperature than at 70 ºC, for ampicillin and amoxicillin. The SPR peak values varies from approximately 0.05 to 0.24 and from 0.06 to 0.40 for ampicillin and amoxicillin, respectively. This corresponds to an increase of 0.04 for ampicillin and 0.07 for amoxicillin, when compared to the results obtained at 70º C. Decreasing the reaction temperature during the reduction of $HAuCl_4$ leads to a decrease in the rate of reduction. This provides a longer time for the interaction of the antibiotic with the $HAuCl_4$ in the solution and leads to the production of more GNPs [33], [51]. In the case of ceftazidime, this does not occur. Ceftazidime is the antibiotic with the lowest maximum absorbance value (0.18), which is lower than when synthesized at 70º C (0.23), indicating that this antibiotic produces less GNPs when left at room temperature or that the reaction was affected by environmental conditions. By increasing the reaction time between the gold

salt and the antibiotic to 24 hours, the sample also becomes more subjectable to changes in the lab conditions, such as temperature and light exposure, which might affect the reaction.

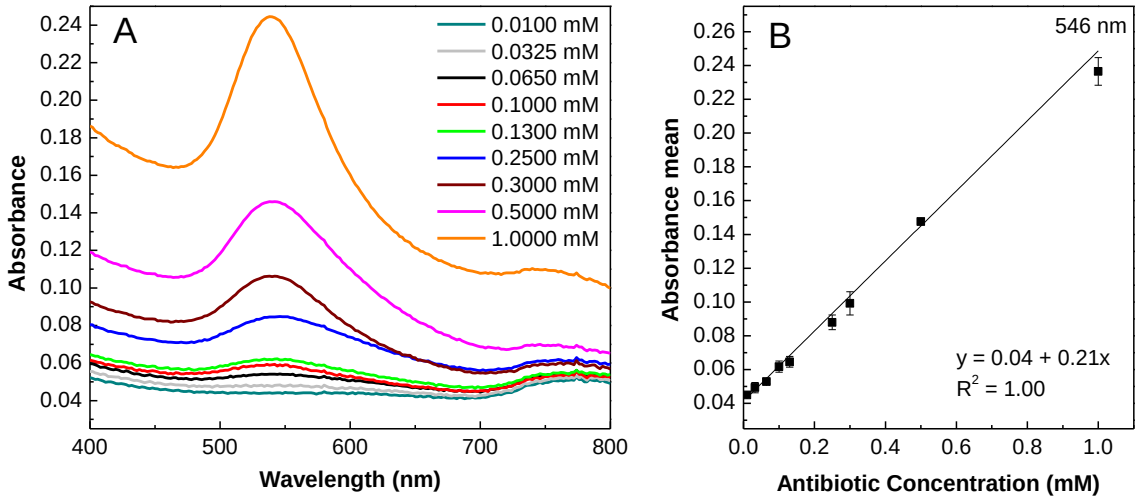

Figure 5.6 UV-Vis spectrophotometry analysis of colloidal GNP solutions upon addition of ampicillin and left at room temperature

A: Absorbance spectrum obtained upon addition of different concentrations of ampicillin; B: Corresponding calibration curve of SPR peak versus antibiotic concentration (n=3).

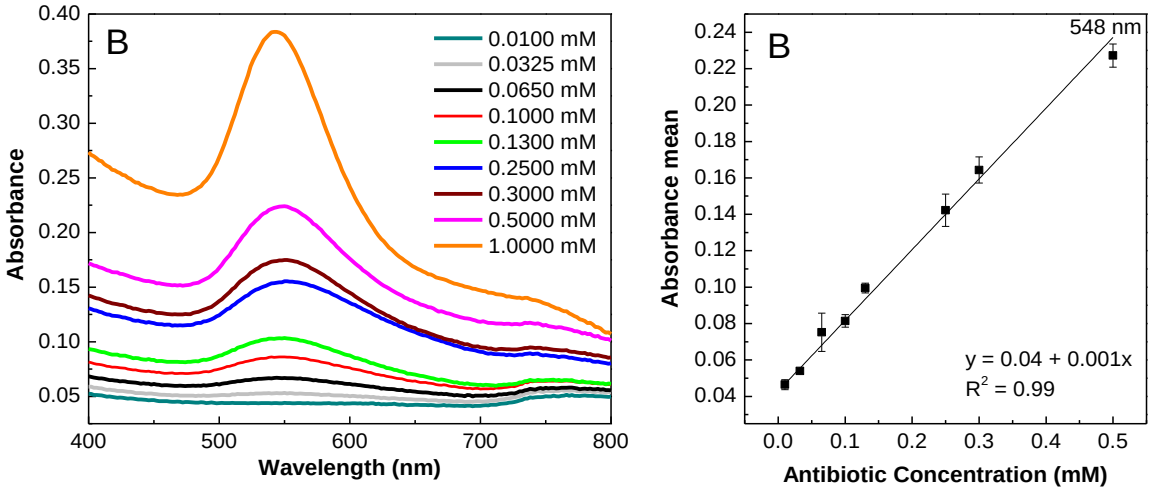

Figure 5.7 UV-Vis spectrophotometry analysis of colloidal GNP solutions upon addition of amoxicillin and left at room temperature

A: Absorbance spectrum obtained upon addition of different concentrations of amoxicillin; B: Calibration curve of SPR peak versus antibiotic concentration (n=3).

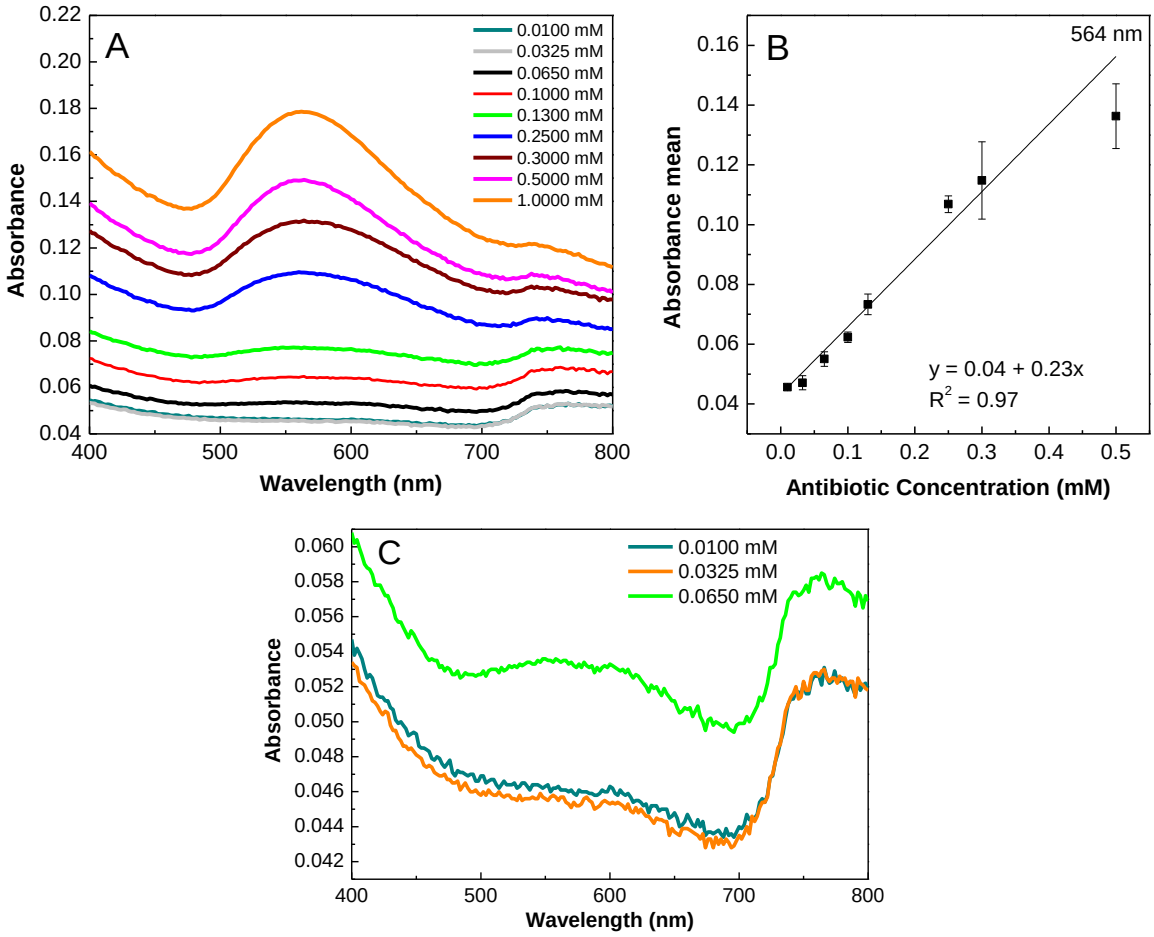

Figure 5.8 UV-Vis spectrophotometry analysis of colloidal GNP solutions upon addition of ceftazidime and left at room temperature

A: Absorbance spectrum obtained upon addition of different concentrations of ceftazidime; B: Calibration curve of SPR peak versus antibiotic concentration (n=3); C: Zoom in the absorbance spectrum (A) at the lowest concentrations of ceftazidime.

From **Figures 5.3 - B, 5.4 - B** and **5.5 -B**, it is possible to observe that the absorbance value of the SPR peaks of the UV-Vis spectrum is also directly proportional to the concentration of antibiotic, as in the GNPs synthesized at 70 ºC. This confirms the increase of absorbance value with the increase of antibiotic concentration. For ampicillin, the direct proportionality occurs up to 1.0000 mM of antibiotic concentration, instead of 0.5000 mM as in the synthesis at 70º C. This increases the range in which the assay maintains the same sensitivity, but only occurs for this antibiotic. Ampicillin is also the antibiotic with lower standard deviation values, which affects the average values of absorbance and consequently, the calibration curve. In addition, the adjusted R^2 of the calibration curves is higher for GNPs synthesized at room temperature than at 70º C, indicating a better linear fit of the terms when synthesized at room temperature. The synthesis of GNPs on paper substrate can occur without the heat source.

5.2 Characterization of the paper substrates

In this thesis, two different types of paper were used as substrates (Whatman No.1 chromatography paper and office paper Portucel) in order to select the best fitted substrate for the paper-based sensor. The types of paper were submitted to different characterization techniques, mentioned in **Chapter 4**, to evaluate their properties.

5.2.1 Scanning Electronic Microscopy

SEM was used to characterize and observe the morphology of the papers' surface. SEM images of Whatman No.1 chromatography paper and office paper are represented in **Figure 5.9** and **Figure 5.10**, respectively.

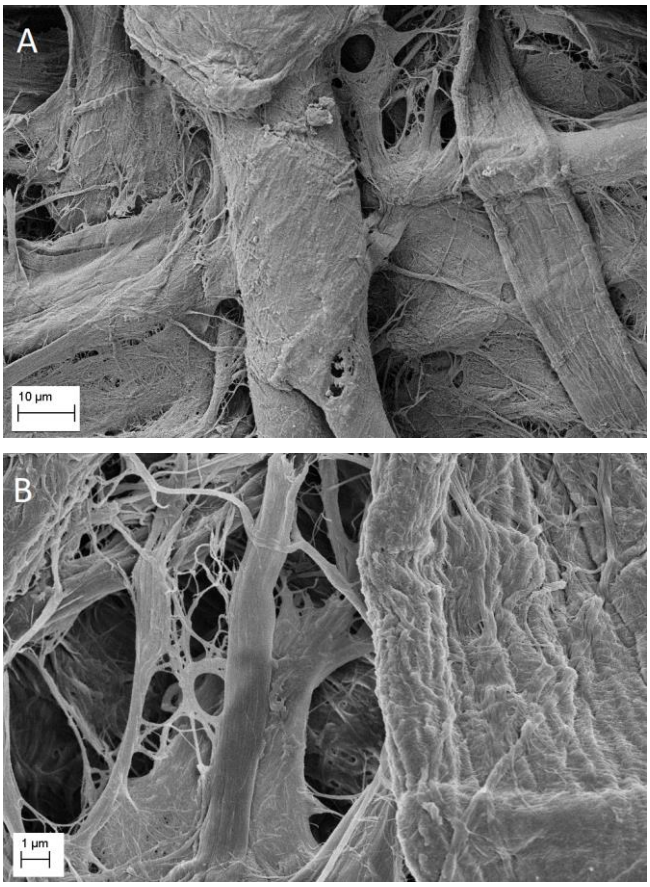

Figure 5.9 SEM images of Whatman No.1 chromatography paper with different magnifications
A: 1000x magnification. B: 5000x magnification

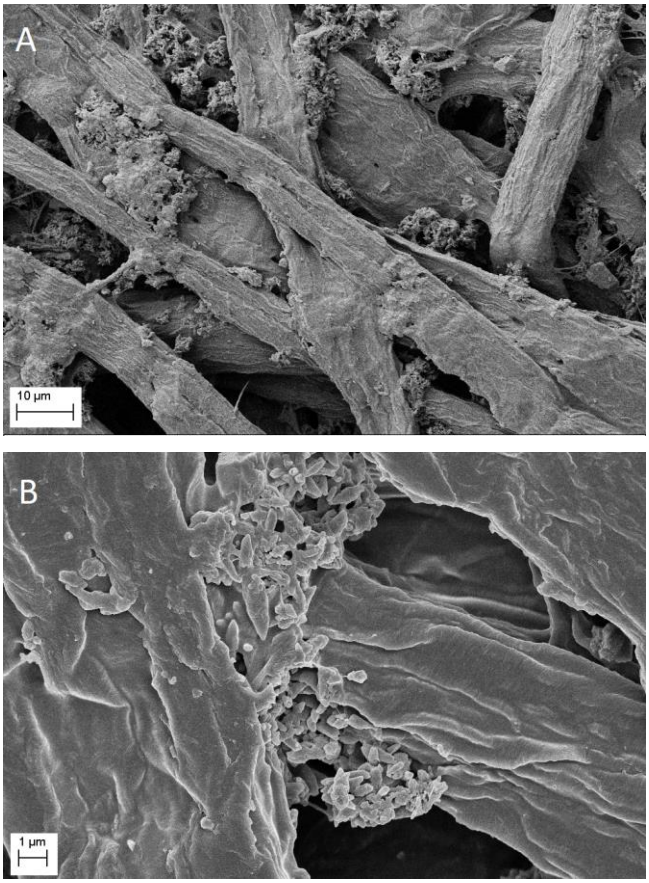

Figure 5.10 SEM images of office paper with different magnifications
A: 1000x magnification. B: 5000x magnification

Comparing the previous SEM images through visual inspection, it is possible to observe some similarities and differences in the morphology of their surfaces. Both substrates are mainly composed by a three-dimensional mesh of cellulose fibres. However, Whatman No.1 chromatography paper presents a more cylindrical geometry and is more porous than the office paper. The office paper has flatter cellulose fibres, which gives it a lower thickness and higher density. It is also possible to detect small crystalline clusters in the office paper that are mainly calcium carbonate, a paper additive used to give higher opacity, brightness and smoothness. These agglomerates fill most of the pores, which makes the office paper less porous and with a more uniform surface.

5.2.2 Fourier Transform Infrared Spectroscopy

FTIR was used to characterize and identify the functional groups present in the paper substrates. By observing the obtained FTIR spectra in **Figure 5.11**, it is possible to identify several infrared peaks that are common to the office paper and the Whatman paper. These common peaks can also be found in the cellulose spectrum and are related to chemical bonds and functional groups present in the cellulose chemical structure, represented in **Figure 5.12**. In the first region

of the infrared spectrum, it is possible to identify three peaks: around 3300 cm^{-1}, 2900 cm^{-1} and 1600 cm^{-1}. The peaks around 3300 cm^{-1} and 2900 cm^{-1} correspond to a hydrogen-bonded O-H stretch and a C-H symmetrical stretch, respectively. The other peak around 1600 cm^{-1} corresponds to the O-H bending of absorbed water [22], [67].

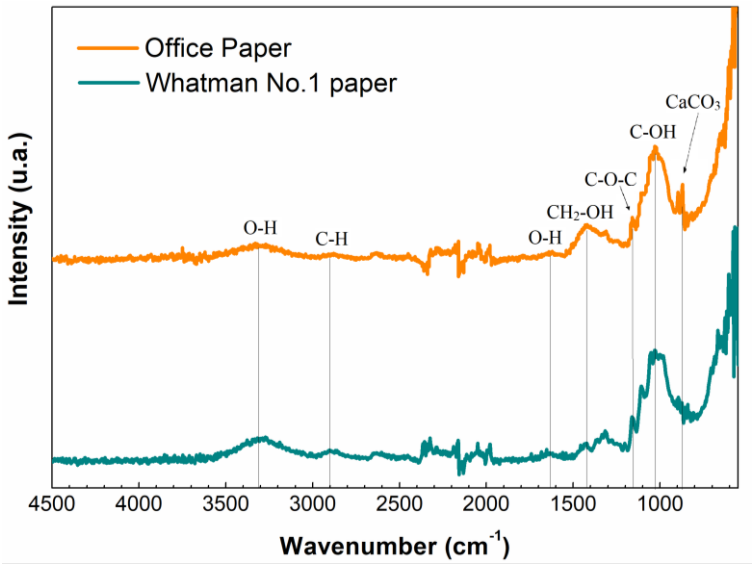

Figure 5.11 FTIR spectra obtained for Whatman and office paper peak identification

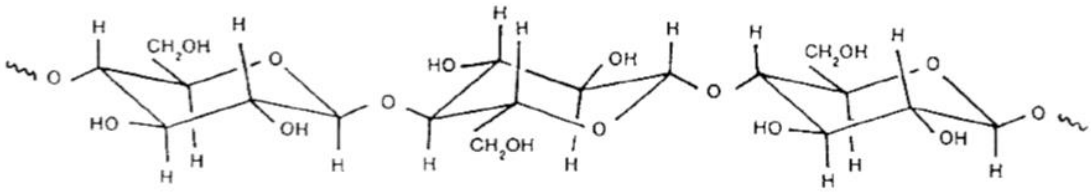

Figure 5.12 Cellulose chemical structure
[22]

In the fingerprint region, between 1500 cm^{-1} and 900 cm^{-1}, it is also possible to identify cellulose characteristic peaks. The peak around 1400 cm^{-1} represents the CH_2 and OH in-plane bending vibrations. Around 1150 cm^{-1}, it can been observed a peak that represents the C-O-C asymmetric vibration, while around 1000 cm^{-1} there is another peak related to the C-OH side group vibration [22], [67]. The difference between the office paper and the Whatman No.1 paper is the presence of a $CaCO_3$ band in the office paper, at 1420 cm^{-1}, that corresponds to the calcium carbonate. This confirms that the small crystalline clusters detected in the office paper by SEM, are calcium carbonate.

5.2.3 X-Ray Diffraction

XRD was used to collect information about the structure of the different types of paper, by analyse of their crystalline materials. The diffractograms obtained for each type of paper are presented in **Figure 5.13**.

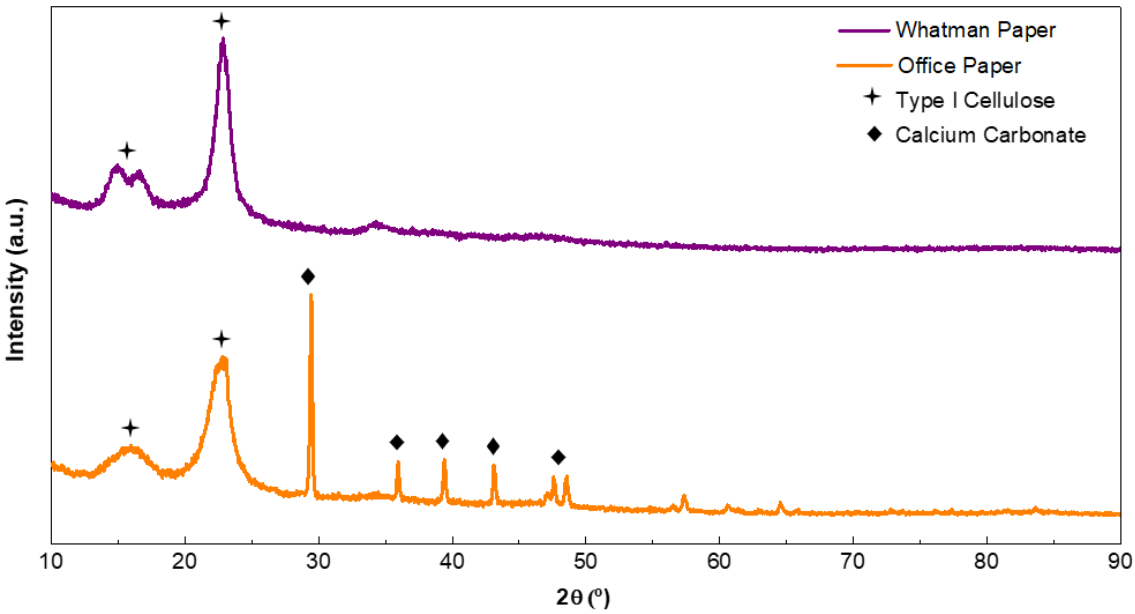

Figure 5.13 XRD diffractogram obtained for Whatman and office paper

When analysing **Figure 5.13**, it is possible to observe that both types of paper present characteristic peaks of type I cellulose (native cellulose). However, Whatman paper has three diffraction peaks (14.93º, 16.60º and 22.88º) unlike the office paper that only has two diffraction peaks (15.97º and 22.82º). This is because "(…) Cellulose I has two polymorphs, a monoclinic structure I_β and a triclinic structure I_α, which coexist in various proportions depending on the cellulose structure (…)" [24]. When the cellulose content is high, as in the case of Whatman paper, it is possible to observe two peaks near 15º, but when the fibre contains high amount of amorphous materials, such as lignin and hemicellulose, as in the office paper, these two peaks are smeared, appearing as one broad peak [24], [68]. Secondly, in the Whatman paper only one crystal structure was identified, as no more diffraction peaks are visible than the cellulose characteristic peaks. On the contrary, in the office paper other diffraction peaks are visible, which correspond to the crystalline structure of calcium carbonate [69]. This confirms the previous results obtained by SEM and FTIR.

The crystalline index (Cr.I.) of each paper was calculated by the empirical method proposed by Segal, mentioned in **Chapter 2**. Whatman paper, with an I_{200} of 22.80º, has a Cr.I. of approximately 74.37%, while office paper, with an I_{200} of 22.82º, has a Cr.I. of approximately 69.17%. From these values, it is possible to confirm that Whatman paper has a higher cellulose content than the office paper. Whatman chromatography paper is manufactured from cotton lines with high percentage of cellulose, which guarantees quality, uniformity, a semi-crystalline structure and a higher degree of crystallinity [25].

5.2.4 Thermogravimetry and Differential Scanning Calorimetry

TG and DSC were used to study the behaviour of the office and Whatman No.1 papers when exposed to increased temperatures. During the procedure of synthesis of GNPs on paper substrate, the paper microplates are heated on a heating plate at 120 ºC, in order to melt and diffuse the wax through the pores of these substrates. Knowing the thermal properties of the final device's substrate is important for its use, transport and storage. The DSC and TG curves of the two types of paper are represented in **Figure 5.14**.

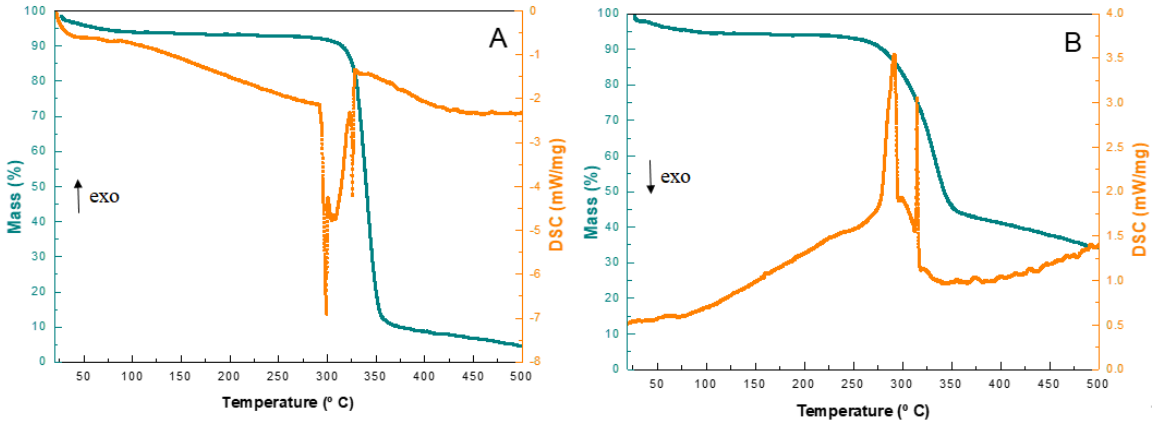

Figure 5.14 DSC and TG curves for Whatman and Office paper
A: Whatman No.1 paper; B: Office paper

Observing the TG curves in **Figure 5.14**, it is possible to verify that there is a gradual mass loss until the temperature reaches approximately 100 ºC, corresponding to water evaporation. The resultant mass loss is of approximately 4.54% for Whatman No.1 paper and 4.63% for office paper. From approximately 300 ºC to 360 ºC for Whatman paper and 250 ºC to 360 ºC for office paper, there is an abrupt mass loss, corresponding to cellulose degradation. At high temperatures, cellulose decomposes very quickly and the products are released intensively within a short time interval [70]. The decomposition of cellulose results in a mass loss of approximately 79.88% for Whatman paper and 49.13% for office paper. The mass loss is lower for the office paper, because of the presence of calcium carbonate that presents higher degradation temperatures. The presence of two endothermic peaks during these temperature intervals (approximately

330 ºC and 370 ºC for Whatman paper and 273 ºC and 324 ºC for office paper), confirm the degradation of the cellulose due to thermal decomposition. From 360 ºC, the mass loss continues gradually. The cellulose degradation temperature, around 300 ºC, is distant from the temperatures used during the heating process in this thesis (120 ºC) and the possible conditions to which the final device will be exposed.

5.3 Synthesis of GNPs on paper substrate

For the synthesis of GNPs by the one-step reduction of a gold salt by antibiotics on paper substrate, the same concentrations of antibiotic as the previous procedure (concentrations between 0.0100 mM and 1.0000 mM) were tested. First this synthesis was done on Whatman No.1 chromatography paper (*GE Healthcare*), but this type of paper was discarded, because the colour appearance in the wells took approximately two weeks and the procedure was sometimes unproducible. As the purpose of this sensor is the rapid detection of falsified antibiotics and in the office paper there is an immediately visible colour change after the drying of the reagents, preference was given to the office paper for the substrate device. As observed in **Section 5.2.1**, Office paper has flatter cellulose fibres, a more uniform surface and is less porous than Whatman paper, which reduces the loss of gold salt by paper fibres.

Regarding the deposition of the reagents, first $HAuCl_4 \cdot 3H_2O$ was deposited and allowed to dry at room temperature, and then the antibiotic was deposited. This procedure was unsuccessful, and the wells would not acquire colour, so then the reagents were deposited sequentially, without letting the first one dry. Adding the antibiotic right after the deposition of $HAuCl_4 \cdot 3H_2O$ and without letting it dry out, allows a greater diffusion and more homogeneous mixing of the reagents, improving the formation of GNPs.

To decide the optimum volumes and concentrations of $HAuCl_4 \cdot 3H_2O$ and antibiotic, that allow the best distinction between the wells with antibiotic and the control well (addition of only $HAuCl_4 \cdot 3H_2O$), different volume ratios between these reagents and different concentrations of gold salt were tested. First the reagent volumes were varied with a fixed concentration of $HAuCl_4 \cdot 3H_2O$ (0.010 M) and then different concentrations of $HAuCl_4 \cdot 3H_2O$ were tested with the best two volumes previously obtained. In **Figures 5.15**, **5.16** and **5.17** it is possible to observe the results obtained after variation of the reagent volumes, using the fixed concentration of $HAuCl_4 \cdot 3H_2O$ of 0.010 M. The volume ratio ($HAuCl_4$:Amoxicillin) 3 µL:3 µL was based on previous projects carried out in CENIMAT|i3N and the volume ratio ($HAuCl_4$:Amoxicillin) 3 µL:7.5 µL was obtained through the volume ratio ($HAuCl_4$:Amoxicillin) 15 µL:38 µL, used in

the synthesis of GNPs in solution. The other volume ratios were decided consonant with the best results obtained after two weeks on the Whatman No.1 chromatography paper.

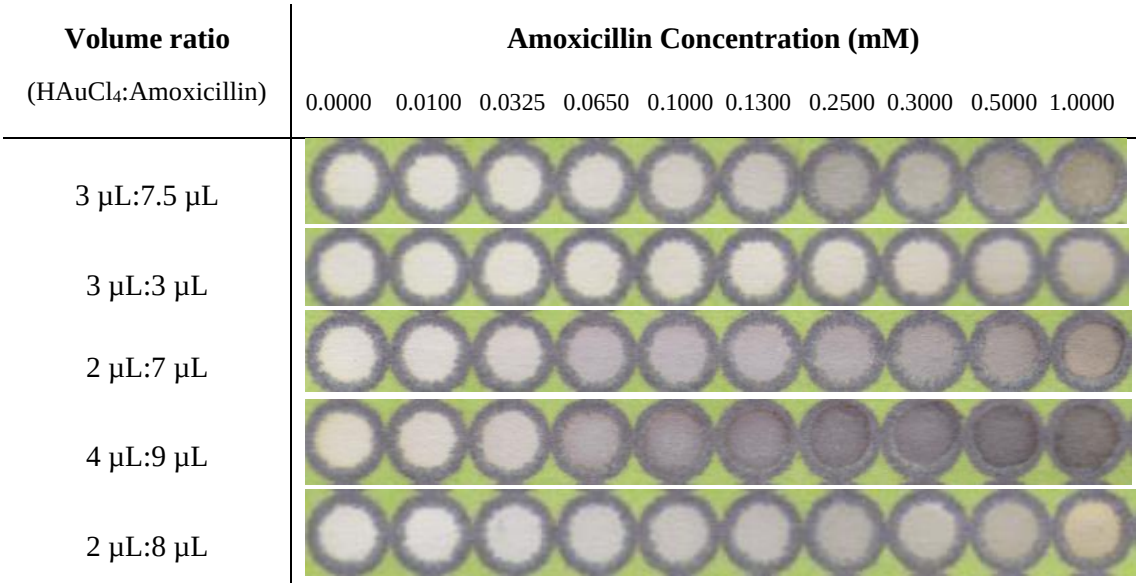

Figure 5.15 Variation of the volumes of $HAuCl_4 \cdot 3H_2O$ and amoxicillin
Along the lines of the microplate varies the concentration of antibiotic from 0.0100 mM to 1.0000 mM and along the columns varies the volume ratio between the gold salt and the antibiotic. The first column of each line corresponds to the control well.

From **Figure 5.15** it is possible to observe that the control wells do not present visible colour formation, indicating the non-formation of GNPs in the absence of antibiotic. In addition, the volume ratio ($HAuCl_4$:Amoxicillin) 3 µL:3 µL is the one with less colour intensity in the wells. It is also the case in which less colour changes, perceptible to the naked eye, occur along the line. The volume ratios ($HAuCl_4$:Amoxicillin) with higher colour intensity and better distinction when compared to the control well are 2 µL:7 µL and 4 µL:9 µL. These cases present an increase of colour intensity with antibiotic concentration, as in the GNP colloidal solutions. As it can also be seen through visual inspection, the resulting GNPs present a greyish colour instead of a red/pink colouration, indicating GNPs aggregation. In the volume ratios 2 µL:7 µL and 4 µL:9 µL, it is possible to see a colour change, visible to the naked eye, from 0.0650 mM, indicating a LOD of 0.0650 mM for the synthesis of GNPs on paper substrate. This demonstrates that the LOD, for amoxicillin, is the same in the synthesis of GNPs in solution and on paper substrate. As common antibiotic dosages are 125 mg/5 mL, 250 mg/5 mL and 500 mg/5 mL and the protocol in this thesis is based on the dilution of the antibiotics, it is possible to dilute the solution to always be above the LOD.

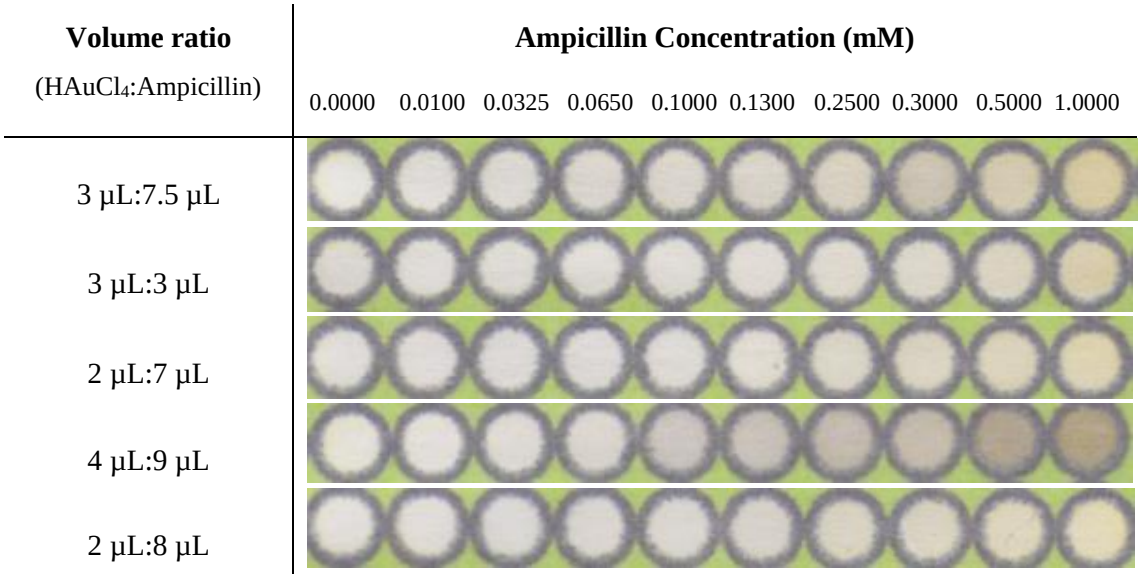

Figure 5.16 Variation of the volumes of $HAuCl_4 \cdot 3H_2O$ and ampicillin
Along the lines of the microplate varies the concentration of antibiotic from 0.0100 mM to 1.0000 mM and along the columns varies the volume ratio between the gold salt and the antibiotic. The first column of each line corresponds to the control well.

From **Figure 5.16** it is possible to observe that ampicillin was the antibiotic that presented the least colour intesity in the wells, after reacting with the gold salt, and colour changes with the increase of antibiotic concentration.This is in line with the results obtained for the synthesis of GNPs in solution at 70º C, where ampicillin had lower absorbance values than amoxicillin and ceftazidime. This may be because of the presence of other reducing groups in amoxicillin and ceftazidime chemical structures, such as -OH and -COOH, that might improve the formation of GNPs on paper substrate [34], [71]. Most of the wells do not present visible colour formation and are not distinct from the control well, indicating the non-formation of GNPs. Only higher concentrations of ampicillin cause a slight colour change, when compared to the control well. The case that presents the most visible colour change with increasing antibiotic concentration, is the volume ratio ($HAuCl_4$:Ampicillin) of 4 µL:9 µL. It is also the volume ratio in which there is a bigger difference between the intensity of the control well and the well with the highest antibiotic concentration. This volume ratio presents a LOD, visible to the naked eye, of 0.1000 mM, which is higher than the LOD for amoxicillin, decreasing the range in which the biosensor can work. This LOD is not so perceptible as in amoxicillin.

Volume ratio ($HAuCl_4$:Ceftazidime)	**Ceftazidime Concentration (mM)** 0.0000 0.0100 0.0325 0.0650 0.1000 0.1300 0.2500 0.3000 0.5000 1.0000
3 µL:7.5 µL	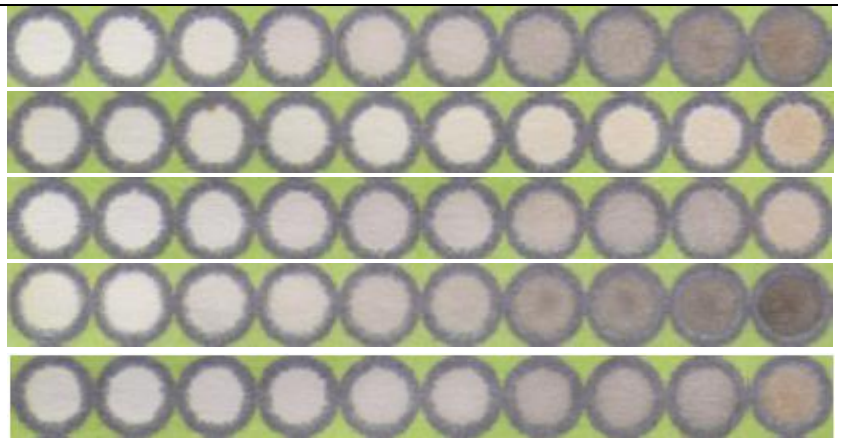
3 µL:3 µL	
2 µL:7 µL	
4 µL:9 µL	
2 µL:8 µL	

Figure 5.17 Variation of the volumes of $HAuCl_4 \cdot 3H_2O$ and ceftazidime
Along the lines of the microplate varies the concentration of antibiotic from 0.0100 mM to 1.0000 mM and along the columns varies the volume ratio between the gold salt and the antibiotic. The first column of each line corresponds to the control well.

In **Figure 5.17** it can be seen that the volume ratio ($HAuCl_4$:Ceftazidime) 3 µL:3 µL is also the one with less colour intensity. The colour changes along the line, for this volume ratio, are almost imperceptible to the naked eye, as in **Figure 5.15** Only higher concentrations of ampicillin cause a slight colour change, when compared to the control well. The volume ratios ($HAuCl_4$:Ceftazidime) with higher colour intensity and better distinction when compared to the control well are 3 µL:7.5 µL and 4 µL:9 µL. These also present an increase in colour intensity with the increase of antibiotic concentration. These resulting GNPs have a brownish/greyish colour instead of a red/pink colouration, indicating GNPs aggregation. The LOD, visible to the naked eye, in these cases is 0.0650 mM, for volume ratio 3 µL:7.5 µL, and 0.1.0000 mM, for volume ratio 4 µL:9 µL. As in the cases before, the protocol is based on the dilution of the antibiotics, so it is possible to dilute the solution to always be above the LOD.

In order to choose the optimum volume ratios between the gold salt and the antibiotic, preference was given to the cases with higher colour intensity and better distinction when compared to the control well, and the cases in which the colour intensity of the wells increases with antibiotic concentration. It was also considered the R-squared and the properties of the calibration curve (colour signal vs. antibiotic concentrations) of each microplate line. For amoxicillin and ceftazidime two volume ratios were chosen while for ampicillin only one volume ratio was selected, due to the low colour intensity and almost imperceptible colour change, along the microplate line, for most of the different volume ratios.

As mentioned before, to decide the optimum volumes and concentrations of reagents for the final device, first different volumes were tested with a fixed concentration of $HAuCl_4 \cdot 3H_2O$ (0.010 M), then different concentrations of $HAuCl_4 \cdot 3H_2O$ were tested with fixed volume ratios (gold salt:antibiotic). In **Figures 5.18**, **5.20**, **5.22**, **5.24** and **5.25** it is possible to observe the results obtained after variation of the concentration of $HAuCl_4 \cdot 3H_2O$, using the best volume ratios obtained from the previous tables. **Figures 5.18** and **5.20** were obtained using the best volume ratios for amoxicillin, **Figure 5.22** was obtained using the best volume ratio for ampicillin and **Figures 5.24** and **5.25** were obtained using the best volume ratios for ceftazidime.

5.3.1 Amoxicillin

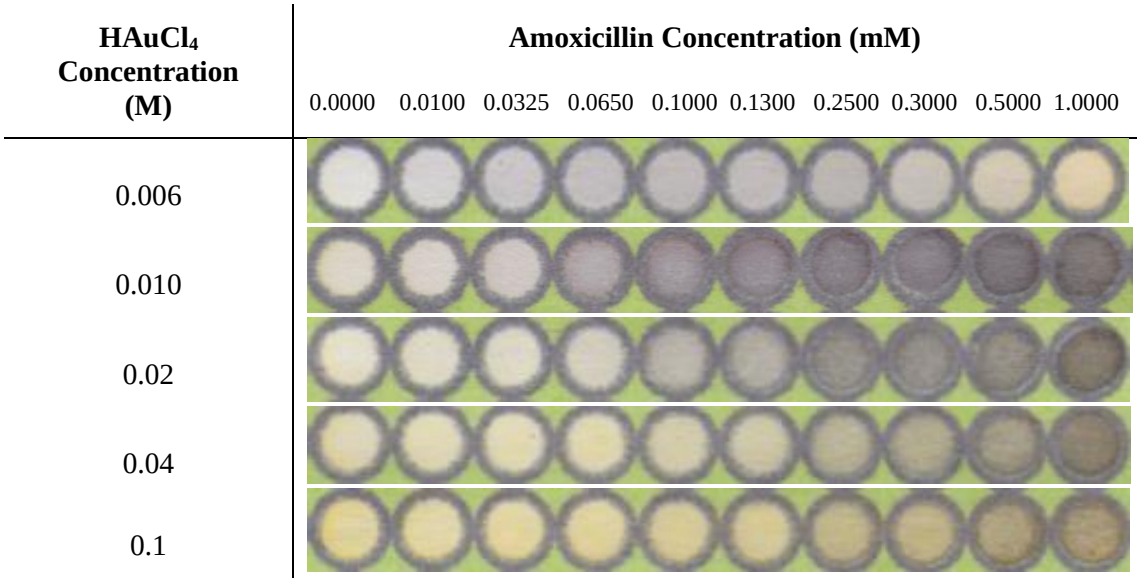

Figure 5.18 Variation of the concentration of $HAuCl_4$ for the volume ratio ($HAuCl_4$:Amoxicillin) of 4 µL:9 µL

Along the lines of the microplate, varies the concentration of antibiotic from 0.0100 mM to 1.0000 mM and along the columns varies the concentration of $HAuCl_4 \cdot 3H_2O$. The first column of each line corresponds to the control well, without antibiotic.

Figure 5.18 presents the results obtained after variation of the $HAuCl_4$ concentration for the volume ratio ($HAuCl_4$:Amoxicillin) of 4 µL:9 µL. It is possible to observe that as $HAuCl_4$ concentration increases, the number of wells with a visible grey colour formation decreases. In other words, as $HAuCl_4$ concentration increases, the LOD visible to the naked eye also increases, decreasing the range in which the biosensor can work. At the lowest concentration of $HAuCl_4$ (0.006 M), the higher antibiotic concentrations no longer form a greyish colour after reacting with the gold salt, indicating that these concentrations do not form GNPs. The $HAuCl_4$ concentrations which present a higher colour intensity and an increase of colour intensity with the increase of antibiotic concentration are 0.010 M and 0.02 M. The calibration curves of these two cases are presented in **Figure 5.19** and the calibration curves of the rest of the cases are presented in **Figure**

B. 1 (in the **Annex**). These calibration curves relate the colour signal of each well with the antibiotic concentration and were obtained after image analysis through *ImageJ* software, based on the ratio between Red and Green channels. These calibration curves allows the antibiotic API dose concentration.

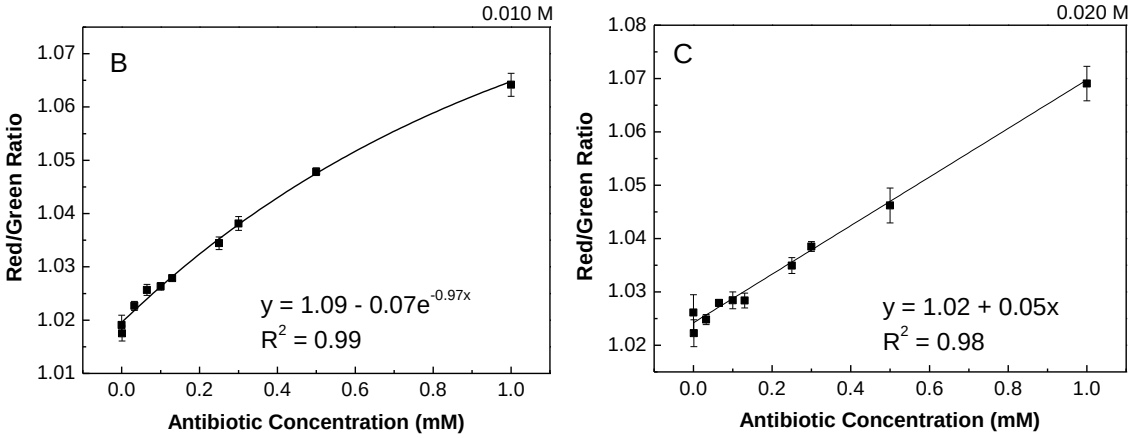

Figure 5.19 Calibration curves corresponding to Figure 5.18

A: Calibration curve correspondent to $HAuCl_4$ concentration of 0.010 M; B: Calibration curve correspondent to $HAuCl_4$ concentration of 0.02 M.

From **Figure B. 1**, it is possible to observe that the calibration curves correspondant to higher $HAuCl_4$ concentrations have lower R-squared, indicating poorest fit of the terms. The calibration curves with higher R-squared are the calibration curves correspondent to $HAuCl_4$ concentration of 0.010 M, 0.006 M and 0.02 M, which are presented in **Figure 5.19** and **Figure B. 1**. As the $HAuCl_4$ concentrations with better visual properties on paper were 0.010 M and 0.02 M (**Figure 5.19**), preference was given to the case with $HAuCl_4$ concentration of 0.010 M, due to a higher R-squared and lower standard deviations. As common antibiotic dosages are 125 mg/5 mL, 250 mg/5 mL and 500 mg/5 mL and the protocol used in this thesis is based on diluted solutions of antibiotics, the user must dilute the antibiotic into solutions with concentrations in the range of antibiotic concentrations used in this protocol.

Figure 5.20 presents the results obtained after variation of the $HAuCl_4$ concentration for the volume ratio ($HAuCl_4$:Amoxicillin) of 2 µL:7 µL. As in the case obtained after variation of the $HAuCl_4$ concentration for the volume ratio ($HAuCl_4$:Amoxicillin) of 4 µL:9 µL, the $HAuCl_4$ concentration with better results is 0.010 M. It presents the highest colour intensity and the wells with better distinction when compared to the control well. The colour changes along the line, for the lowest $HAuCl_4$ concentration (0.006 M), are almost imperceptible to the naked eye. For higher $HAuCl_4$ concentrations than 0.010 M, only higher concentrations of amoxicillin cause a colour change, when compared to the control well. Considering the calibration curves of all the cases, the calibration curves with higher R-squared are the calibration curves corresponding to $HAuCl_4$

concentration of 0.010 M and 0.02 M, which are presented in **Figure 5.21**. The calibration curves of the rest of the cases are presented in **Figure B. 2** (in the **Annex**), where it is possible to observe that the calibration curves corresponding to higher $HAuCl_4$ concentrations have lower R-squared, indicating poorest fit of the terms. Preference was given to the case with $HAuCl_4$ concentration of 0.010 M, due to the better visual properties on paper and a calibration curve with higher R-squared.

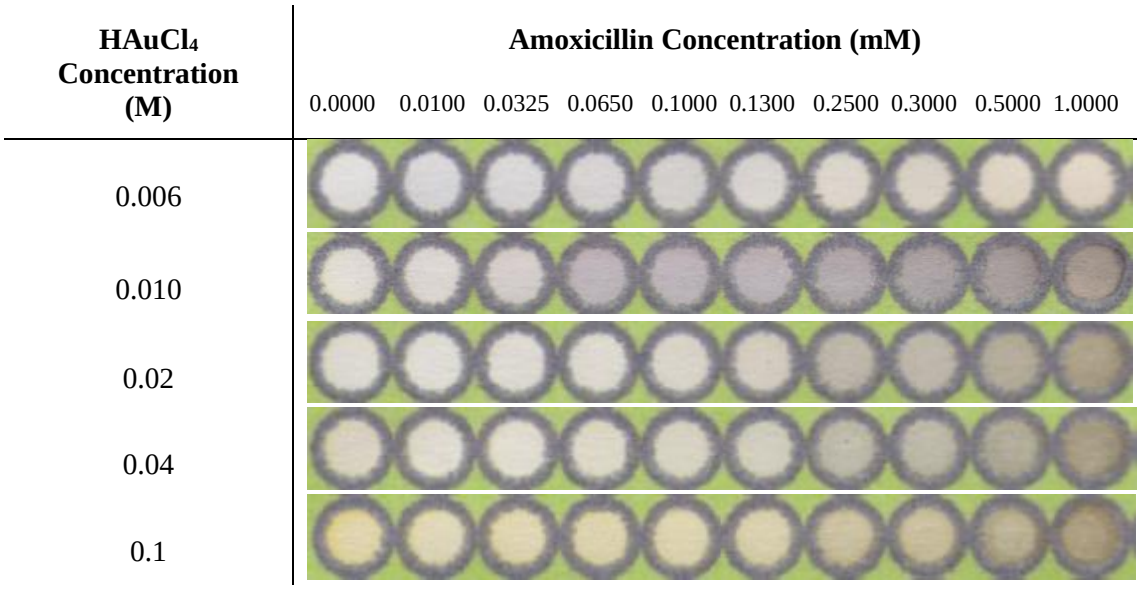

Figure 5.20 Variation of the concentration of $HAuCl_4$ for the volume ratio ($HAuCl_4$:Amoxicillin) of 2 µL:7 µL

Along the lines of the microplate, varies the concentration of antibiotic from 0.0100 mM to 1.0000 mM and along the columns varies the concentration of $HAuCl_4 \cdot 3H_2O$. The first column of each line corresponds to the control well, without antibiotic.

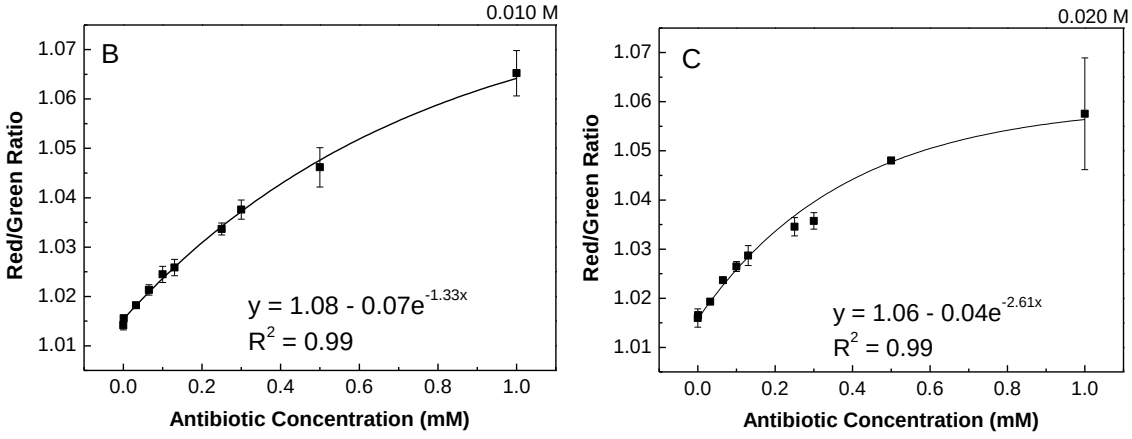

Figure 5.21 Calibration curves corresponding to Figure 5.20

A: Calibration curve correspondent to $HAuCl_4$ concentration of 0.010 M; B: Calibration curve correspondent to $HAuCl_4$ concentration of 0.02 M.

In both of the cases with volume ratios ($HAuCl_4$: Amoxicillin) of 2 µL:7 µL and 4 µL:9 µL, the best results were obtained with a concentration of $HAuCl_4$ of 0.010 M. When comparing

these two results, preference was given to the volume ratio of 4 µL:9 µL, because it presented more colour intensity in the wells and a calibration curve with lower standard deviation for higher antibiotic concentrations.

5.3.2 Ampicillin

Figure 5.22 presents the results obtained after variation of the $HAuCl_4$ concentration for the volume ratio ($HAuCl_4$:Ampicillin) of 4 µL:9 µL. As before in **Figure 5.16**, ampicillin continues to be the antibiotic with less colour intensity and less colour changes along the microplate line. As it can be seen in **Figure 5.22**, the case in which slight colour changes occur, is the case with a concentration of $HAuCl_4$ of 0.010 M. The lowest and highest $HAuCl_4$ concentration do not present visible colour changes with the increase of antibiotic concentration.

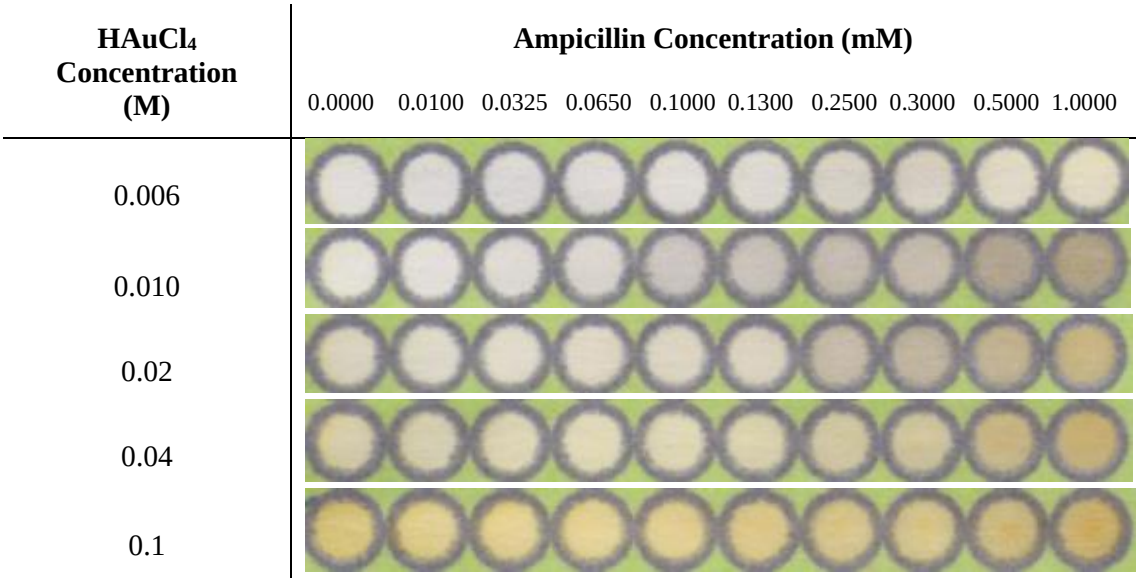

Figure 5.22 Variation of the concentration of $HAuCl_4$ for the volume ratio ($HAuCl_4$:Ampicillin) of 4 µL:9 µL

Along the lines of the microplate, varies the concentration of antibiotic from 0.0100 mM to 1.0000 mM and along the columns varies the concentration of $HAuCl_4 \cdot 3H_2O$. The first column of each line corresponds to the control well, without antibiotic.

The case with a concentration of HAuCl4 of 0.010 M was also the case with a better calibration curve, which is presented in **Figure 5.23**. The calibration curves of the rest of the cases are presented in **Figure C. 1** (in the **Annex**), where it is possible to observe that the calibration curves correspondent to higher HAuCl4 concentrations also have lower R-squared, indicating poorest fit of the terms. The calibration curve with higher R-squared is the calibration curve correspondent to HAuCl4 concentration of 0.010 M. Preference was given to this case, because it had better visual properties on paper and a calibration curve with higher R-squared and an exponential fit, common to paper-based sensors with gold nanoparticles.

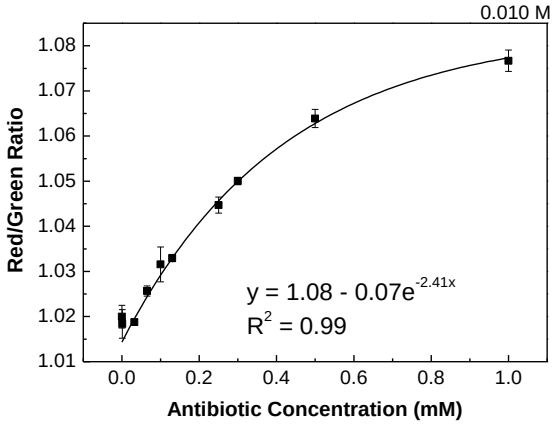

Figure 5.23 Calibration curves corresponding to Figure 2.22
Calibration curve correspondent to $HAuCl_4$ concentration of 0.010 M

5.3.3 Ceftazidime

Figures 5.24 and **5.25** present the results obtained after variation of the $HAuCl_4$ concentration for the volume ratio ($HAuCl_4$:Ceftazidime) of 4 µL:9 µL and 3 µL:7.5 µL, respectively.

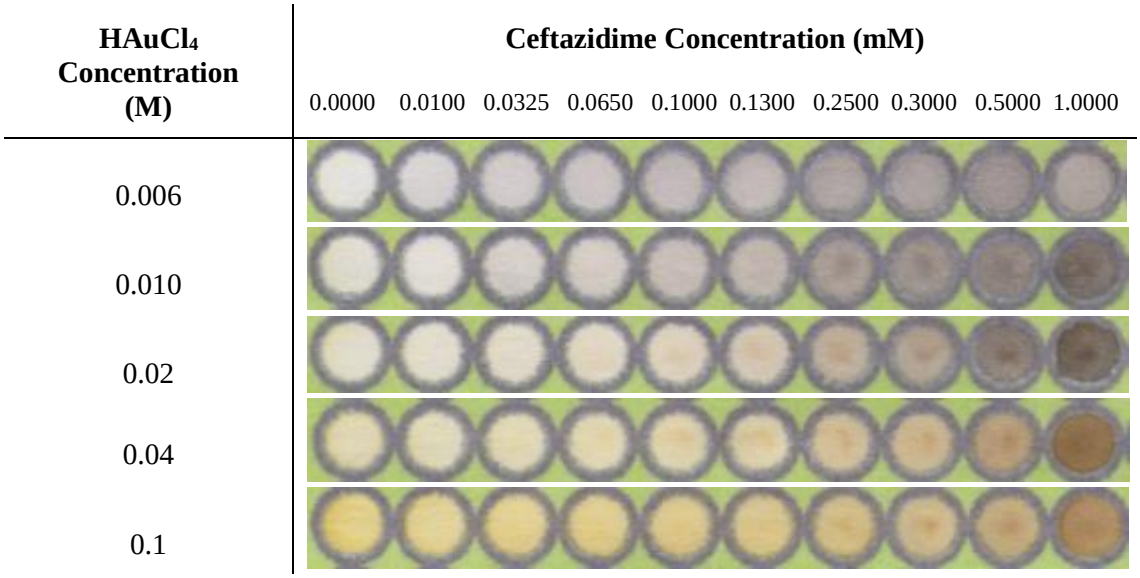

Figure 5.24 Variation of the concentration of $HAuCl_4$ for the volume ratio ($HAuCl_4$: Ceftazidime) of 4 µL:9 µL
Along the lines of the microplate, varies the concentration of antibiotic from 0.0100 mM to 1.0000 mM and along the columns varies the concentration of $HAuCl_4 \cdot 3H_2O$. The first column of each line corresponds to the control well, without antibiotic.

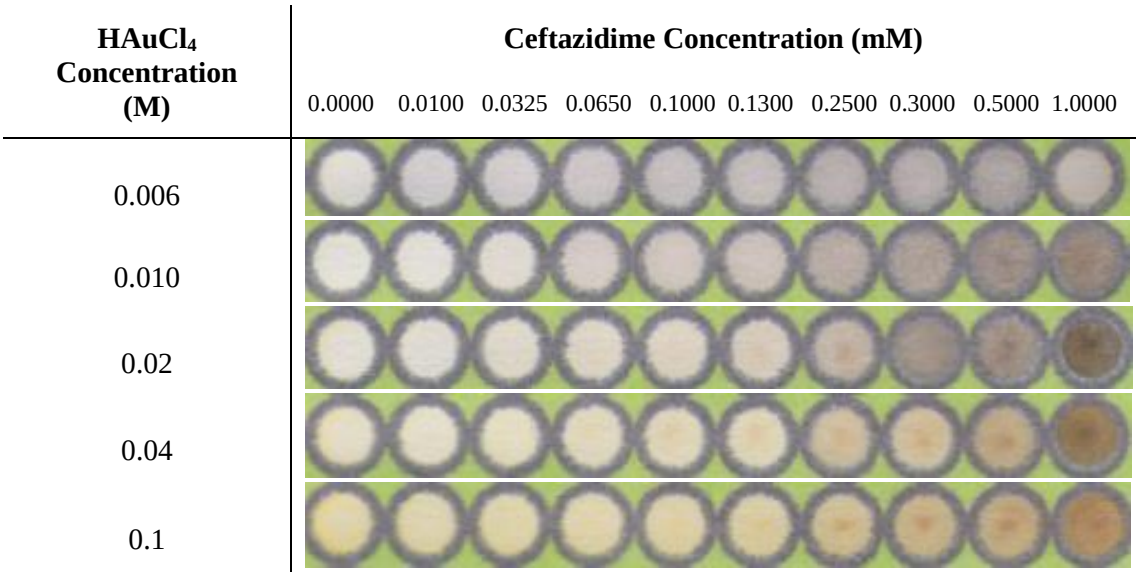

Figure 5.25 Variation of the concentration of $HAuCl_4$ for the volume ratio ($HAuCl_4$: Ceftazidime) of 3 µL:7.5 µL

Along the lines of the microplate, varies the concentration of antibiotic from 0.0100 mM to 1.0000 mM and along the columns varies the concentration of $HAuCl_4 \cdot 3H_2O$. The first column of each line corresponds to the control well, without antibiotic.

In both **Figures 5.24** and **5.25**, it is possible to observe that as $HAuCl_4$ concentration increases, the range in which there is a grey/brown colouration in the wells also increases, rising the LOD visible to the naked eye and decreasing the range in which the sensor works. The cases with a lower LOD visible to the naked eye, correspondent to $HAuCl_4$ concentration of 0.006 M and 0.010 M, present a higher colour intensity and an increase of colour intensity with the increase of antibiotic concentration. Although the highest antibiotic concentration (1.0000 mM) has a colour less intense than the antibiotic concentration before (0.5000 mM), for $HAuCl_4$ concentration of 0.006 M, it is still possible to distinct from the control well.

Considering the calibration curves, is possible to observe that all the calibration curves have high R-squared, indicating a good fit of the terms. The calibration curves with higher R-squared are the calibration curves correspondent to $HAuCl_4$ concentration of 0.006 M and 0.010 M, which is in line with the cases with better optical properties on paper. The calibration curves of these two cases are presented in **Figure 5.26** and **5.27** while the other calibration curves are presented in **Figure D. 1** and **D. 2** (in the **Annex**).

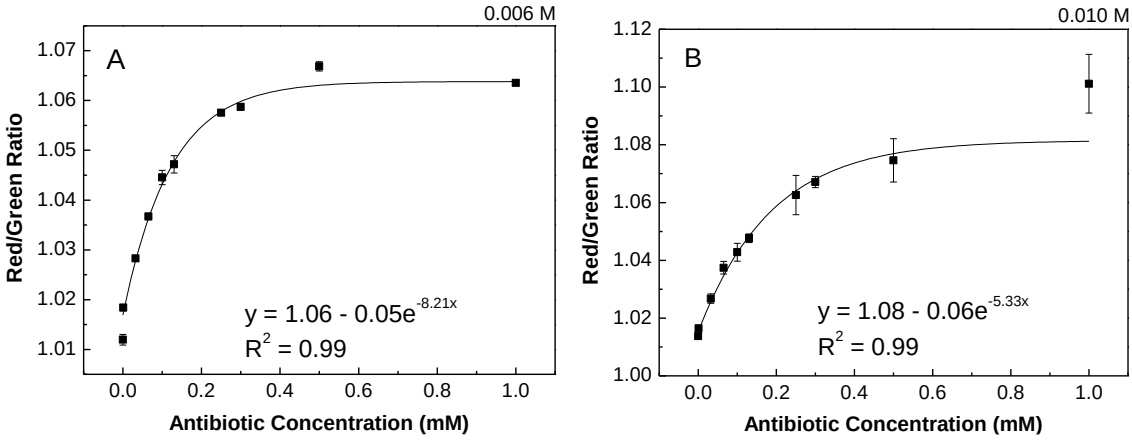

Figure 5.26 Calibration curves corresponding to Figure 5.24

A: Calibration curve correspondent to $HAuCl_4$ concentration of 0.006 M; B: Calibration curve correspondent to $HAuCl_4$ concentration of 0.010 M.

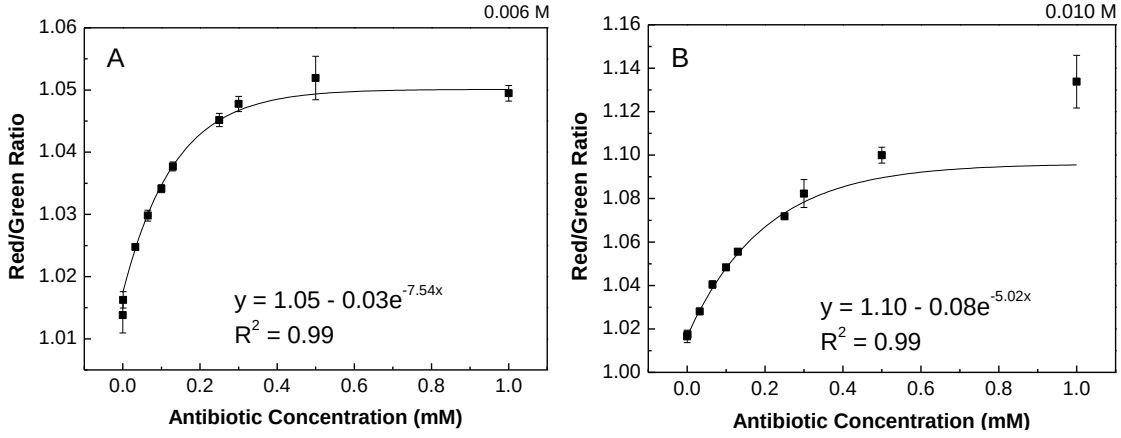

Figure 5.27 Calibration curves corresponding to Figure 5.25

A: Calibration curve correspondent to $HAuCl_4$ concentration of 0.006 M; B: Calibration curve correspondent to $HAuCl_4$ concentration of 0.010 M.

In both of the cases with volume ratios ($HAuCl_4$: Ceftazidime) of 3 µL:7.5 µL and 4 µL:9 µL, preference was given to $HAuCl_4$ concentration of 0.006 M, due to the lower LOD visible to the naked eye (0.010 M) and the better calibration curves, with higher R-squared and a curve that contained the highest antibiotic concentration sample. When comparing these two results, preference is given to the volume ratio of 4 µL:9 µL, because it presents more colour intensity in the wells and a calibration curve with lower standard deviations and a higher Red/Green ratio. It is also the calibration curve which allows a better distinction between the control well (0 mM) and the well with 0.0100 mM of antibiotic.

It can be concluded that the optimum volume ratio $HAuCl_4$: Antibiotic is 4 µL:9 µL for the three antibiotics and that the optimum $HAuCl_4$ concentration is 0.010 M for amoxicillin and ampicillin, and 0.006 M for ceftazidime. These optimum results are summed up in **Figure 5.28**

and their calibration curves are presented in **Figure 5.29**. The LOD visible to the naked eye is 0.0650 mM for amoxicillin, 0.1000 mM for ampicillin and 0.0100 mM for ceftazidime, which indicates that after dilution, the antibiotic to test must have a final concentration between these values and 1.0000 mM.

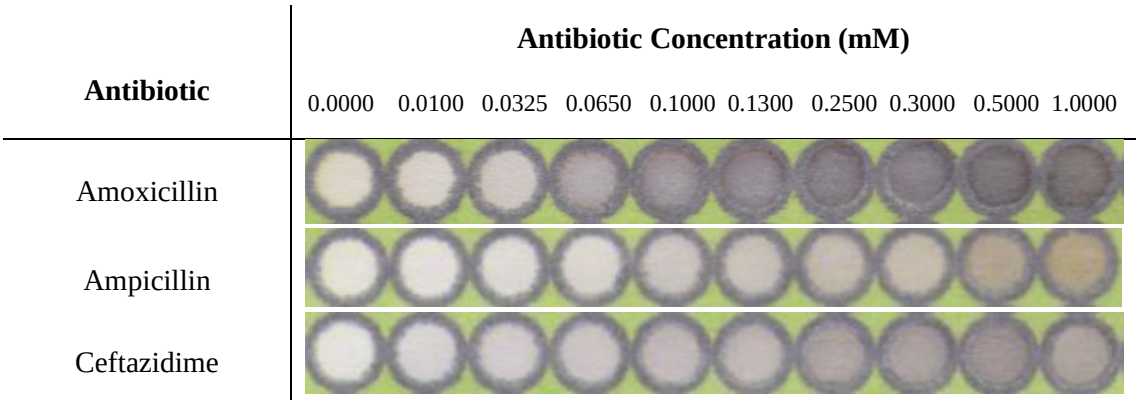

Figure 5.28 Sum up of the optimum results of synthesis of GNPs on paper substrate

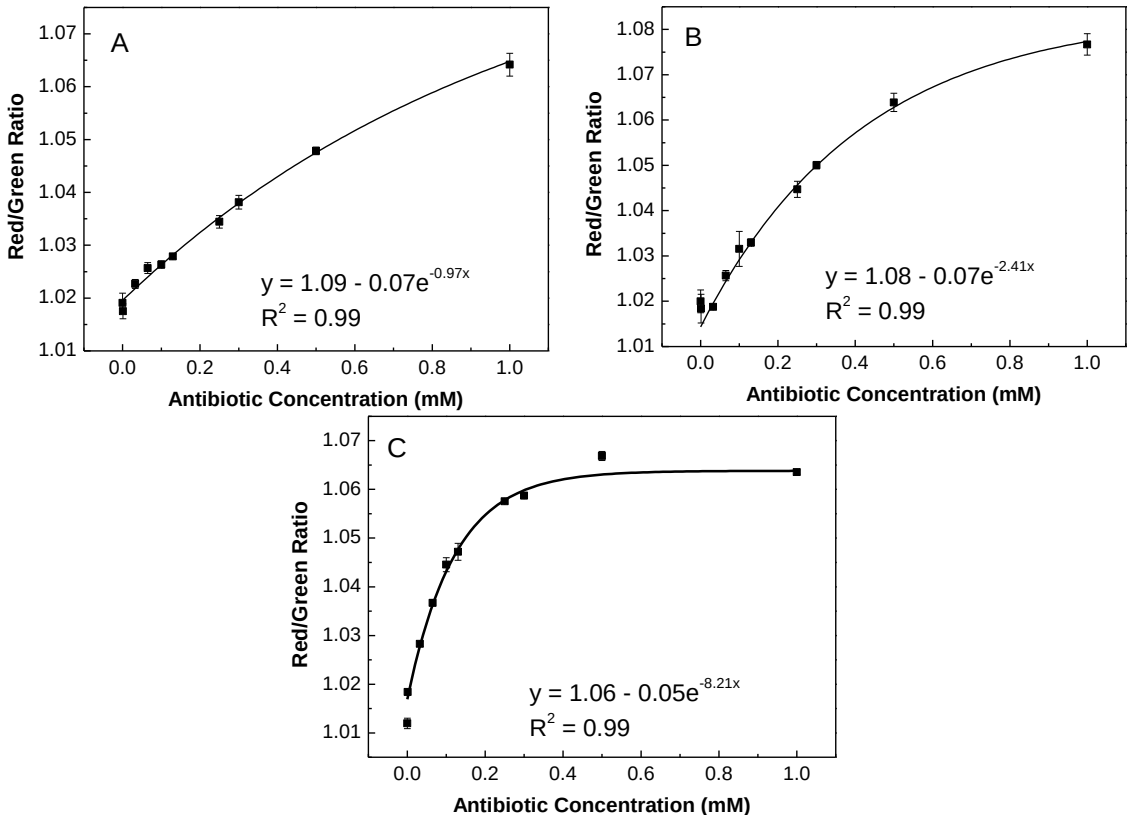

Figure 5.29 Sum up of the calibration curves of the optimum results for synthesis of GNPs on paper substrate

A: Calibration curve of the sensor for Amoxicillin; B: Calibration curve of the sensor for Ampicillin; C: Calibration curve of the sensor for ceftazidime.

In **Figure 5.29**, the calibration curves for the final sensor present an exponential fit, indicating that as the antibiotic concentration continues to increase, a saturation point will be reached. This saturation behaviour is common in these type of devices [72]. In **Figures 5.29 - A** and **5.29 – B** the point of saturation is not reached with the range of antibiotic concentration used in this thesis. In **Figure 5.29 – C** it is possible to observe that the Red/Green Ratio stabilizes from approximately 0.6 mM. Therefore, the range of antibiotic concentrations that this sensor can quantify is up to 0.6 mM. This indicate that the diluted solution of the antibiotic to test must be less than 0.6 mM.

5.4 Testing common drug replacements

To test if the developed system is feasible to be used for the detection of falsified antibiotics, the antibiotics were replaced by gelatine, sodium bicarbonate, acetylsalicylic acid, calcium carbonate, D-(-)-fructose and D-(+)-galactose. First these substitutes were used in the procedure for synthesis of GNPs in solution, then in the procedure for synthesis of GNPs on paper substrate. **Figures 5.30**, **5.31** and **5.32** present the UV-Vis spectrophotometry analysis of solutions upon addition of those ingredients and **Figures 5.33** and **5.34** present the results of the same substitutes on paper substrate. These experiences were repeated three times each and similar results were obtained.

To test common drug replacements, the ingredients previously mentioned were used in concentrations between 0.0100 mM and 1.0000 mM, com exception gelatine and calcium carbonate, and compared with the results obtained in **Sections 5.1** and **5.3**. As mentioned in **Section 4.4**, the tests for calcium carbonate used a smaller range of concentrations (between 0.1300 mM and 0.0100 mM) due to the low solubility of this ingredient in water. Also, the tests for gelatine were done only for concentrations between 0.0325 mM and 1.0000 mM.

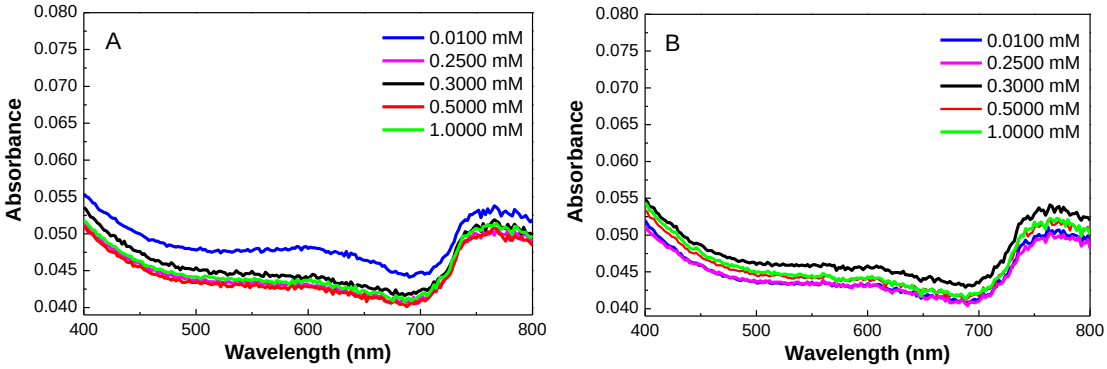

Figure 5.30 UV-Vis spectrophotometry analysis of solutions upon addition of sodium bicarbonate and D-(+)-galactose
A: Sodium bicarbonate; B: D-(+)-galactose.

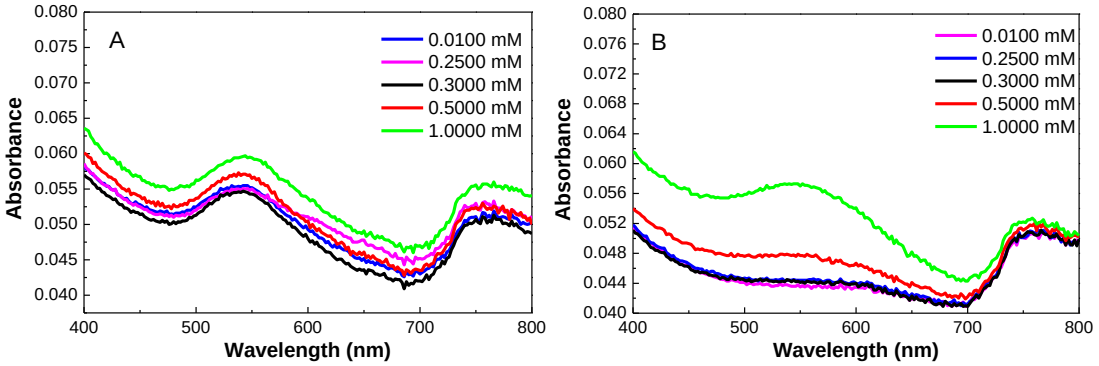

Figure 5.31 UV-Vis spectrophotometry analysis of solutions upon addition of D-(-)-fructose and acetylsalicylic acid

A: D-(-)-fructose; B: Acetylsalicylic acid

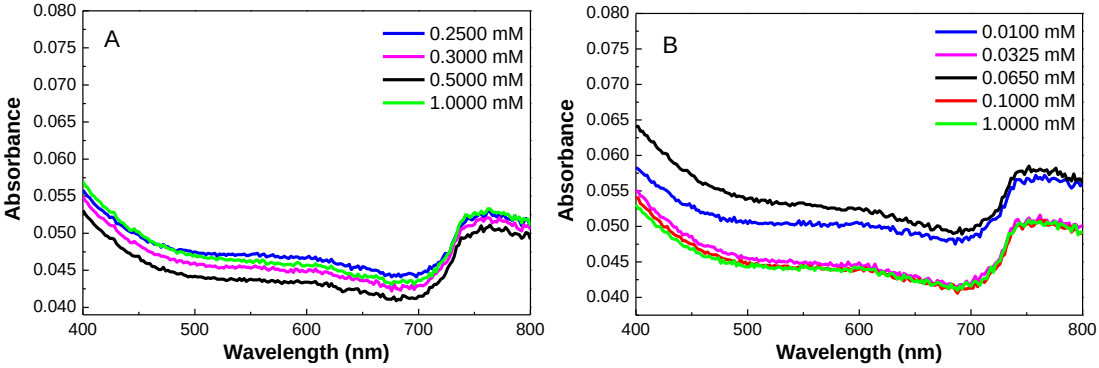

Figure 5.32 UV-Vis spectrophotometry analysis of solutions upon addition of gelatine and calcium carbonate

A: Gelatine; B: Calcium carbonate

In **Figures 5.30** and **5.32** there is no absorption SPR peak in the visible region of the electromagnetic spectrum, characteristic of GNPs, indicating that there is no reduction of $HAuCl_4$ by sodium bicarbonate, D-(+)-galactose, gelatine or calcium carbonate, and consequently, no formation of GNPs. In **Figure 5.31** an absorption SPR peak between 500 nm and 600 nm can be observed, indicating a formation of GNPs. In the case of D-(-)-fructose, all concentrations between 0.0100 mM and 1.0000 mM form GNPs as expected, because fructose has been used to form GNPs [73]. In the case of acetylsalicylic acid, there is only formation of GNPs for the highest concentration (1.0000 mM), due to the presence of monosodium citrate in the *migraspirin* tablet beyond acetylsalicylic acid. Such as fructose, sodium citrate is also used in the formation of GNPs [74]. In addition, theses graphics present more noise than the graphics correspondent to the synthesis of GNPs using antibiotics. A detection based only on the synthesis of GNPs in solution would not be enough to distinguish legitimate antibiotics from falsified antibiotics.

Figures 5.33 and **5.34** present the results of the use of common drug replacements, instead of the antibiotic, in the synthesis of GNPs on paper substrate protocol.

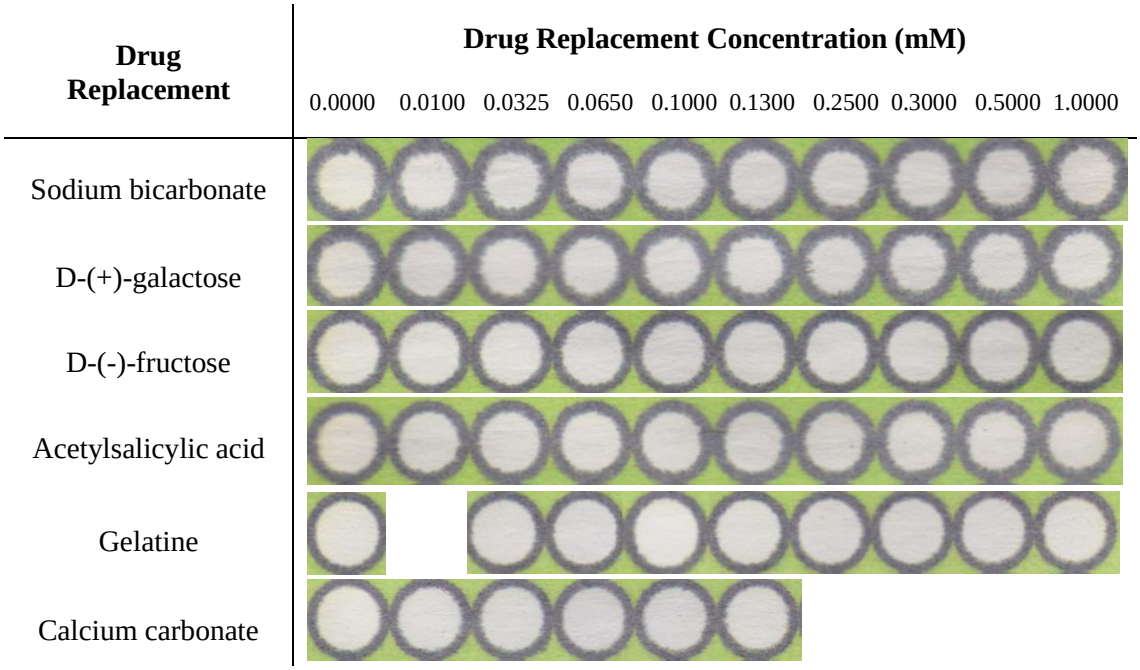

Figure 5.33 Results on paper substrate after addition of common drug replacements and using a $HAuCl_4$ concentration of 0.010 M

The blank space in the gelatine concentration of 0.0100 mM is because this substitute was made only for concentrations between 0.0325 mM and 1.0000 mM.

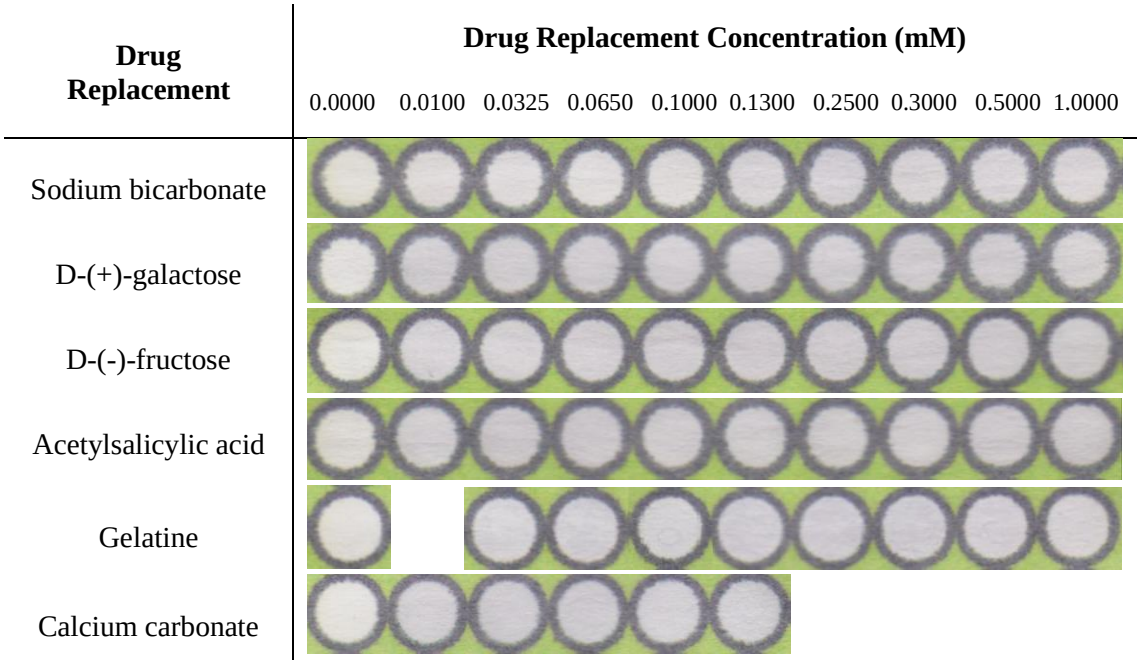

Figure 5.34 Results on paper substrate after addition of common drug replacements and using a $HAuCl_4$ concentration of 0.006 M

The blank space in the gelatine concentration of 0.0100 mM is because this substitute was made only for concentrations between 0.0325 mM and 1.0000 mM.

When comparing the results present in **Figures 5.33** and **5.34** with the results obtained by antibiotics on paper substrate (**Figure 5.28**), it is possible to observe that there are almost no colour changes as the drug replacement concentration increases. There is also a poor distinction between the control well (0 mM) and the wells with the substitute, indicating the non-formation of GNPs on paper substrate or the non-significant formation for colorimetric results. Although there is formation of GNPs in solution when fructose and acetylsalicylic acid are used, on paper substrate that does not occur, and it is possible to distinguish between the antibiotic and the substitute. It can be concluded that it is possible to distinguish between falsified and authentic antibiotics on paper substrate by the method described in this thesis.

Previous microplate paper wells with antibiotic (1.0000 mM of amoxicillin) and drug replacement (1.0000 mM of D-(+)-galactose) were analysed by SEM, to see if the colour change that occurred in the presence of the antibiotic represented the formation of GNPs. **Figure 5.35** presents the SEM images of microplate paper wells containing $HAuCl_4$ and amoxicillin and **Figure 5.36** presents the SEM images of microplate paper wells containing $HAuCl_4$ and D-(+)-galactose.

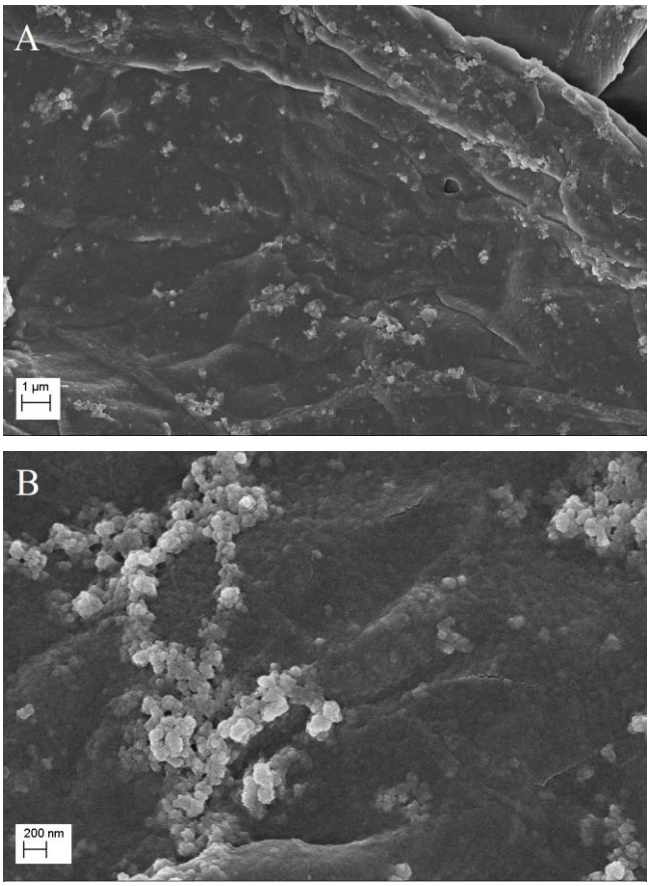

Figure 5.35 SEM images of microplate paper wells containing $HAuCl_4$ and amoxicillin
A: 5000x magnification; B: 20000x magnification.

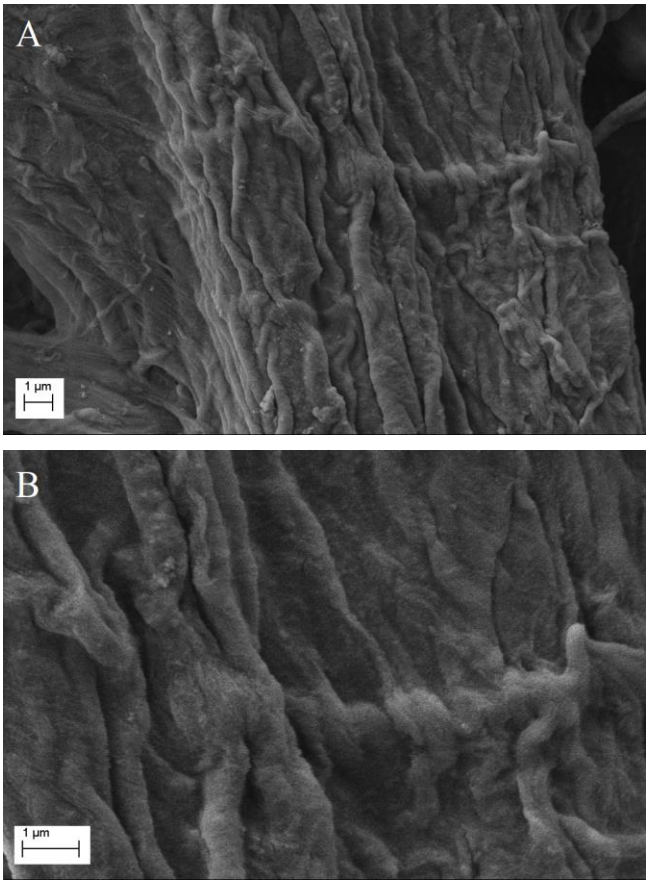

Figure 5.36 SEM images of microplate paper wells containing $HAuCl_4$ D-(+)-galactose
A: 5000x magnification; B: 10000x magnification.

When comparing **Figure 5.35** with **Figure 5.36**, it is possible to observe that the well containing antibiotic presents agglomerates, which may be indicative of the formed GNPs. These agglomerates are not present in the well containing the drug replacement, indicating that the reaction between $HAuCl_4$ and the drug replacements does not form GNPs. It also concludes that the procedure for synthesis of GNPs on office paper can be used to distinguish counterfeit antibiotics to legitimate antibiotics.

As the goal of this sensor is to distinguish, at naked eye, between falsified and legitimate β-lactam antibiotics, the best results occur at higher concentrations of antibiotic, namely from 0.2500 mM. As common antibiotic dosages are 125 mg/5 mL, 250 mg/5 mL and 500 mg/5 mL, which correspond to approximately 0.046 M, 0.091 M and 0.183 M, respectively, the user must dilute the antibiotic to test into solutions with concentrations between 0.2500 mM and 0.6 mM (which corresponds to the saturation point). The colour visible to the naked eye of the well will indicate the presence or absence of the API of the antibiotic, and through the Red/Green ratio and the calibration curves (**Figure 5.29**) it is possible to identify if the API is present in lower concentrations than normal.

5.5 Final Device Protocol

To use the device developed in this thesis, the user must deposit 4 µL of $HAuCl_4 \cdot 3H_2O$ on the control and sample zones and then deposit 9 µL of the antibiotic to test on the sample zone, without letting the $HAuCl_4 \cdot 3H_2O$ dry. Only then, shall the user let the paper-based sensor dry at room temperature. If the antibiotic to test is amoxicillin or ampicillin, the user must use the $HAuCl_4 \cdot 3H_2O$ with a concentration of 0.010 M. If the antibiotic to test is ceftazidime, the user must use the $HAuCl_4 \cdot 3H_2O$ with a concentration of 0.006 M. The antibiotic to test must be diluted into concentrations between 0.2500 mM and 0.6 mM.

If the sample well presents a brownish/greyish colour (**Figure 5.37**), it indicates that the gold salt was reduced by the antibiotic and confirms the presence of the API. The presence of a similar colour to the control well (**Figure 5.38**) indicates the absence of the antibiotic API, implying a counterfeit β-lactam antibiotic. In cases were the presence of API is confirmed, it is necessary to obtain the Red/Green ratio, through digitalization and image analysis software or through a mobile image processing application and compare the value with the calibration curves presented in **Figure 5.29**. This will allow to identify if the API on the antibiotic to test is present in lower concentrations than normal.

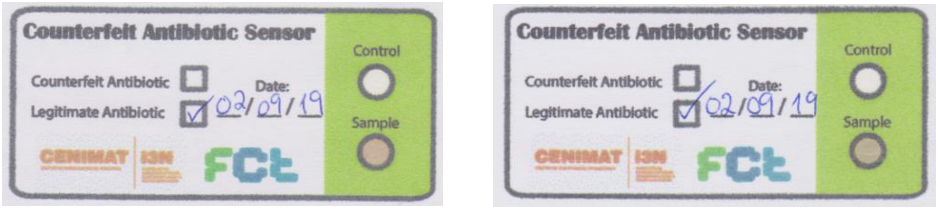

Figure 5.37 Paper-based sensor after addition of legitimate antibiotics

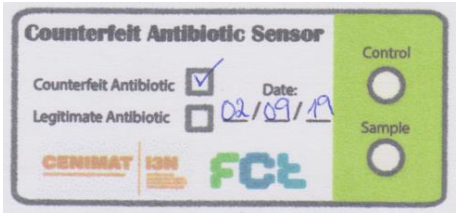

Figure 5.38 Paper-based sensor after addition of counterfeit antibiotics

Table 5.1 shows the cost of raw materials to produce this device, based on the price of each material and reagent required. The expenditures electricity from the appliances were not taken in account. This paper-based sensor is all made of biodegradable materials and reduced volumes of reagents, which reduces production, storage and transportation costs. It has a total cost of 2.3 x 10^{-3} €.

Table 5.1 Cost of raw materials to produce the final device

Materials	Quantity	Cost	Sensor Cost
Office Paper	(5.5 x 2.4) cm^2	1.9 x 10^{-3} €/m^2	2.51 x 10^{-6} €
Printing Wax	2 x (5.5 x 2.4) cm^2	0.28 €/m^2	7.39 x 10^{-4} €
$HAuCl_4 \cdot 3H_2O$ (0.010 M)	4 µL = 0.01006 mg	61.92 €/g	9.91 x 10^{-4} €
$HAuCl_4 \cdot 3H_2O$ (0.006 M)	4 µL = 0.009 mg	61.92 €/g	5.57 x 10^{-4} €
Total Cost			**2.3 x 10^{-3} €**

6

Conclusions and future work

The main goal of this dissertation was to develop a inexpensive and user-friendly device, able to detect counterfeit β-lactam antibiotics, using Lab-on-Paper technology and gold nanoparticles. The use of paper as diagnostic support in this device presents several benefits such as low price, large supply with different formats and properties, compatibility with various chemicals, disposability, easy use and white background, which allows a colorimetric detection and facilitates a digital analysis.

In this thesis, two types of paper were characterized: office paper Portucel and Whatman No.1 chromatography paper. Several characterization techniques were used to evaluate these different types of paper and office paper revealed better properties than Whatman paper, for the development of this device. Office paper was found to have flatter cellulose fibres and a less porous and more uniform surface, due to the presence of calcium carbonate that fill most of the pores, which reduces the diffusion of gold salt by paper fibres. The presence of calcium carbonate was confirmed by FTIR and XRD, in which the office paper presented a lower purity of cellulose and a lower crystallinity index (69.17%), when compared to Whatman paper (74.37%). TG and DSC showed that the cellulose decomposition results in a lower mass loss for office paper (49.13%) than for Whatman paper (79.88%), due to the presence of calcium carbonate, and that the office paper does not present a significant degradation during the heating process.

The enzyme-free protocol developed showed an increase in the absorbance value and colour intensity, of the colloidal solutions, with the increase of antibiotic concentration. The reduction of gold salt by the antibiotic only produced GNPs for antibiotic concentrations from

0.0650 mM, establishing a LOD of 0.0650 mM. This protocol also presented direct proportionality until 0.5000 mM of antibiotic concentration, indicating that the sensitivity is maintained during this range. To be within this range, the antibiotic to be tested must be diluted, as in the procedure of this thesis. Assays without the heat source demonstrated that the GNP synthesis also occurs at room temperature and maintains the same LOD and the direct proportionality between the absorbance value and the antibiotic concentration. These assays presented a better linear fit of the terms than the GNPs synthesized at 70º C and confirmed the possibility of the reaction, between the gold and the antibiotic, occurring on paper substrate at room temperature.

The protocol applied on paper substrate consisted of adding the antibiotic right after the deposition of $HAuCl_4 \cdot 3H_2O$, without letting it dry out. This allowed a greater diffusion and more homogeneous mixing of the reagents, improving the GNP formation. The obtained optimum ratio $HAuCl_4$:Antibiotic was 4 µL:9 µL for the three antibiotics and that the optimum $HAuCl_4$ concentration was 0.010 M for amoxicillin and ampicillin, and 0.006 M for ceftazidime. The resulting LOD visible to the naked eye was 0.0650 mM for amoxicillin, 0.1000 mM for ampicillin and 0.0100 mM for ceftazidime. These conditions presented an increase of colour intensity with antibiotic concentration, a good distinction between the control well and the wells with antibiotic, and calibration curves with lower standard deviations and higher R-squared.

Testing the previous protocols with common drug replacements, such as gelatine, sodium bicarbonate, acetylsalicylic acid, calcium carbonate, D-(-)-fructose and D-(+)-galactose, confirmed the possibility of using this device to detect counterfeit β-lactam antibiotics. Although GNPs were synthesized in solution upon addition of D-(-)-fructose and acetylsalicylic acid, this did not occur when applied on paper substrate. On paper substrate, no significant colour changes occurred with the increase of drug replacement concentration, indicating the non-formation of GNPs or the non-significant formation for colorimetric results. The SEM analysis allowed the observation of agglomerates, probably GNPs, in the microplate well containing antibiotic and its absence in the microplate well containing a common drug replacement. This indicates that the procedure for synthesis of GNPs on office paper can be used to distinguish counterfeit antibiotics to legitimate antibiotics.

As the main goal of the developed sensor is to distinguish, at naked eye, between falsified and legitimate β-lactam antibiotics, the antibiotic concentration range was chosen between 0.2500 mM and 0.6 mM. This range is below the saturation point and presented the wells with higher colour intensity, upon addition of the antibiotic. As common antibiotic dosages are 125 mg/5 mL, 250 mg/5 mL and 500 mg/5 mL, which correspond to approximately 0.046 M, 0.091 M and 0.183 M, respectively, the antibiotic to test must be diluted into concentrations between 0.2500 mM and

0.6 mM. In addition, these values presented Red/Green ratios distinct from each other, allowing the user to calculate the dosage of API and compare it with the results obtained in this thesis. The sensor detection is based on checking for the presence of the active pharmaceutical ingredient in the antibiotic, through a brownish/greyish colour in the sample well and verifying if it is within the correct dosage. When comparing this sensor to the devices mentioned in the State of the Art, this device has the advantage of allowing a quantitative analysis.

This device consisted of a microfluidic paper-based platform, obtained by Lab-on-Paper technology, with an enzyme-free detection, based on the use of gold nanoparticles, which made the final device low-cost and with a longer shelf life than a biosensor with enzymes. This device does not require the use inside a laboratory and can be useful in hospitals, clinics, pharmacies and non-governmental organizations, especially in less developed countries. Users can use this sensor when patients do not respond to medication, to determine if the cause is a counterfeit antibiotic, or as a quality assurance during the purchasing process. To bring this device to general use, improvements and optimizations must be made.

As future work, a trial with more samples must be done, to calculate the false positives and false negatives and consequently, obtain the sensor error. Furthermore, another control well can be added on the final sensor, in which only antibiotic is placed, and other excipients can be tested to see if they reduce the gold salt and may interfere with the results. Also, the evaluation of the size and shape of the GNPs present in the colloidal solutions, through dynamic light scattering and transmission electron microscopy, would be interesting to see if the size and shape vary with the concentration of antibiotic and with the type of antibiotic. Another suggestion is the development of a smartphone application, that automatically analyses the sample well, obtains the API dosage and indicates if the antibiotic is counterfeit or legitimate.

References

[1] E. Pisani, "WHO Global Surveillance and Monitoring System for Substandard and Falsified Medical Products," 2017. [Online]. Available: https://www.who.int/medicines/regulation/ssffc/publications/gsms-report-sf/en/. [Accessed: 23-Jan-2019].

[2] I. P. INFARMED, "Matérias Primas," 2016. [Online]. Available: http://www.infarmed.pt/web/infarmed/entidades/inspecao/inspecao-medicamentos/materias-primas. [Accessed: 23-Jan-2019].

[3] K. E. Boehle, C. S. Carrell, J. Caraway, and C. S. Henry, "Paper-Based Enzyme Competition Assay for Detecting Falsified β-Lactam Antibiotics," *ACS Sensors*, vol. 3, pp. 1299–1307, 2018.

[4] T. Kelesidis and M. E. Falagas, "Substandard/Counterfeit Antimicrobial Drugs," *Clin. Microbiol. Rev.*, vol. 28, no. 2, pp. 443–464, 2015.

[5] E. Etebu and I. Arikekpar, "Antibiotics : Classification and mechanisms of action with emphasis on molecular perspectives," *Int. J. Appl. Microbiol. Biotechnol. Res.*, vol. 4, pp. 90–101, 2016.

[6] B. D. Clayton and Y. N. Stock, "Antimicrobianos," in *Fundamentos de Farmacologia*, 12ª., Lusociência, 2002, p. 594.

[7] G. Dumancas, "Penicillins," *Encyclopedia of Toxicology*. Academic Press, pp. 768–772, 2014.

[8] N. A. Rosário and A. S. Grumach, "Allergy to beta-lactams in pediatrics: a practical approach," *J. Pediatr. (Rio. J).*, vol. 82, no. 5, pp. S181–S188, 2006.

[9] G. J. Tortora, B. R. Funke, and C. L. Case, “Drogas Antimicrobianas,” in *Microbiologia*, 10th ed., Porto Alegre: Artmed Editora SA, 2012, pp. 553–583.

[10] P. R. Murray and K. S. Rosenthal, *Microbiologia Médica*, 7ª edição. Rio de Janeiro: Elsevier Editora Ltda., 2014.

[11] G. J. Tortora, B. R. Funke, and C. L. Case, *Microbiologia*, 10ª edição. Porto Alegre: Artmed Editora SA, 2012.

[12] K. Shahbaz, “Cephalosporins: pharmacology and chemistry,” *Pharm. Biol. Eval.*, vol. 4, no. 6, pp. 234–238, 2017.

[13] D. Kalman and S. L. Barriere, “Review of the Pharmacology, Pharmacokinetics, and Clinical use of Cephalosporins,” *Texas Hear. Inst. J.*, vol. 17, no. 3, pp. 203–214, 1990.

[14] JCGM, “International Vocabulary of metrology - Basic and general concepts and associated terms,” 2012. .

[15] K. Kalantar-zadeh, “Sensors Characteristics,” in *Sensors: An Introductory Course*, New York: Springer Science+Business Media, 2013, pp. 11–28.

[16] H. Kaur, A. Bhosale, and S. Shrivastav, “Biosensors : Classification, Fundamental Characterization and New Trends : A Review,” *Int. J. Heal. Sci. Res.*, vol. 8, no. 6, pp. 315–333, 2018.

[17] R. Pallàs-Areny and J. G. Webster, *Sensors and Signal conditioning*, 2nd editio. New York: John Wiley & Sons, Inc., 2001.

[18] K. W. Britt, “Papermaking,” *Encyclopaedia Britannica*, 2012. [Online]. Available: https://www.britannica.com/technology/papermaking. [Accessed: 11-Sep-2019].

[19] P. Shenoy, “A Study on History of Paper and Possible Paper Free World,” *Int. J. Manag.*, vol. 6, no. 1, pp. 337–355, 2016.

[20] Y. Habibi, L. A. Lucia, and O. J. Rojas, “Cellulose nanocrystals: Chemistry, self-assembly, and applications,” *Chem. Rev.*, vol. 110, no. 6, pp. 3479–3500, 2010.

[21] T. Huber, J. Müssig, O. Curnow, S. Pang, S. Bickerton, and M. P. Staiger, “A critical review of all-cellulose composites,” *J. Mater. Sci.*, vol. 47, no. 3, pp. 1171–1186, 2012.

[22] K. K. Pandey, “A study of chemical structure of soft and hardwood and wood polymers by FTIR spectroscopy,” *J. Appl. Polym. Sci.*, vol. 71, no. 12, pp. 1969–1975, 1999.

[23] S. Park, J. O. Baker, M. E. Himmel, P. A. Parilla, and D. K. Johnson, “Cellulose crystallinity index: Measurement techniques and their impact on interpreting cellulase

performance," *Biotechnol. Biofuels*, vol. 3, pp. 1–10, 2010.

[24] M. Poletto, V. Pistor, and A. J., "Structural Characteristics and Thermal Properties of Native Cellulose," *Cellul. - Fundam. Asp.*, no. January 2015, 2013.

[25] M. N. Costa *et al.*, "A low cost, safe, disposable, rapid and self-sustainable paper-based platform for diagnostic testing: lab-on-paper," *Nanotechnology*, vol. 25, 2014.

[26] L. Fu and Y. Wang, "Detection methods and applications of microfluidic paper-based analytical devices," *Trends Anal. Chem.*, vol. 107, pp. 196–211, 2018.

[27] M. D. Tarn and N. Pamme, "Microfluidics," in *Chemistry, Molecular Sciences and Chemical Engineering*, Elsevier Inc., 2013.

[28] J. Osredkar, "Point-of-Care testing in laboratory medicine," in *Point-of-Care Diagnostics - New Progresses and Perspectives*, 2017, pp. 1–28.

[29] G. Luka *et al.*, "Microfluidics Integrated Biosensors : A Leading Technology towards Lab-on-a-Chip and Sensing Applications," *Sensors*, vol. 15, pp. 30011–30031, 2015.

[30] P. Kim, K. W. Kwon, M. C. Park, S. H. Lee, and S. M. Kim, "Soft Lithography for Microfluidics : a Review," *Biochip J.*, vol. 2, no. 1, pp. 1–11, 2008.

[31] M. Baalousha and T. Hofmann, "Nanoparticles : Structure, Properties, Preparation and Behaviour in Nanoparticles : structure, properties, preparation and behaviour in environmental media," *Ectoxicology*, vol. 17, pp. 326–343, 2008.

[32] M. Hadi, T. Aghaie, A. Avan, A. Vatankhah, M. Reza, and S. Gha, "Colorimetric detection based on gold nano particles (GNPs): An easy, fast, inexpensive, low-cost and short time method in detection of analytes (protein, DNA, and ion)," *Sens. Bio-Sensing Res.*, vol. 20, pp. 1–8, 2018.

[33] M. Demurtas and C. C. Perry, "Facile one-pot synthesis of amoxicillin-coated gold nanoparticles and their antimicrobial activity," *Gold Bull*, vol. 47, pp. 103–107, 2014.

[34] L. Shen, J. Chen, N. Li, P. He, and Z. Li, "Rapid colorimetric sensing of tetracycline antibiotics with in situ growth of gold nanoparticles," *Anal. Chim. Acta*, vol. 839, pp. 83–90, 2014.

[35] P. K. Jain, X. Huang, and I. H. El-sayed, "Review of Some Interesting Surface Plasmon Resonance-enhanced Properties of Noble Metal Nanoparticles and Their Applications to Biosystems," *Plasmonics*, vol. 2, pp. 107–118, 2007.

[36] V. Amendola, R. Pilot, and M. Frasconi, "Surface plasmon resonance in gold

nanoparticles: a review," *J. Phys.*, vol. 29, 2017.

[37] S. Eustis and M. A. El-Sayed, "Why gold nanoparticles are more precious than pretty gold: Noble metal surface plasmon resonance and its enhancement of the radiative and nonradiative properties of nanocrystals of different shapes," *Chem. Soc. Rev.*, vol. 35, no. 3, pp. 209–217, 2006.

[38] Merck, "Gold Nanoparticles: Properties and Applications," 2019. [Online]. Available: https://www.sigmaaldrich.com/technical-documents/articles/materials-science/nanomaterials/gold-nanoparticles.html. [Accessed: 06-Sep-2019].

[39] K. A. Willets and R. P. Van Duyne, "Localized Surface Plasmon Resonance Spectroscopy and Sensing," *Annu. Rev. Phys. Chem.*, vol. 58, no. 1, pp. 267–297, 2006.

[40] S. Kovacs, S. E. Hawes, S. N. Maley, E. Mosites, L. Wong, and A. Stergachis, "Technologies for detecting falsified and substandard drugs in low and middle-income countries," *PLoS One*, vol. 9, no. 3, 2014.

[41] G. Hancu, B. Simon, H. Kelemen, A. Rusu, E. Mircia, and Á. Gyéresi, "Thin layer chromatographic analysis of beta-lactam antibiotics," *Adv. Pharm. Bull.*, vol. 3, no. 2, pp. 367–371, 2013.

[42] S. Vickers, M. Bernier, S. Zambrzycki, F. M. Fernandez, P. N. Newton, and C. Caillet, "Field detection devices for screening the quality of medicines: a systematic review," *BMJ Glob. Heal.*, vol. 3, 2018.

[43] G. J. Buckley and L. O. Gostin, "Countering the Problem of Falsified and Substandard Drugs," 2013. [Online]. Available: http://www.nap.edu/catalog.php?record_id=18272. [Accessed: 26-Jan-2019].

[44] O. Coskun, "Separation Tecniques: CHROMATOGRAPHY," *North. Clin. Istanbul*, vol. 3, no. 2, pp. 156–160, 2016.

[45] R. Das, E. Ali, and S. B. Abd Hamid, "Current Applications of X-ray Powder Diffraction - A Review," *Rev. Adv. Mater. Sci.*, vol. 38, no. 2, pp. 95–109, 2014.

[46] J. K. Maurin, F. Pluciński, A. P. Mazurek, and Z. Fijałek, "The usefulness of simple X-ray powder diffraction analysis for counterfeit control-The Viagra® example," *J. Pharm. Biomed. Anal.*, vol. 43, pp. 1514–1518, 2007.

[47] N. A. Dafale, U. P. Semwal, R. K. Rajput, and G. N. Singh, "Selection of appropriate analytical tools to determine the potency and bioactivity of antibiotics and antibiotic resistance," *J. Pharm. Anal.*, vol. 6, pp. 207–213, 2016.

[48] Global Pharma Health Fund, "GPHF | The GPHF-Minilab™." [Online]. Available: https://www.gphf.org/en/minilab/. [Accessed: 25-Jan-2019].

[49] A. A. Weaver *et al.*, "Paper analytical devices for fast field screening of beta lactam antibiotics and anti-tuberculosis pharmaceuticals," *Anal. Chem.*, vol. 85, no. 13, pp. 6453–6460, 2013.

[50] B. Pagará, "Paper as a Colorimetric Biosensing Platform for Tetracyclines Detection in Milk," (Master's Thesis) Faculdade de Ciências e Tecnologia - Universidade Nova de Lisboa, 2018.

[51] A. Rai, A. Prabhune, and C. C. Perry, "Antibiotic mediated synthesis of gold nanoparticles with potent antimicrobial activity and their application in antimicrobial coatings," *J. Mater. Chem.*, vol. 20, no. 32, pp. 6789–6798, 2010.

[52] Xerox Corporation, "ColorQube 8570, Color Printers: Xerox," *ColorQube™ 8570*. [Online]. Available: https://www.office.xerox.com/en-us/printers/colorqube-8570. [Accessed: 07-Aug-2019].

[53] Euro-Scientific, "Hot plates, ceramic, CERAN 500," *Hot plates, Ceramic, Ceran 500*. [Online]. Available: https://www.euro-scientific.be/en/default/2000309/OUR PRODUCTS/Industry laboratory/Laboratory Equipment/Hot plates/Hot plates, ceramic/Hot plates, ceramic, CERAN 500.aspx. [Accessed: 07-Aug-2019].

[54] C. De Caro and C. Haller, *UV/VIS Spectrophotometry - Fundamentals and Applications*. Suíça: Mettler Toledo, 2015.

[55] ImageJ, "Introduction," 2019. [Online]. Available: https://imagej.nih.gov/ij/docs/intro.html. [Accessed: 13-Sep-2019].

[56] Instituto Pedro Nunes, "Microscopia electrónica de varrimento com sistema EDS e WDS (análise química por raios X)." [Online]. Available: https://www.ipn.pt/laboratorio/LEDMAT/ensaio/15. [Accessed: 27-Jan-2019].

[57] CENIMAT|i3N, "Microscopy - SEM Microscopy Laboratory | CENIMAT." [Online]. Available: https://www.cenimat.fct.unl.pt/services/laboratory-structural-materials/microscopy-sem-microscopy-laboratory. [Accessed: 27-Jan-2019].

[58] W. Zhou and Z. L. Wang, Eds., *Scanning Microscopy for Nanotechnology - Techniques and Applications*. New York: Springer Science+Business Media, 2006.

[59] S. A. Khan, S. B. Khan, L. U. Khan, and A. Farooq, "Fourier Transform Infrared Spectroscopy : Fundamentals and Application in Functional Groups and Nanomaterials

Characterization," in *Handbook of Materials Characterization*, Springer, Cham, 2018, pp. 317–344.

[60] A. A. Bunaciu and H. Y. Aboul-enein, "X-Ray Diffraction : Instrumentation and Applications Critical Revie," *Anal. Chem.*, vol. 45, no. 4, pp. 289–299, 2015.

[61] P. Gill, T. T. Moghadam, and B. Ranjbar, "Differential Scanning Calorimetry Techniques: Applications in Biology and Nanoscience," *J. Biomol. Tech.*, vol. 21, no. 4, pp. 167–93, 2010.

[62] R. Goenka, P. Parthasarathy, N. K. Gupta, N. K. Biyahut, and S. Narayanan, "Kinetic Analysis of Biomass and Comparison of its Chemical Compositions by Thermogravimetry, Wet and Experimental Furnace Methods," *Waste and Biomass Valorization*, vol. 6, no. 6, pp. 989–1002, 2015.

[63] CENIMAT|i3N, "TGA-DSC - STA 449 F3 Jupiter | CENIMAT," 2019. [Online]. Available: https://www.cenimat.fct.unl.pt/services/laboratory-electronic-and-optoelectronic-materials-and-devices/tga-dsc-sta-449-f3-jupiter. [Accessed: 12-Aug-2019].

[64] I. P. INFARMED, "Lista das denominações, formas farmacêuticas, dosagens, vias de administração dos medicamentos, titulares das autorizações de introdução no mercado nos estados-membros," *Anexo Amoxicilina*, 2016. [Online]. Available: http://www.infarmed.pt/web/infarmed/infarmed?p_p_id=101&p_p_lifecycle=0&p_p_state=maximized&p_p_mode=view&_101_struts_action=%2Fasset_publisher%2Fview_content&_101_assetEntryId=1925779&_101_type=document&inheritRedirect=false&redirect=http%3A%2F%2Fwww.inf. [Accessed: 14-Aug-2019].

[65] J. D. S. Newman and G. J. Blanchard, "Formation of gold nanoparticles using amine reducing agents," *Langmuir*, vol. 22, no. 13, pp. 5882–5887, 2006.

[66] C. Subramaniam, R. T. Tom, and T. Pradeep, "On the formation of protected gold nanoparticles from AuCl 4- By the reduction using aromatic amines," *J. Nanoparticle Res.*, vol. 7, no. 2–3, pp. 209–217, 2005.

[67] M. Fan, D. Dai, and B. Huang, "Fourier Transform Infrared Spectroscopy for Natural Fibres," *Fourier Transform - Mater. Anal.*, 2012.

[68] V. Tserki, N. E. Zafeiropoulos, F. Simon, and C. Panayiotou, "A study of the effect of acetylation and propionylation surface treatments on natural fibres," *Compos. Part A Appl. Sci. Manuf.*, vol. 36, no. 8, pp. 1110–1118, 2005.

[69] M. Hariharan *et al.*, “Synthesis and Characterisation of CaCO3 (Calcite) Nano Particles from Cockle Shells Using Chitosan as Precursor,” *Int. J. Sci. Res. Publ.*, vol. 4, no. 10, pp. 1–5, 2014.

[70] D. K. Shen and S. Gu, “The mechanism for thermal decomposition of cellulose and its main products,” *Bioresour. Technol.*, vol. 100, no. 24, pp. 6496–6504, 2009.

[71] N. Yang, X. Jiang, and D.-W. Pang, “Catalytic Applications of Carbon Dots,” in *Carbon Nanoparticles and Nanostructures*, Springer, Cham, 2016, pp. 257–298.

[72] M. Costa, “Desenvolvimento de microfluídica em papel para utilização em biossensores,” (Master's Thesis) Faculdade de Ciências e Tecnologia - Universidade Nova de Lisboa, 2012.

[73] C. F. Castro-Guerrero, A. B. Morales-Cepeda, L. K. Hernández-Vega, and M. R. Díaz-Guillén, “Fructose-mediated gold nanoparticles synthesis,” *Cogent Chem.*, vol. 4, no. 1, pp. 1–7, 2018.

[74] I. Ojea-Jiménez, F. M. Romero, N. G. Bastús, and V. Puntes, “Small gold nanoparticles synthesized with sodium citrate and heavy water: Insights into the reaction mechanism,” *J. Phys. Chem. C*, vol. 114, no. 4, pp. 1800–1804, 2010.

Annex

A. Calculation of the molar concentrations of gelatine

M: Molar mass (g/mol)

C: Molar concentration (mol/L)

C_m: Mass concentration (g/L)

n: number of moles (mol)

m: mass (g)

v: volume (L)

$$n = \frac{m}{M} \qquad C = \frac{n}{v}$$

$$M_{ceftazidime} = 546.58\ g/mol$$

$$C_m = \frac{m}{v} = \frac{n \times M}{v} = \frac{C \times v \times M}{v} = C \times M$$

Table A. 1 Correspondent mass concentration of ceftazidime

Molar concentration of ceftazidime (mM)	Correspondent mass concentration of ceftazidime (mg/mL)
0.0100	5.466×10^{-3}
0.0325	0.0101
0.0650	0.0355
0.1000	0.0547
0.1300	0.0711
0.2500	0.1301
0.3000	0.1640
0.5000	0.2733
1.0000	0.5000

B. Calibration curves corresponding to the paper microplates with amoxicillin

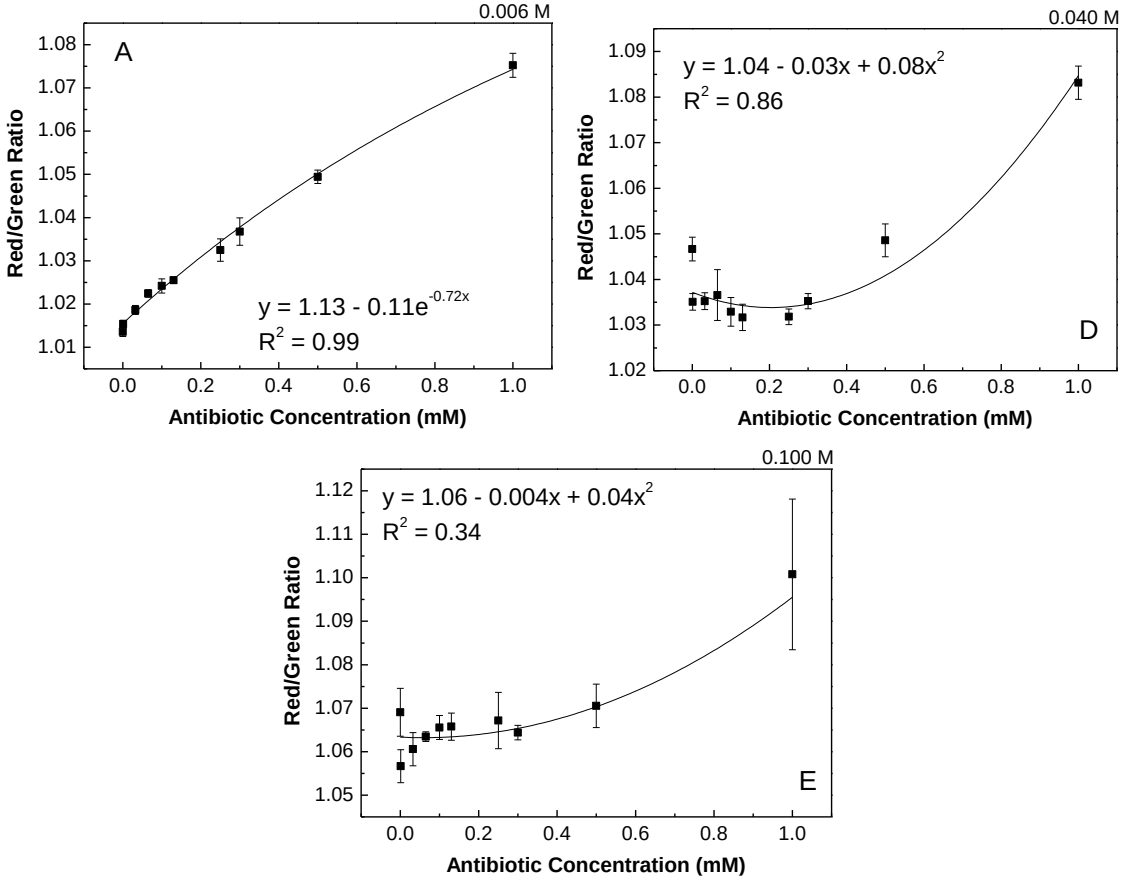

Figure B. 1 Calibration curves corresponding to Figure 5.18

A: Calibration curve correspondent to $HAuCl_4$ concentration of 0.006 M; B: Calibration curve correspondent to $HAuCl_4$ concentration of 0.040 M; C: Calibration curve correspondent to $HAuCl_4$ concentration of 0.100 M

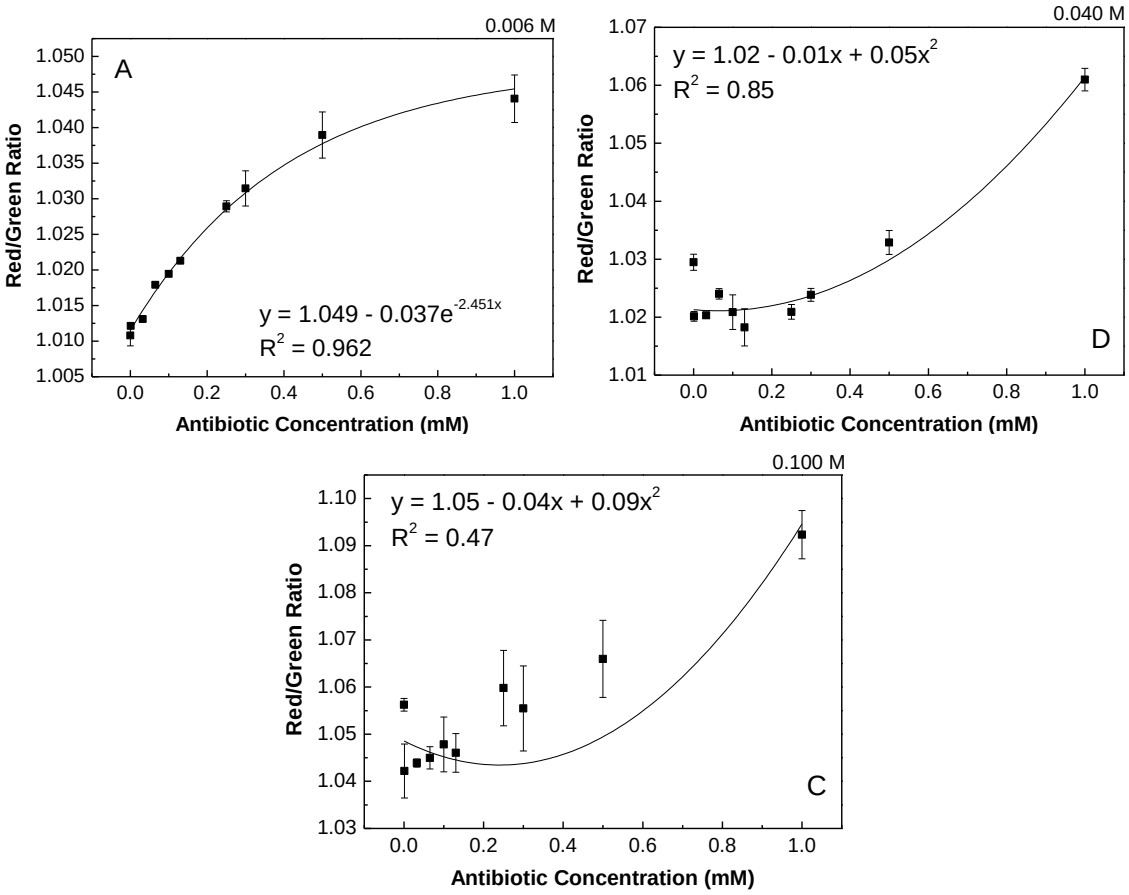

Figure B. 2 Calibration curves corresponding to Figure 5.20

A: Calibration curve correspondent to $HAuCl_4$ concentration of 0.006 M; B: Calibration curve correspondent to $HAuCl_4$ concentration of 0.040 M; C: Calibration curve correspondent to $HAuCl_4$ concentration of 0.100 M

C. Calibration curves corresponding to the paper microplates with ampicillin

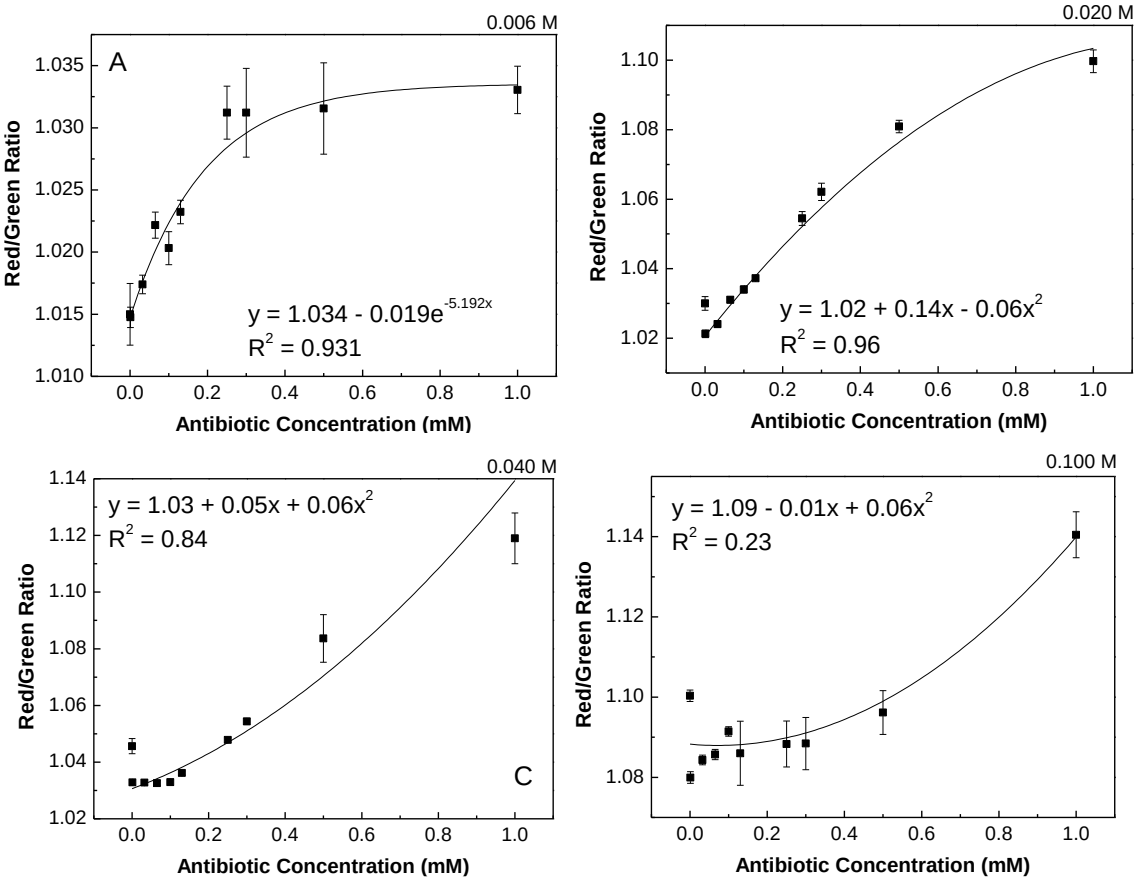

Figure C. 1 Calibration curves corresponding to Figure 2.22

A: Calibration curve correspondent to $HAuCl_4$ concentration of 0.006 M; B: Calibration curve correspondent to $HAuCl_4$ concentration of 0.020 M; C: Calibration curve correspondent to $HAuCl_4$ concentration of 0.040 M; D: Calibration curve correspondent to $HAuCl_4$ concentration of 0.100 M

D. Calibration curves corresponding to the paper microplates with ceftazidime

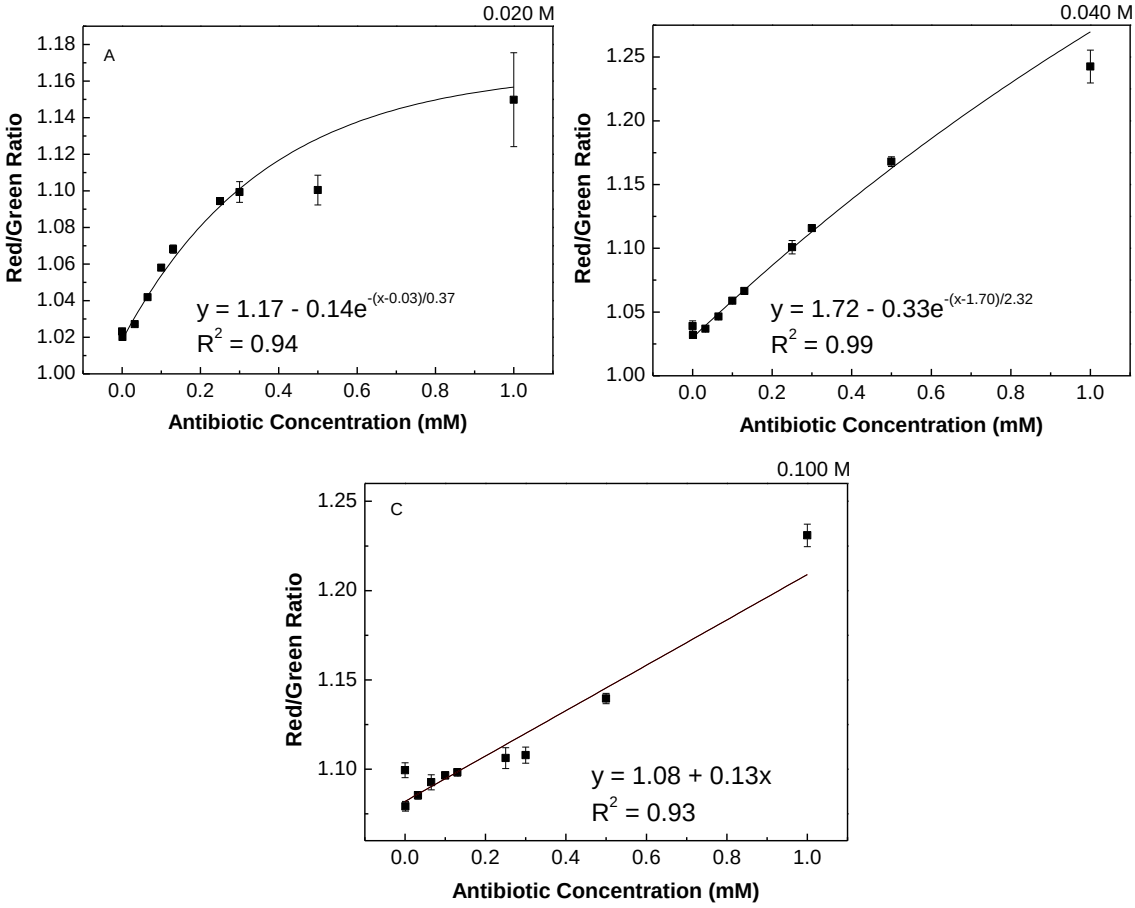

Figure D. 1 Calibration curves corresponding to Figure 5.24

A: Calibration curve correspondent to $HAuCl_4$ concentration of 0.020 M; B: Calibration curve correspondent to $HAuCl_4$ concentration of 0.040 M; C: Calibration curve correspondent to $HAuCl_4$ concentration of 0.100 M

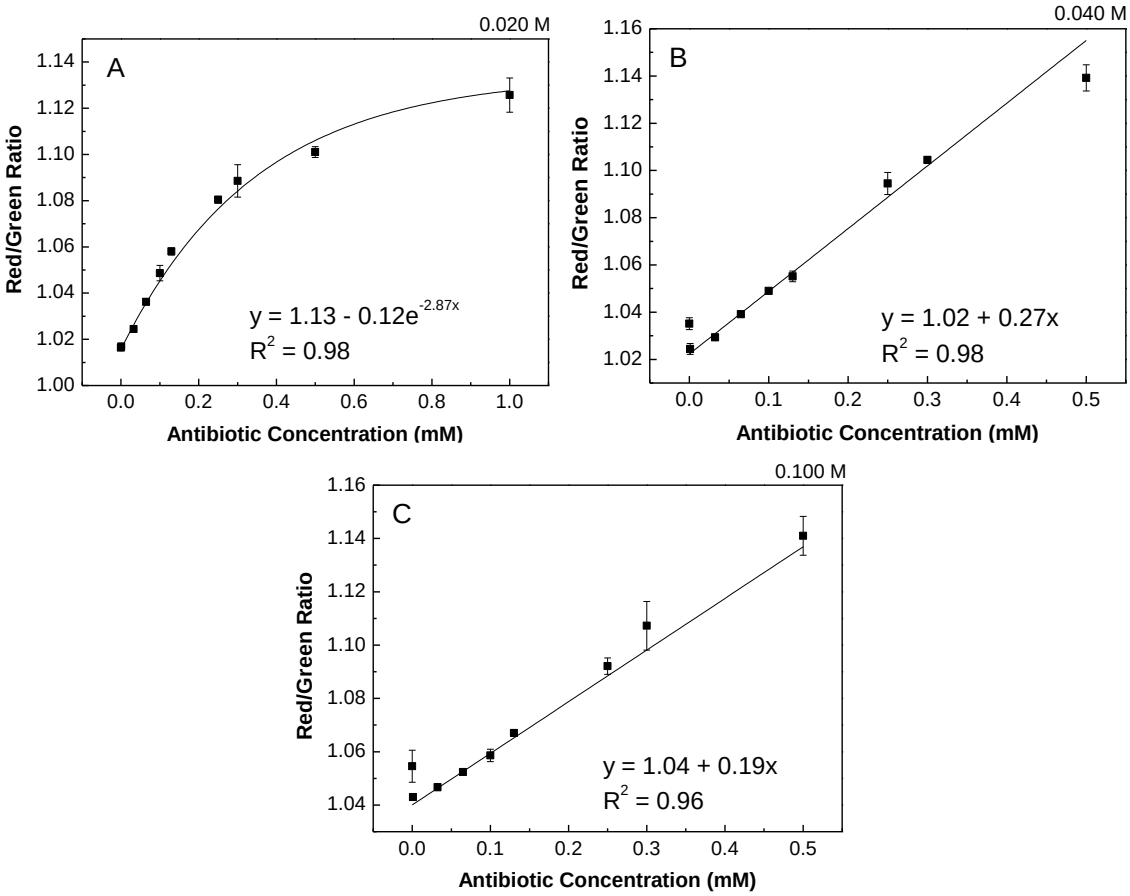

Figure D. 2 Calibration curves corresponding to Figure 5.25

A: Calibration curve correspondent to $HAuCl_4$ concentration of 0.020 M; B: Calibration curve correspondent to $HAuCl_4$ concentration of 0.040 M; C: Calibration curve correspondent to $HAuCl_4$ concentration of 0.100 M